

1981

Inelastic overload analysis of continuous steel multi-girder highway bridges by the finite element method, PhD dissertation (J. C. Hall), June 1981, 201p.

Jeffrey Craig Hall

C. N. Kostem

Follow this and additional works at: <http://preserve.lehigh.edu/engr-civil-environmental-fritz-lab-reports>

---

#### Recommended Citation

Hall, Jeffrey Craig and Kostem, C. N., "Inelastic overload analysis of continuous steel multi-girder highway bridges by the finite element method, PhD dissertation (J. C. Hall), June 1981, 201p." (1981). *Fritz Laboratory Reports*. Paper 500.  
<http://preserve.lehigh.edu/engr-civil-environmental-fritz-lab-reports/500>

This Technical Report is brought to you for free and open access by the Civil and Environmental Engineering at Lehigh Preserve. It has been accepted for inclusion in Fritz Laboratory Reports by an authorized administrator of Lehigh Preserve. For more information, please contact [preserve@lehigh.edu](mailto:preserve@lehigh.edu).

**Lehigh  
University**



LEHIGH UNIVERSITY LIBRARIES



3 9151 00942822 4

ON LOAN 432.6

Due 11/1/81

INELASTIC OVERLOAD ANALYSIS OF  
CONTINUOUS STEEL MULTIGIRDER HIGHWAY BRIDGES  
BY THE FINITE ELEMENT METHOD

FRITZ ENGINEERING  
LABORATORY LIBRARY

BY

JEFFREY C. HALL

CELAL N. KOSTEM

**Fritz  
Engineering  
Laboratory**

FRITZ ENGINEERING LABORATORY REPORT No. 432.6

INELASTIC OVERLOAD ANALYSIS OF CONTINUOUS  
STEEL MULTIGIRDER HIGHWAY BRIDGES BY  
THE FINITE ELEMENT METHOD

by

Jeffrey C. Hall

Celal N. Kostem

FRITZ ENGINEERING  
LABORATORY LIBRARY

Fritz Engineering Laboratory Report

Department of Civil Engineering

Lehigh University

Bethlehem, Pennsylvania

June 1981

Fritz Engineering Laboratory Report No. 432.6

Parts of this work were sponsored by the Pennsylvania Department of Transportation and the United States Department of Transportation, Federal Highway Administration.

The contents of this report reflect the views of the authors, who are responsible for the accuracy of the data presented herein. The contents do not necessarily reflect the official view or policies of the Pennsylvania Department of Transportation or the Federal Highway Administration. This report does not constitute a standard, specification, or regulation.

## TABLE OF CONTENTS

|    |  |    |
|----|--|----|
|    | ABSTRACT   |    |
| 1. | INTRODUCTION   | 2  |
|    | 1.1 Introduction   | 2  |
|    | 1.2 Problem Statement  | 3  |
|    | 1.3 Purpose and Scope of Investigation                               | 5  |
|    | 1.4 Previous Research  | 8  |
|    | 1.5 The Analytical Model   | 11 |
| 2. | MATERIAL BEHAVIOR AND STABILITY CONSIDERATIONS                       | 16 |
|    | 2.1 Introduction   | 16 |
|    | 2.2 Uniaxial Stress-Strain Relationship for Steel                    | 18 |
|    | 2.3 Biaxial Stress-Strain Relationship for<br>Slab Concrete          | 21 |
|    | 2.4 Torsional Buckling of Compression Flange                         | 26 |
|    | 2.5 Buckling of Plate Girder Web Panels and<br>Compression Flanges   | 30 |
|    | 2.5.1 Web Panel Buckling   | 31 |
|    | 2.5.2 Web Panel Post-Buckling Behavior                               | 35 |
|    | 2.5.3 Lateral Buckling of the Compression<br>Flange of Plate Girders | 41 |
| 3. | FINITE ELEMENT ANALYSIS  | 44 |
|    | 3.1 Introduction and Assumptions                                     | 44 |

TABLE OF CONTENTS (continued)

|     |  |    |
|-----|--|----|
| 3.2 | The Finite Element Method                          | 46 |
| 3.3 | The Slab Element                                   | 49 |
| 3.4 | The Beam Element                                   | 54 |
| 3.5 | Concrete Failure and Unloading                     | 61 |
| 3.6 | Buckling Failure                                   | 61 |
| 3.7 | Solution Scheme                                    | 62 |
|     | 3.7.1 Problem Definition                           | 63 |
|     | 3.7.2 Dead Load Solution                           | 63 |
|     | 3.7.3 Scaling Procedure                            | 64 |
|     | 3.7.4 Overload Solution Procedure                  | 65 |
| 4.  | COMPARISONS OF ANALYTICAL AND EXPERIMENTAL RESULTS | 70 |
|     | 4.1 Introduction                                   | 70 |
|     | 4.2 Beam-Slab Bridge Superstructures               | 72 |
|     | 4.2.1 Example No. 1 - Bridge 3B                    | 73 |
|     | AASHTO Bridge Test                                 |    |
|     | 4.2.2 Example No. 2 - Bridge 1 - University        | 78 |
|     | of Tennessee                                       |    |
|     | 4.3 Continuous Composite Beams                     | 82 |
|     | 4.3.1 Example No. 3 - Test CB2                     | 83 |

TABLE OF CONTENTS (continued)

|       |   |     |
|-------|---|-----|
| 4.4   | Transversely Stiffened Unsymmetrical Plate<br>Girders | 85  |
| 4.4.1 | Example 4a, b, c - Tests UG2.1,<br>UG2.2 and UG2.3    | 86  |
| 4.5   | Analysis of a Four-Span Continuous Highway<br>Bridge  | 90  |
| 4.5.1 | FHWA Four-Span Continuous Bridge<br>Superstructure    | 91  |
| 5.    | FURTHER CONSIDERATIONS                                | 96  |
| 5.1   | Introduction  | 96  |
| 5.1.1 | Shear Connector Stiffness                             | 96  |
| 5.1.2 | Fatigue   | 99  |
| 5.1.3 | Torsion of the Beams or Girders                       | 102 |
| 6.    | SUMMARY AND CONCLUSIONS                               | 108 |
| 6.1   | Summary   | 108 |
| 6.2   | Conclusions   | 111 |
| 6.3   | Suggestions for Future Research                       | 112 |
| 7.    | NOMENCLATURE  | 114 |
|       | TABLES  | 121 |
|       | FIGURES   | 139 |
|       | REFERENCES  | 183 |
|       | ACKNOWLEDGMENTS                                       | 192 |

## ABSTRACT

This dissertation describes an analytical technique for predicting the response to overloads of simple-span and continuous multi-girder beam-slab type highway bridge superstructures made of steel beams and reinforced concrete slabs. The nonlinear overload response is obtained by using a tangent stiffness solution process. The analysis scheme also employs the displacement based finite element method of structural analysis, where the superstructure is discretized into a series of beam and slab finite elements, and, in addition, where the elements are further subdivided into a series of layers through their depth. The beam and slab finite elements in this model are allowed to deform in both bending and in-plane displacement modes, while the beam finite elements are also permitted to deform in shear. Each of the element layers is assumed to have its own stiffness properties and to be in a state of plane stress. The nonlinearities included in the model are: inelastic stress-strain relationships, cracking and crushing of concrete, yielding and strain hardening of steel, buckling of beam compression flanges, and buckling of plate girder webs and compression flanges. The method is verified through comparisons of analytical results and laboratory or field overload test results.

## 1. INTRODUCTION

### 1.1 Introduction

This dissertation describes a mathematical model which predicts the overload response resulting from the placement of overweight vehicles on simple-span or continuous multi-girder highway bridge superstructures, with steel beams (girders) and a reinforced concrete deck. Because the overload vehicles lack standardization in size, shape, and load distribution, and because each bridge superstructure is different, the analytical technique presented herein has been made general enough to perform a nonlinear analysis of many different bridge superstructures and loading patterns. This analytical technique can also perform an overload analysis of deteriorated beam-slab bridges, of composite beams, of plate girders, and of concrete slabs.

This algorithm employs the finite element method in which the concrete slab and steel beams (girders) are divided into a series of finite elements (Fig. 1), interconnected at discrete node points (Fig. 2). The beam and slab elements are then further subdivided into layers (Fig. 3), where each layer has its own stiffness properties. This finite element idealization permits a realistic simulation of the structural response of the bridge superstructures. (Refs. 42, 43, 52, 54, 55, 68 and 69).

The solution scheme also uses a tangent stiffness or piecewise linear solution process to simulate the expected inelastic structural response. In this process the loads are applied in a series of load increments or load steps, to allow for changes in the overall structural stiffness due to nonlinear responses, i.e. inelastic stress-strain relationships or buckling. This tangent stiffness solution process provides a continuous description of the structural response from initial load levels in the elastic range up to the collapse load levels.

The reliability of this analytical technique is illustrated by several collations between experimental and analytical results. Comparing the experimental and analytical load versus deformation diagrams and load versus damage assessments for the various test structures, more than adequate correlation exists to verify the reliability of the analytical technique.

## 1.2 Problem Statement

The overloading of beam-slab highway bridges with reinforced concrete slabs and steel beams or girders, hereafter referred to as steel bridges, has become a relatively common occurrence due to basically three factors: (1) increases in the allowable vehicular weight limitations, (2) transportation of heavy industrial and construction equipment, and (3) the issuing of overload permits for specialized overweight and oversized vehicles. As a result of this increased frequency of structural overloads, the bridge

engineer has an urgent requirement to accurately assess the reserve capacity and serviceability limits of any bridge superstructure on which overload vehicles are expected to traverse.

Since an accurate overload analysis requires knowledge of the actual distribution of forces and stresses in the component members, the commonly used reverse design method of analysis is inadequate. This is so because in the reverse design process the loads are distributed to the composite beam and slab according to assumed distribution factors; thus the actual interaction of bridge components to the given load is not considered. In addition, if during an overload the slab cracks, or the beam yields or buckles, it becomes extremely important to know: the location of such a failure; the post-failure strength of the component which has failed; and the manner in which the forces and stresses will redistribute themselves due to the failure. Again, typical analysis procedures which evaluate one beam at a time cannot account for these phenomena because no interaction between bridge components takes place. However, the method presented in this dissertation allows for the consideration of all these phenomena. It should also be noted that while methods have been developed to predict the ultimate capacity of steel bridges or their components, none of these methods adequately predicts the structural response of the bridge in the region between design load levels and ultimate capacity load levels. Therefore, an analysis method is required which reliably predicts both the elastic and inelastic response of a bridge superstructure

as well as that ill-defined region between the design limit and the ultimate capacity. Such an analysis scheme would permit through the application of serviceability limits the defining of the limiting overloads.

Another analysis technique found in the literature realistically predicts the structural response to overloads of concrete slab-concrete beam highway bridge superstructures (Refs. 52, 55), hereafter referred to as concrete bridges. But no method has been previously reported in the literature, with the exception of the technique presented herein, which will reliably predict the entire structural response to overloads in terms of load versus deformation, material failure, and local buckling of bridges with steel beams (girders) with reinforced concrete decks.

### 1.3 Purpose and Scope of Investigation

As was stated earlier, the goal of the overall research program is the development of a mathematical model and analysis technique to reliably predict the complete response of steel highway bridge superstructures when subjected to overloads. Previous research efforts have successfully predicted the overload behavior of slab-beam bridges with reinforced or prestressed concrete beams and concrete decks (Ref. 54, 55); and, simulated the linear elastic behavior of beam-slab structures with steel beams, including the effects of shear deformation of the beam, shear lag in the deck, and slip between the slab and the beam (Ref. 69). The results of these

two research efforts served as a basis for the presently reported work which was divided into three phases:

1. The "integration" of the algorithms for the inelastic slab (Ref. 52) and linear elastic beam (Ref. 64) to produce a composite algorithm, and ultimately a computer program capable of analyzing the overload response of steel bridges. This computer program differs from previous inelastic analytical techniques by including the effects of slip, shear deformation of the beam, and shear lag in the deck, into the inelastic analysis. The accuracy of the developed analytical technique is verified via correlation of analytical and experimental results (Ref. 27).
2. The extension of the inelastic method for analyzing steel bridges, which was developed for phase 1, to include the effects of: strain hardening of the beam steel; buckling of girder webs; and flange buckling (Ref. 28).
3. The determination of the possible effects of torsion in the beams and of the possible occurrence of fatigue cracking in susceptible details when steel bridges are subjected to overloads.

Phase 1 has been reported on and verified in detail (Ref. 27), thus, only those features of phase 1 which are essential for a clear understanding of the contents of this dissertation are to be presented. Phase 2, while being extensively reported upon and verified (Ref. 28), will be presented in detail within the context of this report, because this phase represents the main focus or contribution to the overall research. The investigative results of phase 3 are also presented.

To summarize, this report includes the following material:

1. A brief description of the analytical techniques employed to model the material stress-strain relationships for the concrete and the steel materials (see Chapter 2).
2. A description of the analytical modeling scheme employed to include the predictions of and effects of flange and web buckling (Chapter 2).
3. A brief review of the finite element method and how the finite element method is employed in the analysis scheme presented in this report (Chapter 3).
4. Verification of the method through comparisons with actual test results (Chapter 4).

5. The determination of the possible effects of torsion in the beams and of the possible occurrence of fatigue failure of susceptible details when steel bridges are subjected to overload. (Chapter 5)

#### 1.4 Previous Research

The objective of this research is the determination of the overload response of simple span or continuous steel multi-girder highway bridge superstructures. Therefore, only those works which are reported upon in the literature and which are applicable to the present problem will be reviewed.

Beam-slab highway bridge superstructures can be divided into two categories: those with reinforced or prestressed concrete beams (concrete bridges), and those with steel beams or girders (steel bridges). While many similarities exist when comparing the response characteristics of these two types of bridges, concrete bridges and steel bridges also have many response characteristics which are applicable only to one or the other. For example, one of the primary modes of failure for the concrete bridges is the cracking of the concrete beams, while for the steel bridges the possible modes of failure may be the formation of plastic hinges, or the buckling of webs or flanges. Thus, those response characteristics which are evident in steel bridges may not occur in concrete bridges, and vice versa.

The first developmental work concerning the analysis of structures with concrete decks and steel beams was presented in two papers by Newmark (Refs. 51, 59). The first of these papers did not consider the composite action of the beam and slab. The second paper overcame this deficiency and presented a derivation for the differential equation describing the axial forces of the component parts in the elastic region. However, this equation was applicable only to isolated T-beams and not to multi-girder systems. Others have expanded upon the theory formulated by Newmark to account for non-uniform connector spacing, initial strains, and nonlinear material properties using an iterative solution procedure.

Proctor, Baldwin, Henry and Sweeney at the University of Missouri (Ref. 5) and Yam and Chapman at Imperial College (Ref. 72) treat the boundary value problem as an initial value problem and solve the equations by successive approximation; and Dia, Thiruvengadam and Seiss at the University of Illinois (Ref. 19), Wu at Lehigh University (Ref. 71), and Fu at the University of Maryland (Ref. 25) use finite differences in conjunction with Newmark's work. None of these methods, however, considers fully the problem of shear lag, shear deformation of the beam, slip between the slab and the beam, and continuous structures, whereas, Tumminelli and Kostem (Ref. 64) employing a finite element method

to include the above deficiency into a linear elastic solution process with no inelastic capabilities.

Research by Wegmuller and Kostem (Refs. 68, 69) led to the development of an analysis technique and computer program to predict the elastic-plastic structural response of eccentrically stiffened plate systems. This technique, which employed the finite element method, used the ACM (Ref. 1) rectangular plate element modified for in-plane displacement by Clough (Ref. 18). The elements were layered to monitor the spread of yielding throughout the structure. In addition, the material was assumed to obey a von Mises yield condition. Based on this work Kulicki and Kostem (Refs. 40, 43) extended the model and the technique to incorporate eccentrically placed reinforced concrete or prestressed concrete beams. In this analysis the response characteristics of the concrete beams were realistically modelled, including the cracking and crushing of concrete and yielding of steel. Subsequently, Peterson and Kostem (Refs. 52, 54, 55) further extended the analysis technique to accurately simulate the biaxial behavior of reinforced concrete slabs, and thus in the end, to reliably predict the overload response of concrete highway bridge superstructures. However, this still left the problem of the overload analysis of steel bridges to be solved.

The above research efforts have demonstrated that the finite element method of analysis provided an efficient tool that can be used to perform an inelastic analysis of eccentrically

stiffened slab systems. The complexities in material behavior and losses in stiffness due to yielding, cracking, crushing, or local instability can be directly incorporated into the analysis scheme. Thus, by integrating the works of Tumminelli and Kostem and Peterson and Kostem, and including the effects of strain hardening, flange buckling, and web buckling into a concise finite element computer program, a realistic model for predicting the overload response of continuous steel multi-girder highway bridges can be developed. The main contribution of the material in this dissertation, is the development of such a realistic model.

#### 1.5 The Analytical Model

The analytical model should adequately reflect the structural characteristics of the actual structure. To reliably describe the inelastic response of beam-slab highway bridge superstructures with steel beams or girders, the following must be considered:

1. The out-of-plane or flexural behavior of the structure.
2. The in-plane response of the beam and slab due to the eccentricity of the beams.
3. The coupling action of the in-plane and out-of-plane responses.
4. Material nonlinearities.

5. The possibility of slip between the beam and the slab (i.e. amount of composite action).
6. Shear deformation of the beams or girders.
7. Local instability of the beam and/or girder flanges or webs, and any associated post-buckling behavior.

When bridge superstructures are subjected to vehicular loads, i.e. out-of-plane forces, both longitudinal and transverse bending moments which are out-of-plane responses, and axial forces which are in-plane responses, occur in the slab. At the same time, longitudinal bending moments and axial forces are predominant in the beams and/or girders. The development of these axial forces in the slab and beams is due to the eccentricity of the center of gravity of the beams in relation to the midheight of the slab. Thus, the application of out-of-plane loads to the bridge superstructure produces both in-plane and out-of-plane responses in the slab and beam. This interdependency between in-plane and out-of-plane actions is commonly referred to as coupling action. While coupling action has little effect on the structural response in the elastic region, it has significant effect on the inelastic structural response as explained in detail in Ref. 55.

Since the material nonlinearities have a profound effect on the structural response of the superstructure by causing changes in the structural stiffness, a realistic representation of the material stress-strain relationships of the component parts is

essential. For steel highway bridge superstructures the appropriate material representations needed are:

For the beam or girder:

1. Steel subjected to uniaxial stress states.

For the slab:

1. Concrete subjected to biaxial stress states.
2. Mild steel reinforcing subjected to uniaxial stress states.

Since the response due to overloads is expected to eventually cause nonlinear stress-strain behavior, the appropriate inelastic stress-strain relationships of the component materials must be included. Thus, the present analysis scheme utilizes the biaxial stress-strain relationships developed in Refs. 45, 47, 48, 50, 52, 55 to describe the inelastic behavior of concrete slabs, and in addition, utilizes the uniaxial stress-strain relations developed in Refs. 27, 28, 39, 40, 42, 57 to describe the inelastic response of steel.

To adequately reflect the variation in material stiffness properties through the depth of the beam or slab members, due to cracking of concrete or yielding of steel, or some other material failure, the finite elements are subdivided into a series of layers. Each layer is assumed to be in a state of biaxial or uniaxial stress and each assumed to have distinct material properties. Then by defining the stress-strain relationship on a layer by layer basis, the progression of nonlinear material behavior

through the structure can be monitored. Through the utilization of the layering technique good agreement has been obtained between analytical and test results (Refs. 6, 30, 31, 40, 43, 53, 66, 70).

Typical analytical models for composite structures assume that no slip occurs between the slab and the beams. But if there does not exist sufficient linkage between the slab and the beam, then slip will occur and the percentage of load shared by the beam and the slab will change. Thus, the analytical model should be able to account for the possibility of slip. In addition, due to shear deformation, beams and particularly plate girders with thin webs, will deflect considerably more than standard beam theory would predict. Thus the model should be able to adequately reflect the effects of shear deformation.

Finally, because beams and plate girders are of thin walled open cross-sections, they are susceptible to local buckling phenomena, prior to attaining maximum stress conditions. Therefore, the analytical technique should be capable of predicting the occurrence of local buckling and any post-buckling strength of such sections.

The preceding paragraphs contain the major structural phenomena which have significant effect on the structural behavior of steel bridge superstructures. The underlying premise of the entire nonlinear response and ultimate collapse of the bridge superstructure is that the primary response of the structure is flexural in nature with the associated in-plane and coupling

actions. While the effects of torsion of the beams is considered to be of minor importance, and, therefore, not included in the analytical method, an investigation into the effects of torsion of the beams in the elastic region is still presented. Other structural phenomena considered to be of secondary importance and excluded from the analysis technique are:

1. Minor axis bending of the beams. This will affect the forces in the bracing and hence the major axis bending moments, but the contribution to the overall structural response is considered extremely minimal.
2. Shear punch failure of the slab. Because in normal bridge superstructures the loads are transmitted through the vehicle tires, such failures are highly unlikely due to the large distribution of load (Ref. 74).
3. Dynamic and impact effects. It is assumed that the speed of the overload vehicle would be slow enough so as not to produce any dynamic or impact effects (Ref. 75).
4. Superelevation. Comparisons of analytical and experimental results of bridges which had large superelevation, but were modelled with no superelevation showed that little or no noticeable error occurs by ignoring the effects of superelevation (Refs. 54, 55).

## 2. MATERIAL BEHAVIOR AND STABILITY CONSIDERATIONS

### 2.1 Introduction

This chapter presents the material stress-strain relationships and stability criterion employed in the reported analytical technique. Material stress-strain relations are defined for the beam steel, reinforcing bar steel, and for the slab concrete. In addition, the equations defining the initiation of buckling in the flanges and webs of the beams (girders) and the post-buckling response of the beams (girders) are described. These relations and equations are later used to establish the stiffness properties of the bridge components.

The behavior of concrete and steel is dependent upon the particular stress state, i.e. tension or compression, and whether or not the stress field is uniaxial or biaxial. A beam, for example, may be idealized as a one-dimensional structural element in which major axis bending produces a uniaxial state of stress (Ref. 40). A slab, on the other hand, may be envisioned as a two-dimensional structural element in which bending and in-plane actions in both the longitudinal and transverse directions produce a biaxial stress state (Refs. 52, 55). Thus, the beam (girder) steel is assumed to be in a uniaxial state of stress, while the slab concrete is assumed to be in a biaxial state of stress.

The inelastic uniaxial stress-strain relationship of the beam (girder) steel is analytically defined in this model by a modified Ramberg-Osgood formulation (Refs. 27, 28, 57). Similarly, the nonlinear biaxial stress-strain relationship of the concrete slab is analytically described by empirical formulae which are presented in detail in Ref. 52 and briefly outlined herein. In addition, since the flanges and webs of the beams or girders may buckle, empirical and theoretical formulae are employed to predict the initiation of buckling and any post-buckling behavior of the beam (Ref. 28).

By differentiation of these stress-strain equations the instantaneous slope, tangent modulus, of the particular stress-strain curve is obtained. This tangent modulus and a reduced modulus due to the buckling phenomena are then used to formulate the element elasticity matrix, [D], which relates the stress increment to the strain increment.

$$\{\dot{\sigma}\} = [D] \{\dot{\epsilon}\} \quad (2.1)$$

The elasticity matrix is then utilized to establish the slab and beam (girder) finite element stiffness properties (Chapter 3).

Throughout this dissertation the stress-strain relationships are discussed in terms of both incremental and total stresses and strains. To distinguish between the two type of stress and strain, the incremental quantities will be designated with the customary dot (.) over the appropriate quantity, e.g. Eq. 2.1.

## 2.2 Uniaxial Stress-Strain Relationship for Steel

The uniaxial nonlinear stress-strain relationship for the steel of the beams (girders) and slab reinforcement has been established for the layered finite element model using a Ramberg-Osgood formulation (Refs. 27, 28, 40, 43, 57):

$$\epsilon = \left\{ \sigma + \left( \frac{1-m}{m} \right) \frac{\sigma^n}{\sigma_y^{n-1}} \right\} \frac{1}{E_i} \quad (2.2)$$

where

$\sigma$  = stress

$\epsilon$  = strain

$E_i$  = initial modulus of elasticity

$\sigma_y$  = yield stress

$m$  = 0.7 for mild steel reinforcement

0.67 for beam steel

$n$  = 300 for mild steel reinforcement

400 for beam steel

The instantaneous slope, tangent modulus, of this stress-strain curve is then given by (Refs. 27, 28, 40, 43, 57):

$$\frac{d\sigma}{d\epsilon} = \frac{E_i}{1 + n \cdot \left( \frac{1-m}{m} \right) \left( \frac{\sigma}{\sigma_y} \right)^{n-1}} \quad (2.3)$$

However, when the limiting strain of the plastic range,  $\epsilon_{st}$ , is attained in a layer, a parabolic post-plastic strain-hardening relationship is assumed to exist (Refs. 28, 29). Thus, when

$$|\epsilon| \geq \epsilon_{st} = \text{limit of plastic range} \quad (2.4)$$

then

$$\sigma = \alpha_b + \sqrt{\beta_b + \gamma_b \epsilon} \quad (2.5)$$

where

$$\alpha_b = \frac{[\sigma_u^2 - \sigma_y^2 - 2E_{st} \sigma_y (\epsilon_u - \epsilon_{st})]}{2 [\sigma_u - \sigma_y - E_{st} (\epsilon_u - \epsilon_{st})]}$$

$$\beta_b = (\sigma_y - \alpha_b - 2E_{st} \epsilon_{st})(\sigma_y - \alpha_b)$$

$$\gamma_b = 2 E_{st} (\sigma_y - \alpha_b)$$

and  $\sigma_u$  = the ultimate stress on stress-strain curve (Fig. 5)

$\epsilon_u$  = the strain corresponding to ultimate stress,  $\sigma_u$

$E_{st}$  = initial strain hardening modulus.

The complete stress-strain curve for steel (Fig. 5) is, thus, established analytically. The tangent modulus,  $E_t$ , for the strain-hardening portion of the curve is then determined from Eq. 2.5 to be (Ref. 28):

$$E_t = \frac{d\sigma}{d\varepsilon} = \frac{1}{2} \frac{\gamma_b}{\sigma - \alpha_b} \quad (2.5)$$

In the elastic portion of the stress-strain curve, the instantaneous shearing modulus,  $G$ , is assumed to be equal to (Ref. 28):

$$G = \frac{E_i}{2(1 + \nu)} \quad (2.6)$$

where  $\nu$  = Poisson's ratio = 0.3 for steel. However, according to Lay (Ref. 46), the shearing modulus in the post-plastic range can be given by:

$$G_t = \frac{2G}{1 + \frac{E_i}{4E_t(1 + \nu)}} \quad (2.7)$$

Using Eqs. 2.5, 2.6 and 2.7 the instantaneous shearing modulus in the strain-hardening range (i.e.  $|\varepsilon| > \varepsilon_{st}$ ), becomes:

$$G_t = \frac{2 \gamma_b E_i}{2 \gamma_b (1 + \nu) + E_i (\sigma - \alpha_b)} \quad (2.8)$$

From the initiation of yielding to the initiation of strain-hardening, the instantaneous shear modulus is assumed to vary linearly with respect to the strain,  $\varepsilon$ , from an initial value given by Eq. 2.6 to a final value given by Eq. 2.8.

### 2.3 Biaxial Stress-Strain Relationship for Slab Concrete

Based upon experimental investigations into the biaxial behavior of concrete (Refs. 45, 48, 49, 50) and employing analytical expressions developed by Liu (Refs. 48, 49), for the biaxial principal stress-strain relations of concrete, Peterson and Kostem (Refs. 52, 54, 55) developed effective linear and non-linear biaxial stress-strain relationships for concrete slabs. The nonlinear principal stress-strain curve, in compression dominant regions, can be given by (Refs. 27, 52, 55):

$$\sigma = \frac{\epsilon E_c}{(1 - \nu\alpha)(1 + C\epsilon + D\epsilon^2)} \quad (2.9)$$

where

$\sigma$  = principal stress in direction of  
interest

$\epsilon$  = strain in direction of interest

$\nu$  = Poisson's ratio = 0.20 (concrete)

$\alpha$  = ratio of principal stresses

$E_c$  = initial uniaxial tangent modulus for concrete

C, D = constants which depend upon  $E_c$ ,  $\nu$ ,  $\alpha$

and the peak stress,  $\sigma_p$ , strain,  $\epsilon_p$ , and  
modulus,  $E_p$ .

The peak stress values of Eq. 2.9 can be obtained from the idealized nondimensional biaxial failure envelope (Fig. 6). Then, from experiments and analytical approximations, corresponding values of peak strain and peak modulus can also be found (Ref. 52, 55). Thus, once the initial stress-state, defined by  $\alpha$ , is known, the complete nonlinear stress-strain relation is analytically determined.

From Eq. 2.9 the instantaneous slope, tangent modulus, is determined to be (Refs. 27, 52, 55):

$$E_b = \frac{d\sigma}{d\varepsilon} = \frac{E_c}{(1 - \nu\alpha)} \frac{(1 - D\varepsilon^2)}{(1 + C\varepsilon + D\varepsilon^2)^2} \quad (2.10)$$

It should be noted that a separate tangent modulus exists for each principal stress direction.

While Eq. 2.9 and 2.10 are applicable in compression dominant regions, the linear biaxial stress-strain relation for concrete in tension dominant regions is given by (Refs. 27, 52, 57):

$$E_b = \frac{d\sigma}{d\varepsilon} = \frac{\sigma_p}{\varepsilon_p} \quad (2.11)$$

To relate the principal biaxial stress state to the principal biaxial strain state, the following anisotropic constitutive relationship is required (Ref. 48):

$$\begin{Bmatrix} \dot{\sigma}_1 \\ \dot{\sigma}_2 \\ \dot{\tau}_{12} \end{Bmatrix} = [\bar{D}] \begin{Bmatrix} \dot{\epsilon}_1 \\ \dot{\epsilon}_2 \\ \dot{\gamma}_{12} \end{Bmatrix} \quad (2.12)$$

where

$$[\bar{D}] = \begin{bmatrix} \frac{E'_{1b}}{1 - \nu_1 \nu_2} & \frac{\nu_2 E'_{1b}}{1 - \nu_1 \nu_2} & 0 \\ \frac{\nu_1 E'_{2b}}{1 - \nu_1 \nu_2} & \frac{E'_{2b}}{1 - \nu_1 \nu_2} & 0 \\ 0 & 0 & \frac{E'_{1b} E'_{2b}}{E'_{1b} + E'_{2b} + 2 \nu_1 E'_{2b}} \end{bmatrix} \quad (2.13)$$

and subscripts 1, 2 denote principal stress directions. It should be noted that  $E_b$  in Eqs. 2.10 and 2.11 relates the stress in a particular direction to the strain in that same direction, and only that direction, while  $E'_{1b}$  and  $E'_{2b}$  represent the actual tangent moduli, where the principal stress is related to the strains in both principal directions and to the shearing strain. The relationship which exists between  $E_b$  and  $E'_b$  is (Ref. 55):

$$E'_{1b} = E_{1b} (1 - \nu_1 \alpha_1) \quad (2.14a)$$

and

$$E'_{2b} = E_{2b} (1 - \nu_2 \alpha_2) \quad (2.14b)$$

Thus, all the terms required for determining the elasticity matrix,  $[\bar{D}]$ , are now defined analytically. However, since the  $[\bar{D}]$  matrix relates only stresses and strains in the principal stress directions, a transformation must take place to relate the stresses and strains in the global x-y coordinated system (Eq. 2.15). Such a transformation is required, so that the slab element stiffnesses in the x-y directions may be computed.

$$\begin{Bmatrix} \dot{\sigma}_x \\ \dot{\sigma}_y \\ \dot{\tau}_{xy} \end{Bmatrix} = [D] \begin{Bmatrix} \dot{\epsilon}_x \\ \dot{\epsilon}_y \\ \dot{\gamma}_{xy} \end{Bmatrix} \quad (2.15)$$

$$\text{where } [D] = [T] [\bar{D}] [T]^T \quad (2.16)$$

and  $[T]$  is a transformation matrix relating the 1, 2 coordinate system to the x, y coordinate system (Ref. 55).

In the analytical model when the principal stress exceeds the idealized peak stress as defined by Fig. 6, cracking or crushing of the concrete is assumed to occur (Refs. 52, 54, 55). As a result of this cracking or crushing the concrete layer is assumed to have a stiffness only in the uncracked or uncrushed direction. Thus, if cracking or crushing occurs in the "2" direction, the resulting constitutive stress-strain relationship would become:

$$\begin{Bmatrix} \dot{\sigma}_1 \\ \dot{\sigma}_2 \\ \dot{\tau}_{12} \end{Bmatrix} = \begin{bmatrix} E_{1b} & 0 & 0 \\ 0 & 0 & 0 \\ 0 & 0 & 0 \end{bmatrix} \begin{Bmatrix} \dot{\epsilon}_1 \\ \dot{\epsilon}_2 \\ \dot{\gamma}_{12} \end{Bmatrix} \quad (2.17)$$

It should be noted that the shearing stiffness term,  $D_{33}$ , is also set equal to zero. This is done because previous research has shown that slabs in flexure are insensitive to the value for the shearing stiffness once cracking has occurred (Refs. 30, 31, 47).

After failure of the concrete layer due to cracking or crushing, the layer would be incapable of sustaining the stress that caused the failure, and, thus this stress must be reduced to zero within the layer while maintaining external and internal equilibrium. This unloading of stress and redistribution of forces to neighboring layers is accomplished through the application of a fictitious force matrix (Refs. 52, 54, 55). However, in the actual overload analysis of continuous steel highway bridges it becomes possible at extremely high load levels for the concrete slab to become completely cracked, i.e. cracked through the entire depth of the slab. Such complete cracking of the slab can occur, for example, over interior supports in the transverse direction or over the beams in the longitudinal direction. When complete cracking does occur in the finite element model the slab element stiffness in the direction perpendicular to the crack would become zero. However, experience has shown that when the slab element stiffness becomes zero in one principal direction, numerical difficulties often occur in the solution process and inaccurate solutions can result. To avoid this possibility of numerical instability in the solution process the cracked or crushed layer is given an artificial stiffness equal to  $E_c/1,000,000$  rather than zero. It should be noted that there is

no loss of accuracy in employing this approximation. A similar procedure will be used frequently throughout this dissertation to prevent mathematical instabilities in the solution process when failures occur.

#### 2.4 Torsional Buckling of Compression Flange

In continuous composite beams the strength in the positive moment region is generally controlled by the yielding of steel in tension or by the crushing of concrete in compression; however, in the negative moment region the strength may be limited by torsional buckling of the compression flange. According to Lay (Ref. 46) torsional flange buckling of conventional wide flange shapes is essentially an inelastic phenomena. It should be noted, however, that the inelastic plate buckling equation can also be applied in the elastic range with some modifications.

Typically, the compression flange is envisioned as being partially restrained against twisting by a torsional spring (Fig. 8a). The assumed deformed shape of a torsionally buckled compression flange is presented in Fig. 7. In the case of elastic plate buckling the critical stress for torsional buckling,  $\sigma_{cr}$ , is based upon the width to thickness ratio of the flange,  $2t/b$ , and the assumed stiffness coefficient,  $k_v$ .

$$\sigma_{cr} = k_v \frac{\pi^2 E}{12 (1 - \nu)} \left( \frac{2t}{b} \right)^2 \quad (2.18)$$

The stiffness coefficient is related to the torsional restraint provided by the beam web. If the web is flexible and provides only vertical support then  $k_v = 0.425$  (Ref. 39); however, if the web is exceedingly stiff and provides vertical support and considerable torsional restraint then  $k_v = 1.277$  (Ref. 39) (Figs. 8b and 8c). In order to relate the coefficient  $k_v$  directly to the dimensions of the web and, therefore, the web's elastic torsional restraint capacity, Lay's inelastic torsional buckling equation, Eq. 2.19, will be modified for elastic conditions (Ref. 28).

$$bt \sigma_{cr} = \frac{1}{\frac{r_o^2}{2}} \left\{ G_t K_T + \left( \frac{n\pi}{L} \right)^2 E_t I_\omega + k_t \left( \frac{L}{n\pi} \right)^2 \right\} \quad (2.19)$$

where:

$G_t$  = inelastic shearing modulus

$E_t$  = inelastic tangent modulus

$k_t$  = torsional stiffness of web

$$K_T = \frac{bt^3}{3}$$

$$I_\omega = \frac{7}{16} \left\{ \frac{b^3 t^3}{144} \right\}$$

$\frac{L}{n}$  = half wave length of buckle

$$\frac{1}{\frac{r_o^2}{2}} = \frac{12}{b^2}$$

If the above inelastic equation is assumed to apply also in the elastic range, then the elastic values for  $G$  and  $E$  can be

substituted for the inelastic values,  $G_t$  and  $E_t$ . By then solving Eq. 2.19, with  $G$  and  $E$ , for the lowest value of  $n\pi/L$  and substituting that value back into Eq. 2.19, the following equation is obtained:

$$bt \sigma_{cr} = \frac{1}{r_o^2} \left\{ GK_T + 2 \sqrt{k_t E I_\omega} \right\} \quad (2.20)$$

The torsional stiffness,  $k_t$ , derived from the deformed shape of the web (Fig. 7) is:

$$k_t \approx \frac{E w^3}{3 (1 - \nu^2) d} \quad (2.21)$$

Substituting the values for  $K_T$ ,  $1/r_o^2$ ,  $I_\omega$ , and  $k_t$  into Eq. 2.20 gives the following elastic critical stress equation:

$$\sigma_{cr} = \left\{ \frac{2}{1 + \nu} + \frac{3}{2} \sqrt{\frac{7}{27} \left(\frac{w}{t}\right)^3 \frac{b}{d} \frac{1}{(1 - \nu^2)}} \right\} E \left(\frac{t}{b}\right)^2 \quad (2.22)$$

By comparing Eqs. 2.18 and 2.22 with  $\nu = 0.3$ , the stiffness coefficient,  $k_v$ , is found to be:

$$k_v = 0.4255 + 0.2215 \sqrt{\left(\frac{w}{t}\right)^3 \frac{b}{d}} \leq 1.277 \quad (2.23)$$

Thus, for any given beam cross-section the critical elastic torsional flange buckling stress,  $\sigma_{cr}$ , can be calculated analytically using Eqs. 2.18 and 2.23. However, it should be noted that

experiments by Winter (Ref. 39) have shown that due to the presence of residual stresses and due to the effects of shear lag in the flanges, there can exist a nonuniform stress distribution in the flanges, and, thus even if the average stress value in the flange is less than the critical value,  $\sigma_{cr}$ , buckling can occur. Based upon experimental results and employing an effective flange width type concept, i.e. only part of the flange is capable of resisting the load, Winter has proposed a semi-empirically derived critical buckling stress transition equation for plates supported at one edge (Ref. 39):

$$\sigma_{av} = 1.19 \sqrt{\sigma_{cr} \sigma_y} (1 - 0.3 \sqrt{\sigma_{cr}/\sigma_y}) \quad (2.24a)$$

The relationship between Eq. 2.18 and 2.24 is shown graphically in Fig. 4, where

$$\lambda = \frac{b}{2t} \sqrt{\frac{\sigma_y}{E} \frac{12(1-\nu^2)}{\pi^2 k_v}} \quad (2.24b)$$

If  $\lambda \geq 1.3$  then Eq. 2.18 controls, and if  $\lambda < 1.3$  and  $\sigma < \sigma_y$  then Eq. 2.24 controls.

If the strain,  $\epsilon$ , in the flange exceeds the yield strain,  $\epsilon_y$ , then the inelastic torsional flange buckling stress equation derived from Eq. 2.19 must be employed (Refs. 28 and 46):

$$\sigma_{cr,in} = \left\{ G_t + \sqrt{\frac{7}{48} E_t G_t \left(\frac{w}{t}\right)^3 \left(\frac{b}{d}\right)} \right\} \left(\frac{2t}{b}\right)^2 \quad (2.25)$$

where  $k_t$  in Eq. 2.19 is equal to  $G_t w^3/3d$ . The values for  $E_t$  and  $G_t$  come from the equations established in Section 2.2 for inelastic behavior of steel.

When the average stress, of all the layers which make up the compression flange of any beam element, exceeds the critical torsional buckling stress, the flange is assumed to buckle. Since the beam finite element cannot deform as shown in Fig. 7, the buckling and post-buckling behavior of the beam compression flange must be simulated as follows. Ideally the flange would have either a negative stiffness value, to permit a redistribution of stress within the beam element, or have a zero stiffness value. Experience and experimental correlations indicate that adequate agreement between experimental and analytical results can be obtained by assigning an artificially low stiffness value of  $(E_t/100,000)$  to all the critical compression flange layers. If the flange stiffness had been set equal to zero, numerical instabilities may have occurred in the solution process (see Section 2.3).

## 2.5 Buckling of Plate Girder Web Panels and Compression of Flanges

In the past one of the design criteria for plate girders was based upon the assumption that the load-carrying capacity of the web plate was limited by buckling of the web; however, experiments indicated that transversely stiffened web plate panels have considerable post-buckling strength. Basler was one of the first to present a definitive analysis of the strength of plate girders

under pure bending, pure shear, and combined bending and shear loading conditions (Refs. 7, 8, 9). The results of Basler's experiments showed that plate girder strength was limited by: (1) web buckling due to shear, or combined shear and bending; (2) vertical buckling of the compression flange; (3) lateral buckling of the compression flange; (4) torsional buckling of compression flange; and (5) yielding. In a simple span composite slab-girder structure the compression flange is laterally and torsionally restrained by the concrete deck; thus, instability of the compression flange is unlikely. In addition, the web panel, in a simple span structure, is unlikely to buckle under combined shear and bending because bending forces will be dominant. In a continuous slab-girder superstructure, however, there exists an increased likelihood of flange or web panel buckling in the vicinity of the interior supports, due to a lack of complete lateral support for the compression flange and the high shear condition for the web. The problem of web panel failure will be dealt with in Sections 2.5.1 and 2.5.2, while the problem of compression flange failure will be covered in Section 2.5.3.

#### 2.5.1 Web Panel Buckling

Since the publication of Basler's works, numerous models have been proposed to predict the initiation of web buckling and any associated post-buckling behavior of transversely stiffened plate girders (Refs. 15, 16, 17, 39, 58). Each of the new models seeks to eliminate the deficiencies in Basler's original tension

field model. While all of the proposed models can reasonably predict the ultimate load capacity of the plate girders, the Chern and Ostapenko formulation (Refs. 15, 16, 17) forms the basis for the present analysis scheme because of its simplicity and reliability.

A typical section of a transversely stiffened plate girder is depicted in Fig. 11. When the plate girder is subjected to combined bending and shear, the resultant stress pattern on the web panel can be idealized as shown in Fig. 9, where the horizontal boundaries of the web plate panel are determined by the flanges, and the vertical boundaries by the transverse stiffeners. The stress distribution at the initiation of web buckling can be determined with sufficient accuracy by means of the following interaction equation (Refs. 17 and 39):

$$\left(\frac{\sigma_{cc}}{\sigma_{ccr}}\right) + \left(\frac{\sigma_b}{\sigma_{bcr}}\right)^2 + \left(\frac{\tau_c}{\tau_{ccr}}\right)^2 = 1.0 \quad (2.26a)$$

where

$$\begin{aligned} \tau_c &= \text{shear buckling stress under combined loads} \\ \tau_{ccr} &= k_s \frac{\pi^2 E}{12(1 - \nu^2)} \left(\frac{w}{d}\right)^2, \text{ buckling stress} \\ &\quad \text{under pure shear condition} \quad (2.26b) \\ \sigma_b &= \text{bending buckling stress at the extreme compression fiber under combined loads} \end{aligned}$$

$$\sigma_{bcr} = k_b \frac{\pi^2 E}{12(1 - \nu^2)} \left( \frac{w}{d} \right)^2, \text{ buckling stress under}$$

pure bending condition (2.26c)

$\sigma_{cc}$  = compressive buckling stress under combined loads

$$\sigma_{ccr} = k_c \frac{\pi^2 E}{12(1 - \nu^2)} \left( \frac{w}{d} \right)^2, \text{ buckling stress under}$$

pure compression. (2.26d)

The buckling coefficients,  $k_s$ ,  $k_b$ , and  $k_c$  are dependent upon whether the unloaded horizontal edge of the web plate panel is assumed to act as a fixed edge, i.e. stiff flanges, or to act as a simply supported edge, i.e. flexible flanges. The fixed edge condition will be designated by an asterisk superscript, and the simply supported condition by no superscript.

$$k_s^* = \frac{5.34}{\alpha_p^2} + \frac{2.31}{\alpha_p} - 3.44 + 8.39 \alpha_p$$

$$k_s = 4.0 + \frac{5.34}{\alpha_p}$$

for  $\alpha_p \leq 1.0$

$$k_s^* = 8.98 + \frac{5.61}{\alpha_p^2} - \frac{1.99}{\alpha_p^3}$$

$$k_s = 5.34 + \frac{4.00}{\alpha_p}$$

for  $\alpha_p \geq 1.0$

$\alpha_p = \frac{a}{d}$ , panel aspect ratio, or ratio of panel width to panel depth.

$$k_b^* = 39.6, \quad k_b = 23.9$$

$$k_c^* = 6.97, \quad k_c = 4.0$$

The critical stress values given by Eqs. 2.26b, 2.26c, and 2.26d are elastic buckling values. However, experiments have shown that due to the presence of residual stresses, initial imperfections and strain hardening that buckling can occur prior to reaching the maximum stress of  $\tau_{ccr}$  or  $\sigma_{bcr}$ . Thus, the following transitional relations are employed for calculating  $\tau_{ccr}$  (Ref. 15):

$$\text{for } 0.58 \leq \lambda_v \leq \sqrt{2}$$

$$\tau_{ccr} = \tau_y \{1 - 0.615 (\lambda_v - 0.58)^{1.18}\} \quad (2.26e)$$

$$\text{for } \lambda_v \leq 0.58$$

$$\tau_{ccr} = \tau_y \{1 + 4.30 (0.58 - \lambda_v)^{1.58}\} \quad (2.26f)$$

where

$$\lambda_v = \sqrt[3]{\frac{\tau_y}{k_s} \frac{12 (1 - \nu^2)}{\pi^2 E} \left(\frac{d}{w}\right)^2}$$

$$\tau_y = \sigma_y / \sqrt{3}$$

Likewise when the pure bending stress,  $\sigma_{bcr}$  in Eq. 2.26c, exceeds  $0.8 \sigma_y$  the following additional relationship is employed to compute  $\sigma_{bcr}$  (Ref. 77):

$$\text{for } \sigma_{bcr} \geq 0.8 \sigma_y$$

$$\sigma_{bcr} = \sigma_y \left\{1 - \frac{0.16 \sigma_y}{\sigma_{bcr}}\right\} \quad (2.26g)$$

When the stress condition under combined loads is such that Eq. 2.26a is satisfied, the web panel is assumed to buckle. Thus, the total shear force carried by the web panel at the initiation of buckling becomes:

$$V_{\tau_c} = \tau_c A_w = \tau_c wd \quad (2.27)$$

### 2.5.2 Web Panel Post-Buckling Behavior

After the web panel buckles, considerable post-buckling strength may be realized by the development of a web panel tension field (Fig. 11). In evaluating this post-buckling strength the following assumptions are made: (1) the web buckling stresses,  $\sigma_{cc}$ ,  $\sigma_b$ , and  $\tau_c$ , remain constant after the web plate buckled, i.e. no unloading; (2) the linearly varying bending stress,  $\sigma_b$ , and constant compressive stress,  $\sigma_c$ , are replaced by their average,  $\sigma_{bc}$  (Fig. 13); and (3) the ultimate strength of the web is reached when the combined stress state of shear stress,  $\tau_c$ ; of average bending and compressive stress,  $\sigma_{bc}$ ; and of the tension field stress,  $\sigma_{tc}$  (Fig. 13); satisfy a von Mises yield condition. An approximation for the expected tension field stress distribution (Figs. 12a, b) has been made for simplicity in the following derivations (Ref. 17). It should be noted that the direction of action of the tension field is at the as yet unknown angle  $\phi_c$  (Fig. 13).

By superimposing the tension field stress state,  $\sigma_{tc}$ , upon the buckling stress state,  $\tau_c$  and  $\sigma_{bc}$ , and imposing the von Mises

yield criteria, the following relation for  $\sigma_{tc}$  (where  $\sigma_{tc}$  and  $\phi_c$  are the only unknowns) is arrived at:

$$\sigma_{tc} = \sigma_{yw} \left\{ \sqrt{1 - 3R^2 - S^2 + [0.5S + 1.5R \sin(2\phi_c + 2\delta)]^2} - (0.5S + 1.5R \sin(2\phi_c + 2\delta)) \right\} \quad (2.28)$$

where

$\sigma_{yw}$  = yield stress of web

$$S = - \frac{C \sigma_{bc}}{4 \sigma_{yw}}$$

$C$  = ratio of maximum tensile stress to maximum compressive stress

$$C = \frac{-\sigma_b + \sigma_{cc}}{\sigma_b + \sigma_{cc}}$$

$$R = \sqrt{S^2 + \left(\frac{\tau_c}{\sigma_{yw}}\right)^2}$$

$$\delta = \frac{1}{2} \tan^{-1} \left( \frac{S \sigma_{yw}}{\tau_c} \right)$$

The tension field shear force of the web plate panel,  $V_{\sigma c}$ , can be determined from Fig. 12b.

$$V_{\sigma c} = \frac{1}{2} wd \sigma_{tc} (\sin 2\phi_c - 0.5 \alpha_p + 0.5 \alpha_p \cos 2\phi_c)$$

(2.29)

Since all of the terms in Eq. 2.29 with the exception of  $\sigma_{tc}$  and  $\phi_c$  are known, and since from Eq. 2.28  $\sigma_{tc}$  is known to be a

function of  $\phi_c$  only, then  $V_{\sigma_c}$  is also a function of  $\phi_c$  only. The maximum tension field action shear force,  $V_{\sigma_c}$ , can then be obtained by differentiating Eq. 2.29 with respect to  $\phi_c$ , setting the derivative equal to zero, and then solving for  $\phi_{co}$ :

$$[\sin 2 \phi_{co} - 0.5 \alpha_p + 0.5 \alpha_p \cos 2 \phi_{co}] \frac{d \sigma_{tc}}{d \phi_{co}} + 2 [\cos 2 \phi_{co} - 0.5 \alpha_p \sin 2 \phi_{co}] \sigma_{tc} = 0 \quad (2.30)$$

where  $\phi_{co}$  denotes the value of  $\phi_c$  obtained when solving Eq. 2.30. The solution of Eq. 2.30 for  $\phi_{co}$  is found by the Newton-Raphson iteration method where the left hand side of the equation is defined as  $F(\phi)$ . Then, since  $\phi_{co}$  is known to be between  $0^\circ$  and  $45^\circ$  an initial trial value of  $\phi_1$  is made using Basler's original formulation, Eq. 2.31, and then computing the function  $F(\phi_1)$ .

$$\phi_1 = \arctan (\sqrt{1 - \alpha_p^2} - \alpha_p) \quad (2.31).$$

If  $F(\phi_1)$  is not within a reasonable tolerance, 0.000001, of the value zero, then a new value of  $F(\phi_2)$  is computed where  $\phi_2$  is ten percent greater than  $\phi_1$ . If  $F(\phi_2)$  is still not within the required tolerance, then the following recursion equation is employed to solve for the new  $\phi$ :

$$\phi_{i+2} = \phi_i - (\phi_{i+1} - \phi_i) \frac{F(\phi_i)}{F(\phi_{i+1}) - F(\phi_i)} \quad (2.32)$$

The operation expressed in the above equation is then repeated until the required accuracy is obtained. By substituting the value of  $\theta_{co}$  back into Eqs. 2.28 and 2.29 the maximum tension field shear becomes:

$$V_{\sigma c} = \frac{1}{2} wd \alpha_{tc} [\sin 2\theta_{co} - 0.5 \alpha_p + 0.5 \alpha_p \cos 2\theta_{co}] \quad (2.33)$$

After buckling of the web plate panel only the stresses parallel to the tension field direction are assumed to increase. Thus, the panel is assumed to have a stiffness only in the tension field direction and no stiffness in the orthogonal direction. Referring to the anisotropic elasticity relation presented in Eq. 2.13, and assuming a similar relationship now exists for the web panel except that  $E_{1b} = E_i$  and  $E_{2b} = 0$ , the following web plate panel constitutive relationship can be assumed to exist:

$$\begin{Bmatrix} \dot{\sigma}_1 \\ \dot{\sigma}_2 \\ \dot{\tau}_{12} \end{Bmatrix} = \begin{bmatrix} E_i & 0 & 0 \\ 0 & 0 & 0 \\ 0 & 0 & 0 \end{bmatrix} \begin{Bmatrix} \dot{\epsilon}_1 \\ \dot{\epsilon}_2 \\ \dot{\gamma}_{12} \end{Bmatrix} \quad (2.34)$$

where the 1, 2 coordinate axes are shown in Fig. 14. Transforming this state of stress to the  $x, z'$  coordinate system (Fig. 14) by means of transformation matrix, [T],

$$[T] = \begin{bmatrix} \cos^2\theta & \sin^2\theta & -2 \cos\theta \sin\theta \\ \sin^2\theta & \cos^2\theta & 2 \cos\theta \sin\theta \\ \cos\theta \sin\theta & -\cos\theta \sin\theta & \cos^2\theta - \sin^2\theta \end{bmatrix} \quad (2.35)$$

where  $\theta = -\phi_{co}$ , and employing Eq. 2.16, the  $x, z'$  coordinate axes stress-strain relationship becomes:

$$\begin{Bmatrix} \dot{\sigma}_x \\ \dot{\sigma}_{z'} \\ \dot{\tau}_{xz'} \end{Bmatrix} = \begin{bmatrix} \cos^4\theta & \sin^2\theta \cos^2\theta & \cos^3\theta \sin\theta \\ \sin^2\theta \cos^2\theta & \sin^4\theta & \cos\theta \sin^3\theta \\ \cos^3\theta \sin\theta & \cos\theta \sin^3\theta & \cos^2\theta \sin^2\theta \end{bmatrix} E_i \begin{Bmatrix} \dot{\epsilon}_x \\ \dot{\epsilon}_{z'} \\ \dot{\gamma}_{xz'} \end{Bmatrix} \quad (2.36)$$

However, since the layered finite element beam formulation considers only the tangent stiffness modulus and the shearing stiffness modulus corresponding to the  $x$ -axis direction, Eq. 2.36 can be simplified to:

$$\begin{Bmatrix} \dot{\sigma}_x \\ \dot{\sigma}_{z'} \\ \dot{\tau}_{xz'} \end{Bmatrix} = \begin{bmatrix} E_i \cos^4\theta & 0 & 0 \\ 0 & 0 & 0 \\ 0 & 0 & E_i \cos^2\theta \sin^2\theta \end{bmatrix} \begin{Bmatrix} \dot{\epsilon}_x \\ \dot{\epsilon}_{z'} \\ \dot{\gamma}_{xz'} \end{Bmatrix} \quad (2.37a)$$

or

$$\dot{\sigma}_x = E_i \cos^4 \theta \dot{\epsilon}_x = E_{pb} \dot{\epsilon}_x \quad (2.37b)$$

$$\dot{\tau}_{xz} = E_i \cos^2 \theta \sin^2 \theta \dot{\gamma}_{xz} = G_{pb} \dot{\gamma}_{xz} \quad (2.37c)$$

where  $E_{pb}$  and  $G_{pb}$  represent the effective post-buckling tangent stiffness modulus and shearing stiffness modulus for the web plate panel. However, the initial attempts to model the actual post-buckling behavior of the web plate panel using the above relations, indicated that the overall post-buckling panel behavior was stiffer than that observed in experiments. Based upon the distribution of the tension field stress a reduction factor,  $C_1$ , was derived to sufficiently decrease the post-buckling stiffness parameters,  $E_{pb}$  and  $G_{pb}$ , to more accurately model the post-buckling web plate panel behavior.

By assuming that only part of the entire web panel is fully effective in contributing to the post-buckling stiffness, a reduction factor is feasible. Thus, considering only that portion of the web plate panel not subjected to the full tension field (i.e. the outer tension field portion) as contributing fully to the stiffness properties of the web panel, the reduction factor becomes (Fig. 14):

$$C_1 = \frac{a \left| a \tan \phi_{co} \right|}{a d} = \frac{\left| a \tan \phi_{co} \right|}{d} \quad (2.38)$$

= area of outer tension field/area web plate panel,

and the resulting moduli become:

$$E_{pb} = C_1 E_i \cos^4 \theta \quad (2.39a)$$

$$G_{pb} = C_1 E_i \cos^2 \theta \sin^2 \theta \quad (2.39b)$$

As will be shown later in the experimental correlations, these assumed post-buckling stiffness parameters provide reasonable agreement with the test results.

The failure load for the limit of the post-buckling behavior occurs when the total web plate panel shear force given by Eq. 2.40 is attained.

$$V_{TH} = V_{TC} + V_{\sigma c} \quad (2.40)$$

where  $V_{TC}$  and  $V_{\sigma c}$  are given by Eqs. 2.27 and 2.33 respectively. Beyond this point the web panel is incapable of sustaining additional load and as with the case of flange buckling this loss of stiffness due to the complete failure of the plate girder panel is simulated by setting the panel stiffness equal to  $E_i/100000$ .

### 2.5.3 Lateral Buckling of the Compression Flange of Plate Girders

As has been mentioned previously when a transversely stiffened plate girder is subjected to combined shear and bending loads one or more of the plate girder panels may fail due to buckling of the web, buckling of the compression flange, or both. While buckling of the web is the predominant mode of failure when a panel is subjected to high shear stress, lateral buckling of the compression flange is the (Fig. 15) predominant mode of

failure when a panel is subjected to large bending stresses.

According to the theory originally proposed by Basler, the critical flange buckling stress for plate girders can be given by:

$$\sigma_{\lambda_{cr}} = \frac{\pi^2 E_i}{(\lambda_b/r^2)} = \frac{\sigma_y}{\lambda_\ell^2} \quad (2.41a)$$

where

$\lambda_b$  = unbraced length of the compression flange

$$r = \sqrt{\frac{bt^3/12}{bt + \frac{1}{6}wd}} = \text{radius of gyration}$$

$$\lambda_\ell = \frac{\lambda_b}{r} \sqrt{\frac{\sigma_y}{\pi^2 E_i}} \geq 2$$

If, however,  $\lambda_\ell < \sqrt{2}$  then a transition equation is required to calculate the flange buckling stress:

$$\sigma_{\lambda_{cr}} = \sigma_y \left(1 - \frac{\lambda_\ell^2}{4}\right) \text{ for } 0 \leq \lambda_\ell \leq 2 \quad (2.41b)$$

Ostapenko and Chern (Ref. 16) however, modified this relationship slightly by assuming the radius of gyration to be:

$$r = \sqrt{\frac{b^3 t/12}{bt + 30 \omega^2}} \quad (2.42)$$

Thus, employing Eqs. 2.41a, b and 2.42 the lateral flange buckling stress can be calculated for any plate girder flange. The unbraced length of the plate girder compression flange can be taken as equal to the distance between points of lateral support in the plate

girder. This assumption is conservative because Eqs. 2.41a, b assume that the flange is in a state of uniform compression throughout its length, while an actual plate girder flange will be in a continually varying stress state due to moment gradients.

Once the compression flange buckles, the flange is unable to sustain any additional increase in load. To simulate the loss of stiffness, the post-buckling flange stiffness should be set equal to  $E_i/100000$ , as before. However, comparisons to experimental results indicate that such a reduction in stiffness is inadequate to effectively model the post-buckling strength of the plate girder. Reliable modelling of the post-buckling stiffness was obtained, however, by assuming that both the flange and the web plate panel suffered a complete loss of stiffness upon reaching the buckling load.

In the preceding paragraphs and sections an attempt has been made to show how the major modes of failure and any post-failure strength of transversely stiffened plate girders can be effectively modelled. As will be shown later in the chapter on experimental correlations, the failure to include these stability considerations into the analyses would lead to highly inaccurate results. However, the present analysis scheme produces reasonably accurate results in terms of load versus deformation curves, load versus stress, and load versus damage records.

### 3. FINITE ELEMENT ANALYSIS

#### 3.1 Introduction and Assumptions

As has been indicated previously, the analytical technique employed in the reported research is based upon the finite element method of analysis (i.e. Refs. 63, 73). A detailed treatment of the finite element method as applied to this research is presented in a number of other related reports, Refs. 27, 40, 43, 52, 54, 64. Thus, only those fundamentals of the method which are necessary for clarity, and those basic assumptions which pertain to the specific features of the analysis, are presented herein.

The following assumptions are made with regards to the development of the analytical model:

1. Geometry - The bridge superstructures to be analyzed are limited essentially to bridges with no skew, i.e. right bridges. However, previous research (Refs. 55 and 75) has indicated that bridges with moderate skew, i.e.  $\phi = 90^\circ$  to  $\phi = 60^\circ$ , can be analyzed as right bridges with no loss in accuracy.
2. Strain Distribution - Plane sections remain plane before and after deformation of the slab and beam, except that a Timoshenko

approach has been employed to include shearing deformation in the beam. In addition, the slab is assumed to behave as a thin plate; and, the beam and slab are assumed not to change thickness.

It should be noted that these common assumptions reduce a three-dimensional problem to one of flexure and one of two-dimensional plate bending where the strain distribution is linear in both cases.

3. Deformations - The deformations are assumed small in comparison to dimensions of the slab, thus, all calculations are based upon the undeformed geometry. Again, it should be noted that previous experience with bridge overloading (Ref. 54) supports this assumption.
4. Strains - Small strains are assumed thus, first order linear strain-displacement relationships can be employed (Ref. 54).
5. Layering - The slab and beam finite elements are layered, each layer having its own stiffness properties, so as to accurately model material nonlinearities and progressive material failure.

6. Stability Failures - When the average stress, of all of the compression flange layers of any beam element, exceeds the critical stress, the compression flange is assumed to buckle, and all of the critical layers are assigned artificially low stiffness values ( $E_i/1000000$ ). Similarly, when the average stress state of the web plate panel reaches the critical conditions, all of the web layers of the entire web plate panel are assigned new stiffness values.

### 3.2 The Finite Element Method

In the finite element method of structural analysis the continuum, i.e. structure, is subdivided into an assemblage of discrete subunits called finite elements, which are interconnected at discrete node points. The behavior of each finite element can be described by the element stiffness matrix,  $[k_i]^e$ , which relates node point forces to node point displacements.

$$\{F\}^e = [k_i]^e \{\delta\}^e \quad (3.1)$$

where

$\{F\}^e$  = vector of element node point forces

$\{\delta\}^e$  = vector of element node point displacements

By stacking all of the element stiffness matrices and considering the applied node point loads and node point constraints the following set of equilibrium equations results:

$$\{F\} = [K] \{\delta\} \quad (3.2)$$

where

$\{F\}$  = vector of applied forces at node points

$[K] = \Sigma \{k_i\}^e$  = global stiffness matrix

$\{\delta\}$  = vector of displacements at node points

The primary concern of the analysis becomes the determination of the element stiffness matrices,  $[k_i]^e$ , for the slab and the girder (Refs. 27, 52, and 69). It can be shown that this element stiffness matrix can be determined by use of Eq. 3.3.

$$[k_i]^e = \int_V [B]^T [D] [B] dV \quad (3.3)$$

where

$[B]$  = strain-displacement matrix

$[D]$  = stress-strain (elasticity) matrix

$V$  = volume of element

The evaluation of these matrices begins by assuming a displacement field, usually a polynomial function, to describe the element deformations.

$$\{f\} = [P(x,y)] \{\zeta\} \quad (3.4)$$

where

$\{f\}$  = displacement field of the element

$[P(x,y)]$  = functions of  $x$  and  $y$  used to describe the shape of displacement field

$\{\zeta\}$  = coefficients of  $x$  and  $y$  functions of  $[P(x,y)]$ .

By enforcing the element boundary conditions at the nodes, and in addition, equilibrium and/or compatibility conditions, Eq. 3.4 can be used to define the element node point displacements  $\{\delta\}^e$ ,

$$\{\delta\}^e = [C] \{\zeta\} \quad (3.5)$$

where

$[C] = [P(x_n, y_n)]$  or the polynomial evaluated at all the element node points.

Solving Eq. 3.5 for the constant coefficients,  $\{\zeta\}$ ,

$$\{\zeta\} = [C]^{-1} \{\delta\}^e \quad (3.6)$$

and then substituting back into Eq. 3.4 gives the following relationship:

$$\{f\} = [P(x,y)][C]^{-1} \{\delta\}^e = [N] \{\delta\}^e \quad (3.7)$$

where

$[N]$  = shape function matrix.

The element strains are found by then differentiating the displacement field, with respect to either  $x$ ,  $y$ , or  $xy$ :

$$\{\epsilon\} = [\Gamma] \{f\} = [\Gamma][P(x,y)][C]^{-1} \{\delta\}^e \quad (3.8a)$$

where

$\{\epsilon\}$  = vector of element strains

$[\Gamma]$  = differential operator matrix

or

$$\{\epsilon\} = [Q][C]^{-1} \{\delta\}^e = [B] \{\delta\}^e \quad (3.8b)$$

where

$$[Q] = [\Gamma][P(x,y)] = \text{connection matrix.}$$

With matrix [B] of Eq. 3.3 now defined, only the elasticity matrix, [D], is still required. Assuming that no initial stresses or strains exist in the element to start, the element constitutive relationship can be given by (Refs. 27, 52 and 69):

$$\{\sigma\} = [D] \{\epsilon\} \quad (3.9)$$

where

$$\{\sigma\} = \text{vector of element stresses.}$$

Thus, with the appropriate choice for the displacement fields to model the desired phenomena, and the correctly chosen constitutive relations for the particular type of element, the element stiffness matrices can be explicitly determined.

### 3.3 The Slab Element

Explicit and in-depth derivations of the layered slab element are presented in Refs. 27, 52, 54, and 55. Only the salient features of slab element development are presented herein. For a detailed treatment of the element development the reader should refer to one of the above references.

The layered slab finite element has a total of four corner point nodes, each with five degrees of freedom (Fig. 16): the vertical z-axis displacement, W; the rotation about x-axis,  $\theta_x$ ; the rotation about y-axis,  $\theta_y$ ; the displacement in the x-direction, U;

and displacement on the y-direction, V. A twelve term polynomial, which is a function of x and y, is used to describe the vertical displacements (Ref. 1). Two four term polynomials are used to describe the longitudinal and transverse displacements. The rotations are obtained by differentiation of the vertical displacement field.

For computational efficiency the displacement field is partitioned into those displacements involving bending action only and those displacements involving in-plane action only:

$$\begin{Bmatrix} \delta_u \\ \delta_\phi \end{Bmatrix} = \begin{bmatrix} P_{u(x,y)} & | & 0 \\ \hline 0 & | & P_{\phi(x,y)} \end{bmatrix} \begin{Bmatrix} \zeta_u \\ \zeta_\phi \end{Bmatrix} \quad (3.10)$$

where the subscript u and  $\phi$ , designate in-plane and bending displacement respectively. Then the element strain obtained by differentiation of the element displacement functions are:

$$\{\epsilon\}_z = \begin{Bmatrix} \epsilon_x \\ \epsilon_y \\ \gamma_{xy} \end{Bmatrix}_z = \begin{Bmatrix} \frac{\partial U}{\partial x} \\ \frac{\partial V}{\partial y} \\ \frac{\partial U}{\partial y} + \frac{\partial V}{\partial x} \end{Bmatrix} + z \begin{Bmatrix} -\frac{\partial^2 W}{\partial x^2} \\ -\frac{\partial^2 W}{\partial y^2} \\ -\frac{\partial^2 W}{\partial x \partial y} \end{Bmatrix} \quad (3.11)$$

where

$z$  = distance from midheight of slab to the point  
under consideration

$(\epsilon_x)_z, (\epsilon_y)_z, (\gamma_{xy})_z$  = strain in x-direction, y-direction, and  
shearing strain at depth  $z$

$\frac{\partial U}{\partial x}, \frac{\partial V}{\partial y}$ , etc = differentiation of respective polynomial  
function with respect to  $x, y$ , or  $xy$ .

Performing the operations outlined in Section 3.2,

Eq. 3.11 becomes:

$$\{\epsilon\}_z = [B_u] \{\delta_u\}^e + z [B_\emptyset] \{\delta\}^e \quad (3.12)$$

As has been mentioned earlier, the slab finite element is subdivided into a series of layers, each layer having its own elasticity matrix,  $[D_i]$ , which depends upon the average stress state in the layer,  $\{\bar{\sigma}_i\}$ . This average stress, which is located at the mid-depth of the slab layer and at a distance  $\bar{z}_i$  from the mid-height of the slab, is obtained by multiplying the elasticity matrix by the integrated average strain of Eq. 3.12:

$$\{\bar{\sigma}_i\} = \frac{[D_i]}{4} \int_a^b \int_p^p [B_u] dx dy \{\delta_u\}^e + z_i \int_x^x \int_y^y [B_\emptyset] dx dy \{\delta_\emptyset\}^e \quad (3.13)$$

Since the elasticity matrix,  $[D_i]$ , depends upon the current total stress state, and the current total stress state depends upon the elasticity matrix, an iterative solution procedure is required to obtain a solution of Eq. 3.13 (see Section 3.6). The steel reinforcing bar layers are included in the integration processes in the same manner as the concrete layers except that the direction of action of the elasticity matrix is uniaxial.

The partitioned slab element stiffness matrix obtained by employing Eq. 3.3 is:

$$[k]^e = \int_V \left[ \begin{array}{c|c} [B_u]^T [D] [B_u] & z [B_u]^T [D] [B_\emptyset] \\ \hline z [B_\emptyset]^T [D] [B_u] & z^2 [B_\emptyset]^T [D] [B_\emptyset] \end{array} \right] dV \quad (3.14a)$$

or

$$[k]^e = \left[ \begin{array}{c|c} [k_{uu}]^e & [k_{u\emptyset}]^e \\ \hline [k_{u\emptyset}]^{eT} & [k_{\emptyset\emptyset}]^e \end{array} \right] \quad (3.14b)$$

where

$[k_{uu}]^e$  = the in-plane stiffness matrix

$[k_{u\phi}]^e$  = the coupling stiffness matrix  
which relates in-plane and  
bending actions

$[k_{\phi\phi}]^e$  = the bending stiffness matrix

Noting from previous discussions that the elasticity matrix is dependent only upon  $z$  and that the strain displacement matrices are dependent only upon  $x$  and  $y$ , the stiffness matrices become:

$$[k_{uu}]^e = \int_x \int_y [B_u]^T [D_{uu}] [B_u] dx dy$$

$$[k_{u\phi}]^e = \int_x \int_y [B_u]^T [D_{u\phi}] [B_\phi] dx dy$$

$$[k_{\phi\phi}]^e = \int_x \int_y [B_\phi]^T [D_{\phi\phi}] [B_\phi] dx dy$$

(3.15)

where

$$\begin{aligned}
 [D_{uu}] &= \sum_{i+1}^L [D_i] (z_{i+1} - z_i) \\
 [D_{u\theta}] &= \sum_{i+1}^L [D_i] \frac{1}{2} (z_{i+1}^2 - z_i^2) \\
 [D_{\theta\theta}] &= \sum_{i+1}^L [D_i] \frac{1}{3} (z_{i+1}^3 - z_i^3)
 \end{aligned} \tag{3.16}$$

and where the summation is over all of the layers, and  $z_{i+1}$  and  $z_i$  are the distances from the mid-height of slab to top and bottom of layer  $i$ , respectively.

In Appendix A of Ref. 27 the slab element stiffness matrix (Eq. 3.14) and submatrices obtained by performing the integration indicated by Eq. 3.15 are given. It should be noted that prior to presentation of the results in Appendix A of Ref. 27 all of the matrix operations performed in Eq. 3.15 were completed by the computer, whereas now the slab element stiffness matrix can be calculated by direct substitution alone.

### 3.4 The Beam Element

Extensive coverage of the theoretical development of the elastic composite beam finite element is presented in Ref. 64, and a similarly detailed development of the inelastic layered composite

beam model is presented in Ref. 27. The key features of those developments will now be presented. For a more detailed presentation of the material the reader should refer to the above mentioned references.

The typical arrangement of the beam and slab node points is depicted in Fig. 2, where the slab and beam node point deformations and sign conventions are given in Fig. 17. The vertical displacement,  $W$ , for the beam and slab finite element are assumed to be identical. The layered beam finite element has one node point at each end of the element, with each node point having two degrees of freedom: the displacement in the x-axis direction,  $U_B$ ; and the rotation of the beam about the y-axis,  $\theta_B$ . A separate rotation field is required for the beam because the rotation of the beam is not equal to the rotation of the slab node. This is due to the additional change in rotation caused by the shearing strain,  $\gamma_B$ . The above displacements,  $U_B$  and  $\theta_B$ , are described by separate three-term polynomials. The related slab displacements

$$W, \theta_A = \frac{dw}{dx}, \text{ and } U_A \text{ (Fig. 17),}$$

are obtained from the polynomials presented in Section 3.3 with  $y$  held constant (Ref. 27).

Enforcing compatibility between the node point displacements and the displacement fields, leads to the generation of the [C1] matrix, which relates ten displacement terms, (Fig. 17), to

thirteen coefficient terms (Ref. 27):

$$\{\delta\}^e [C1] \{\zeta\} \quad (3.17)$$

It should be noted that Eq. 3.6 cannot be used to solve for the constant coefficients,  $\{\zeta\}$ , because of the three additional coefficients. However, by considering the equilibrium of the axial forces, the interface shear flow,  $s$ , between the beam and slab (Fig. 18), and by then enforcing compatibility between the vertical displacement fields and the rotation fields, (Eq. 3.18), three additional equations relating the constant coefficients are obtained, (Eq. 3.19)

$$0 = \frac{dw}{dx} + \theta_B + \gamma_B \quad (3.18)$$

$$\{0\} = [C2] \{\zeta\} \quad (3.19).$$

Eqs. 3.17 and 3.19 can then be combined to form Eq. 3.20:

$$\begin{Bmatrix} \{\delta\}^e \\ \{0\} \end{Bmatrix} = \begin{bmatrix} C1 \\ - - - \\ C2 \end{bmatrix} \{\zeta\} \quad (3.20)$$

which can in turn be solved according to Eq. 3.6:

$$\{\zeta\} = [C]^{-1} \begin{Bmatrix} \{\delta\}^e \\ \{0\} \end{Bmatrix} \begin{bmatrix} CC & | & CX \\ \hline & & \end{bmatrix} \begin{Bmatrix} \{\delta\}^e \\ \{0\} \end{Bmatrix} \quad (3.21)$$

where

$[CC]$  = coefficient displacement matrix consisting of the first ten columns of  $[C]^{-1}$  (Ref. 27,64).

The [CC] matrix can be further partitioned to handle the displacement fields separately:

$$[CC] = [CA \mid CB \mid CW \mid CD]^T \quad (3.22)$$

where [CA], [CB], [CW], and [CD] are the coefficient-displacement matrices for the  $U_A$ ,  $U_B$ ,  $W$ , and  $\theta_B$  fields respectively. From the above coefficient-displacement matrices the beam finite element stiffness matrices can be derived.

This is done by first performing the required operations on the displacement fields as indicated by  $[\Gamma]$  in Eq. 3.8a and substituting the coefficient-displacement matrices as in 3.8b to give the following strain-displacement matrices:

axial strain in beam;

$$\epsilon_{xB} = \frac{dU_B}{dx} - z \frac{d\theta_B}{dx} \quad (3.23a)$$

leads to

$$\epsilon_{xB} = [B_B]_b \{\delta\}^e \quad (3.23b)$$

shearing strain in the beam;

$$\gamma_B = \frac{dw}{dx} - \theta_B \quad (3.24a)$$

becomes

$$\gamma_B = [B_B]_s \{\delta\}^e \quad (3.24b)$$

slip at interface of beam and slab;

$$\delta U = (U_A - z_{iA} \frac{dw}{dx}) - (U_B - z_{iB} \theta_B) \quad (3.25a)$$

becomes

$$\delta U = [B]_d \{\delta\}^e \quad (3.25b)$$

Then with the above expressions for the strain-displacement matrices, and the appropriate elasticity relations (Chapter 2) the component stiffness matrices, via Eq. 3.3, become:

$$[k_B]_b = \int_V [B_B]_b^T [E_B] [B_B]_b dV \quad (3.26a)$$

$$[k_B]_s = \int_V [B_B]_s^T [G_B] [B_B]_s dV \quad (3.26b)$$

$$[k]_d = \int_L [B]_d^T [k_{sc}] [B]_d dx \quad (3.26c)$$

where

$[k_B]_b$  = beam stiffness due to flexure

$[E_B]$  = beam elasticity matrix (flexure)

$[k_B]_s$  = beam stiffness due to shear

$[G_B]$  = beam elasticity matrix (shear)

$[k]_d$  = beam stiffness due to slip

$[k_{sc}]$  = the stiffness of the uniform connection used

to mathematically describe the shear connectors.

It should be noted that explicit value for  $k_{sc}$  have not as yet been directly related to the number of shear connectors or their arrangement, but that an upper bound approximation for the values of  $k_{sc}$  needed to insure composite action can be given by (Ref. 28 and Section 5.11).

$$(k_{sc})_{\max.} = \frac{10}{d^2 L^2} \left( EA_A (e^2) + EA_B (Z_{BB} - e)^2 \right) \quad (3.27)$$

where

$EA_A$  = axial rigidity of slab

$EA_B$  = axial rigidity of beam

$Z_{3B}$  = distance between midheight of slab and  
centroid of beam

$$e = \frac{EA_B |Z_{BB}|}{EA_A + EA_B}$$

$$d = Z_{BB}$$

$L$  = beam element length.

The beam finite element, like the slab finite element, is subdivided into a series of layers as shown in Fig. 3, with each layer having its own  $[E_j]$  and  $[G_j]$  elasticity terms. In order to form the element stiffness matrices of Eqs. 3.26a, b, c, the following four terms must be defined by summation of all of the individual layer stiffnesses:

$$EA_B = \sum_{j=1}^n E_j A_j \quad (3.28a)$$

$$ES_B = \sum_{j=1}^n E_j A_j z_j \quad (3.28b)$$

$$EI_B = \sum_{j=1}^n E_j (I_j + A_j z_j^2) \quad (3.28c)$$

$$GA_{sB} = \sum_{j=1}^n G_j A_{sB_j} \quad (3.28d)$$

where

$E_j, G_j$  = the tangent modulus and corresponding shearing modulus for beam layer  $j$

$A_j, A_{sB_j}, I_j$  = the area, shear area, and moment of inertia for layer  $j$

$z_j$  = the distance from beam reference plane to the layer  $j$  centroid.

Once the terms of Eq. 3.28 are determined the beam finite element stiffness matrices of Eq. 3.26 can be defined explicitly as shown in detail in Appendix B of Ref. 27. In addition, it should be noted that the layer elasticity terms,  $E_j$  and  $G_j$ , are dependent

upon the stress level, and vice versa. Thus, as was the case with the slab elements an iterative process is required to accurately determine the layer stiffness corresponding to a given load level.

### 3.5 Concrete Failure and Unloading

As was noted in Section 2.3 when a concrete layer has cracked or crushed, the layer is incapable of sustaining the stress that caused the failure. Thus, the layer stress perpendicular to crack must be reduced to zero, while at the same time redistributing the stress to uncracked or uncrushed layers. In order to maintain equilibrium, a statically equivalent fictitious force vector must be applied to the structure to redistribute the stress loss due to the failure. In Ref. 54 the equations needed for computing the required fictitious force vector are presented in detail. The reader need only to be aware of the necessity of, and not the specifics of, this fictitious force vector to understand its contribution to the solution process.

### 3.6 Buckling Failure

As was noted in Sections 2.4 and 2.5 when compression flanges buckle or web plate panels reach their ultimate capacity in shear, the flange and/or web of the beam or girder cannot sustain any additional force. Unlike the concrete failure where unloading is required, the loss of stiffness can be effectively modelled by assigning the flange or web an artificially low stiffness of

1/100000 times its original stiffness (see detailed discussion Sec. 2.4 and 2.5). Since the failed flange and/or web has little stiffness, any additional force is automatically redistributed to neighboring elements. Experimental correlations in Chapter 4 verify the reliability of this approximation for post-buckling behavior.

### 3.7 Solution Scheme

The developed solution scheme solves the overload problem in a logical sequence of operations, while including the material and stability relations presented in the preceding sections of Chapter 2 and 3. In addition, Eq. 3.2 is solved for various load levels while providing node point deformations, element layer stresses, layer-failures, and buckling failures at each load level. This solution process consists of four main phases:

1. Problem Definition
  - a. Bridge Description
  - b. Bridge Loading
2. Dead Load Solutions
3. Scaling Procedure
4. Overload Solution Procedure

These phases have been incorporated into a computer program, BOVAS (Bridge Overload Analysis - Steel) (Ref. 76). A simplified flow chart of the relationship between the above phases is shown in Fig. 19, with detailed descriptions of these phases being presented in the following sections.

### 3.7.1 Problem Definition

To define the problem, essentially two operations are required: (1) the bridge description and (2) the bridge loadings. In order to fully describe the superstructure the following information must be provided: the bridge superstructure geometry and finite element discretization in terms of elements and layers; the type and location of slab concrete and reinforcement, and beam steel; the material property parameters needed to fully define the complete stress-strain relationships for each of the varied materials; the location of any web plate panels; and the boundary or support conditions needed for the analysis, employing lines of symmetry where appropriate. With this information all the initial stiffness properties and node point constraints, i.e. boundary conditions, are determined. However, to fully establish the set of equilibrium equations given by Eq. 3.2, the force vector, i.e. the loads, are still required.

The bridge loadings are composed of three parts; the dead loads acting on the beams, i.e. the dead weight of concrete and steel; the dead loads acting on the composite structure, i.e. weight of curbs, parapets, and future wearing surface; and the live load or overload vehicle weights and their position. Once this information is provided the solution process can begin.

### 3.7.2 Dead Load Solution

Since the analytical technique employed considers material nonlinearities, which are stress dependent, an accurate assessment

of the stress state prior to the application of the overloads is required. It should be noted that due to the expected nonlinear behavior of the structure, the principle of superposition cannot be employed. Therefore, the superstructure must be analyzed to obtain the following stresses prior to the application of the overload: the stresses in the beams due to the dead weight of the slab and beams; and the stresses in the beams and slabs due to the dead weight of parapets, curbs, or future wearing surface. The initial stress state and any material failures or nonlinearities due to the application of these dead loads will thus be reflected prior to the application of the overloads.

### 3.7.3 Scaling Procedure

As long as the initial solution due to the overloads produces elastic response, i.e. no nonlinear response, the load is increased proportionally to the lowest load level corresponding to one of the following element stress limitations: 60% of the compressive strength of concrete, 90% of the tensile strength of concrete, 97.5% of the yield strength of steel, and 100% of the buckling stress, whichever is the smallest. Because this technique scales up the initial load level; only one elastic solution is obtained, i.e. subsequent solutions will have nonlinear response. Thus, the number of elastic solutions are kept to a minimum. If, however, the initial solution causes any material or stability failure, i.e. nonlinear response, the initial live load is scaled down so that a linear solution can be obtained. Then the scaled down load is

incremented until nonlinear response occurs. Once nonlinear response begins, i.e. cracking, yielding, or buckling begins, the overload solution procedure is employed.

#### 3.7.4 Overload Solution Procedure

The structural response to an overload vehicle is obtained by solving the set of equilibrium equations expressed by:

$$\{F\} = [K] \{\delta\} \quad (3.1)$$

Because the response is eventually expected to be nonlinear in nature, a piecewise linear or incremental approach must be employed.

$$\{\dot{F}\} = [K (\sigma + \dot{\sigma})] \{\dot{\delta}\} \quad (3.29)$$

The force vector,  $\{\dot{F}\}$ , is considered to be the increment of the node point forces applied to the structure, and,  $\{\dot{\delta}\}$ , the corresponding incremental node point displacement vector. The total forces and displacements are obtained by addition of the various increments. The stiffness matrix  $[K (\sigma + \dot{\sigma})]$  reflects the instantaneous stiffness of the bridge superstructure, and depends upon the current total stress state,  $\sigma$ , and an unknown stress increment,  $\dot{\sigma}$ . Because the unknown stress increment is dependent upon the stiffness and the stiffness is in turn dependent upon the stress increment, conventional linear elastic solution techniques cannot be employed.

However, using a tangent stiffness approach or piecewise linearization of the nonlinear phenomena, the overload problem can

be solved. In such an approach, the system of equations expressed by 3.29 are assumed to be linear in a given load increment. Then by computing the tangent to the stress-strain curve for each layer, based upon the current stress state, the layer stiffnesses, element stiffness, and ultimately the global stiffness matrix can be calculated. Equation 3.29 is then solved for the incremental node point displacements, from which the incremental element strains are calculated. From these element strains the incremental layer strains are calculated. Then by employing the material stress-strain relationships the corresponding layer stress values are obtained. These incremental stress values are added to the total stress state which existed prior to application of the load increment, thus arriving at a new current stress state. The new current stress state is in turn used to recompute the stiffness matrices, and thus, to resolve Eq. 3.29 for the incremental node point displacements. This process is repeated, i.e. iterations take place, until the solution for the increment converges. Should a layer fail during the application of the load increment, the load increment is scaled down so that the layer stress just barely causes failure. Thus, in this method which is called the "incremental-iterative" method, the stiffness matrices are continually updated within each load increment or step. As an approximation to the "incremental-iterative" method it is possible to update the stiffness matrix only at the start of the load increment, i.e. "incremental" method; however, in such a solution scheme, where

no updating of the stiffness matrix takes place within the load increment, error is introduced in the first increment and continually compounded in subsequent increments. For this reason, the "incremental" method has not been used in the present research. An explicit description of the "incremental" method as used in the analysis of concrete bridges is presented in Ref. 54. The "incremental iterative" technique as used in the overload analysis of steel bridges appears in the flow chart of Fig. 20 with the detail descriptions of the steps appearing below:

1. Formulate the element stiffness matrices based on current total stress levels.
2. Stack the element stiffness matrices to form the global stiffness matrix.
3. Solve for the incremental node point displacement using the global stiffness matrix and incremental force vector. Compute the incremental strains and then stresses.
4. If the incremental displacements have converged to the specified tolerance, 20%, go to Step 7; otherwise continue.
5. If the maximum number of iterations, 3, within a load increment has been reached, go to Step 7; otherwise continue.

6. If the stress state exceeds the upper tolerance specified which would cause yielding, cracking, crushing, strain hardening, or buckling, then scale down the applied force increment such that a state of incipient failure exists and go back to Step 1.
7. Unload the excess concrete layer stresses and compute the corresponding fictitious force vector for unloading, if applicable.
8. If the current total stress level, or total strain has exceeded the lower tolerance specified which would cause yielding ( $\sigma \geq 0.975 \sigma_y$ ), cracking ( $\sigma \geq 0.9 f_t$ ), crushing ( $\sigma \geq 0.9 f'_c$ ), strain hardening ( $\epsilon_t \geq 1.0 \epsilon_{st}$ ), or buckling ( $\sigma \geq 1.0 \sigma_{cr}$ ), then set the codes to indicate which layers, flanges, web panels have failed.
9. Compute the total stress, strain, displacement, and force vectors by adding together the old totals and the new increments.

10. Check the live load stress range of various specified details to see if allowable fatigue stress range values have been exceeded, and if so, note this fact. (Only applicable when details are specified.)

11. Apply new force increment and go to Step 1.

It should be noted that the initial solution of each load cycle is based upon zero stress and displacement increment values, thus, the first iteration of each step is based upon the stiffness matrix of the previous load cycle.

The overload analysis process terminates when one of the specified termination checks is exceeded. The termination checks are defined in terms of allowable values of: deflections, live loads, stresses, strains, number of failed layers, or crack widths. Thus, an efficient solution procedure is developed to meet the requirements of the analyst.

## 4. COMPARISONS OF ANALYTICAL AND EXPERIMENTAL RESULTS

### 4.1 Introduction

This chapter contains comparisons of experimental and analytical results. The investigations involve: simple span and continuous beam-slab highway bridge superstructures; continuous composite beam structures; and transversely stiffened plate girder structures. In addition, a simulated overload analysis of a four-span continuous plate girder-slab bridge superstructure is presented as an example of the implementation of the analytical technique. The above comparisons are made so as to provide a basis for the verification of the reported mathematical model. The experimental studies are obtained from the available literature and were not conducted as part of this investigation.

The analytical studies were made by employing the reported method. First, a total of four concrete slab and steel beam structures, which had been previously subjected to overload testing were analyzed. Two of the test structures were full size bridge superstructures, while the remaining two were scaled structural models. The representative results of the full size bridge superstructure comparisons are presented herein. A detailed description of all four tests and the comparative results can be found in Ref. 27.

It should be noted that because the above investigations occurred during phase 1 of the research (Section 1.3), the stability considerations were not as yet a part of the analysis scheme. Thus, if buckling of a component member had occurred the method would not have predicted any buckling. However, due to the proportions of the slab and beams, buckling did not occur in any of the tests with the exception of the University of Tennessee test. In that test, buckling took place only after the formation of a plastic hinge and at a load level of approximately 97% of the ultimate load. Thus, there is no loss of accuracy in three of the analytical results and negligible loss of accuracy in the other analytical prediction by not having included buckling considerations.

The remaining experimental tests were selected because buckling was a major mode of failure. Thus, the reliability of the analytical method in predicting the occurrence of buckling and any post-buckling behavior could be verified. A comparison of the analytical and experimental results of two composite beam tests and seven plate girder tests was presented in detail in Ref. 28. Since similar results were obtained in all cases only one of the composite beam tests and three of the plate girder tests will be presented herein.

Also, as an example of the implementation of the analytical method, an analysis is performed on a typical continuous plate girder bridge, which is taken from the Federal Highway Administration's standard drawings (Ref. 67). While there are no

experimental results which can be used for comparison with the analytical predictions, the analysis will show the applicability of the method and the expected types of nonlinear behavior and distress that should occur in a typical continuous plate girder bridge. While this particular analysis does not verify the validity of the method, the proven reliability of the technique as demonstrated in the other experimental and analytical comparisons, indicates that the results of this plate girder bridge analysis should also be reliable.

#### 4.2 Beam-Slab Bridge Superstructures

Comparisons have been made between experimental results and analytical results of four beam-slab highway bridge superstructures which were subjected to overloads (Ref. 27). The comparisons, which are listed below along with the reference in which the experimental results were presented, were conducted to verify the validity of the developed analytical model. It should be noted that the analytical model does not consider any response due to diaphragms.

No. 1: A simply supported right bridge with a span length of 15.24 m (50') and a width of 4.57 m (15') having three W18x60 steel beams with partial length coverplates (Bridge 3B, Refs. 33 and 34).

No. 2: A four-span continuous right bridge with span lengths of 21.34 m, 27.43 m, 27.43 m, 21.34 m (70', 90', 90', 70') and a width of 10.52 m (34'-3") and having

four W36x170 steel beams with W36x160 beams with coverplates over interior supports (Bridge 1, Test 1300, Refs. 14 and 21).

No. 3: A two-span continuous right bridge model with two span lengths of 2.74 m (9') and a width of 1.6 m (5'-3") with three S6x12.5 steel beams and partial length coverplates. (Two-span model of Refs. 12, 13, 25 and 32).

No. 4: A three-span continuous right bridge model with three span lengths of 1.83 m (6') and a width of 1.6 m (5'-3") with three S5x10 steel beams and partial length coverplates. (Refs. 12, 13, 25, and 32).

Only examples No. 1 and No. 2 of the above list will be presented herein, and they will be referred to as "Bridge 3B - AASHTO Bridge Test" and "Test 1 - University of Tennessee", respectively.

#### 4.2.1 Example No. 1 - Bridge 3B - AASHTO Bridge Test

This bridge was constructed as part of the AASHTO Road Test conducted in the early 1960's (Refs. 33 and 34). The testing consisted of three phases: (1) a regular test traffic program of 500,000 trips, (2) dynamic load tests, and (3) increasing load tests, i.e. overload tests. Bridge 3B was designed as a simply supported composite slab and steel girder bridge with a span length of 15.24 m (50') center-to-center of bearing. The

deck slab for the bridge had an average measured depth of 164 mm (6.45") and was 4.57 m (15') wide. Three W18x60 steel beams were placed 1.52 m (5') apart with 11.1 mm x 152 mm (7/16" x 6") cover-plates extending over 5.64 m (18'-6") of the middle of the span. Figures 21 and 22 show the elevational and cross-sectional views of Bridge 3B.

The loads were applied to the superstructure by moving overload vehicles. For the testing of Bridge 3B three different overload vehicles were used (vehicles 97, 98 and 99 as shown in Fig. 23). The loading procedure consisted of placing weights on the overload vehicle which would then travel across the bridge, usually thirty times. During the loading process the midspan deflections of each beam were monitored and recorded. The load was then increased and another set of runs made. The procedure was continued until the bridge superstructure collapsed onto the safety crib below the bridge superstructure.

Because the loads were not applied in a static manner but by moving vehicles, the moment envelope produced by the passage of the overload vehicle is of interest. Since the finite element program requires a static loading pattern which will then be incremented, an equivalent static loading pattern which would correspond to a realistic simulation is required. In addition, because three different overload vehicles were used, three different moment envelopes must be simulated by one constant loading

pattern. Based upon previous experience and numerical computations, the moment envelope could be best simulated by a line load over the beams (Ref. 55).

Figure 24 shows the superstructure discretized into a series of finite elements. The node points, element numbering, and element dimensions are indicated in the figure. Since the structure was assumed to be symmetric in geometry and loading, only one-quarter of the structure need be analyzed. A total of eighteen slab elements and twelve beam elements were used. It should be noted that because a line of symmetry lies along the axis of the interior beam, only one-half of the interior beam cross-section is included in the model. The line load was simulated by a series of concentrated loads indicated by the cross-hatched squares.

The layered slab and beam models are shown in Fig. 25. A total of six layers of concrete and four layers of steel reinforcement were used in the slab finite element. The direction of action of the reinforcement is indicated by the cross-hatched area and is given along with the thickness, and bar size/spacing in Table 1A. The beam finite element consists of a total of eleven layers as indicated. The cross-hatched layer, which represents the coverplate, has two sets of material properties. In the region where no coverplate exists in the actual structure, the material stiffness properties are set to artificially low values to simulate the absence of the coverplate. In the area where there is a

coverplate the properties of steel were used. In Table 2 are presented the material properties of the steel and concrete used in Bridge 3B, and the corresponding material properties used in the finite element simulation.

At the end of the regular test traffic program one of the three beams of Bridge 3B was discovered to have a fatigue crack at the end of the coverplate. Even so, it was determined that the small permanent set in the bridge at that stage was due to cracking of the concrete slab and yielding of the steel; thus, the fatigue crack had no effect on the stiffness of the bridge. Prior to the overload test the fatigue crack was repaired with a butt weld in order to prevent premature failure.

The bridge failed in a flexure mode and in Ref. 34 the overload behavior of the bridge is presented in terms of a plot of the maximum static moment at midspan caused by the overload vehicle versus the average displacement at midspan of the three beams. Figure 26 shows the midspan moment displacement history of the bridge. The analytical results of program BOVAS and the test results are presented by the (□) and (○) symbols as noted. As can be observed from the plots, the results produced by the two methods agree relatively well, especially at the beginning, and from a deflection of 102 mm (4") (1/150 deflection to span ratio) to about 254 mm (10") (1/60 deflection to span ratio). The main discrepancies between test results and the calculated response occur within two regions: first, from approximately 33 mm to 102 mm

(1.3" to 4.0") deflection, and secondly, from about 254 mm (10") in deflection to the termination of the test.

Some difference between test results and computed results is to be expected because the loads were applied to the test structure by three different overload vehicles in motion and the finite element program applied an approximate equivalent static loading pattern in an incremental fashion. In addition, as with any finite element model, there exists the effect of the size of the discretization used. However, in the second region of disagreement the difference in maximum loads is only around seven percent and thus within acceptable modeling limits. A considerable improvement can be made in the modeling scheme if the effects of residual stresses in the steel beams are included. Residual stress measurements in the beams were made and reported on in Ref. 33. Assuming a parabolic distribution of residual stresses in both the flanges and the web, an average value of residual stress in each of these parts of the cross-section is calculated. Using these values of residual stress as initial stress values in the beams and repeating the finite element analysis, much better agreement with test results is obtained, as indicated on Fig. 26.

A qualitative description of the extent of damage at different load levels, as reported in Ref. 34 is compared to damage as predicted by program BOVAS in Table 3. In general the damage record shows that the method of failure and the loads at which

different types of structural damage occurred can be predicted by program BOVAS.

#### 4.2.2 Example No. 2 - Bridge 1 - University of Tennessee

This bridge was one of four bridges which were to be inundated as part of a reservoir in Tennessee (Ref. 14). Bridge 1, referred to as such by the experimental researchers, was a four-span continuous composite structure with span lengths of 21.34 m, 27.43 m, 27.43 m and 21.34 m (70', 90', 90' and 70'). It was constructed in 1963 and designed for HS-20 loading. The deck slab was 178 mm (7") deep and was 10.52 m (34'-6") wide, including the curb (Fig. 27). For the finite element analysis the curb portion of the superstructure was considered to be in the same plane and of the same thickness as the slab. A total of four W36x170 steel beams were used to support the deck with 2.54 m (8'-4") spacing center-to-center between the beam. In the negative moment regions there were W36x160 steel beams with 267 mm x 25.4 mm (10-1/2" by 1") coverplates. A plan view of the superstructure and the location of the applied loads and points where readings were taken are shown in Fig. 28.

The loads were applied to the bridge deck by 890 kN (200 k) center hole jacks resting on bearing grills. The bearing grills were constructed from two W14x30 steel beams 1.17 m (46") long and 0.76 m (30") center-to-center, and resting on concrete pads poured directly on the bridge deck. The location of the grills is shown in Fig. 28 by cross-hatched areas.

Due to the symmetry of the loads only one-half the structure needs to be discretized. The node points, element numbering, and element dimensions of the discretized structure are indicated in Fig. 29. The cross-hatched areas represent the location of the patch loads that must be applied to the idealized structure. A total of 42 slab finite elements and 28 beam elements were used, resulting in 90 nodes and 360 degrees of freedom. The area of main structural interest was the portion of the bridge near the midspan of the loaded span; therefore, the element discretization is finer in this region and much coarser in other spans. While the coarse discretization of the unloaded spans will be sufficient to model accurately the stiffness of the bridge, deflections and stresses in these regions will not be reliable because of the element size.

The layered slab and beam finite elements are shown in Fig. 30. A total of six layers of concrete and four layers of steel reinforcement were used. The direction of action of the slab reinforcement is perpendicular to the cross-hatched area and is specified, along with the thickness and bar size/spacing, in Table 1B. The exact reinforcement and pattern in the slab were not specified in Ref. 14, so a reinforcement distribution based upon the existing design practices was chosen. The beam finite element consists of eleven layers as indicated. Because the length of the coverplated sections were not specified, the same beam element, i.e. W36x170, was used throughout.

In Table 4 the actual material properties of the steel and concrete used in Bridge 1 and the material properties and parameters assumed for the finite element analysis are listed.

Bridge 1 was described as being "structurally sound" prior to the beginning of the experimental tests (Refs. 14 and 21). The bridge had been in service for approximately five years and, prior to the testing, the average daily traffic was 600 vehicles per day. Before the ultimate load test was conducted, other load tests involving lateral load distribution studies and dynamic response studies to rolling and vibratory loading were carried out, Refs. 14 and 21 contain all the information concerning the results of these other tests.

A plot of the load and corresponding average deflection at the midspan of the loaded span is presented in Fig. 31 for both the analytical ( $\square$ ) and experimental ( $\odot$ ) results. In general, the two curves are in close agreement except in the range of about 127 mm (5") (1/216 deflection to span ratio) to 330 mm (13") (1/83 deflection to span ratio) deflection. However, even in this range the maximum difference in load is only five percent.

Qualitative bridge damage, as reported in Refs. 14 and 21, is compared to damage as predicted by program BOVAS in Table 5. As can be seen, considerable difference can be observed between the first cracking loads for the experiment and the analytical predictions. This noticeable difference is not all that disturbing if one evaluates all the facts. First, the real structure had

coverplated sections over the piers, making the composite section in that area more resistant to cracking. Second, and most important, the finite element discretization in the region near the support piers is extremely coarse. This leads to poor element stress distribution and, therefore, damage predictions. As mentioned before, however, the coarse discretization still produces reliable stiffness properties (i.e. overall load versus deflection results). Lastly, the visual observation of cracking in the slab does not give any quantitative information on the extent of cracking through the slab. The reported cracking thus may be either "surface deep" or halfway through the depth of the slab. Looking at other recorded damage the observation of first yield in the beams differs by only ten percent, and considering the qualitative nature of the observation, this is within acceptable limits.

As reported in Refs. 14 and 21, at a load just above first yielding the bridge "lifted off" the abutment nearest the load. The present version of the finite element model is not capable of simulating this behavior, but as indicated in Fig. 31 the experimental and analytical results are not very different. This is, in part, due to the fact that when the "lift off" occurred, the moment capacity of the composite section over the first pier had reached much is its capacity. Considering coarseness of the discretization, the leaving out of the coverplated sections, and the lifting off of the bridge from the abutment, the BOVAS results are remarkably good.

#### 4.3 Continuous Composite Beams

Comparisons were made between the analytical results and experimental results of two continuous composite beams which were subjected to overloads (Ref. 28). The comparisons, which were conducted to verify the reliability of the developed analytical technique in predicting the occurrence of torsional buckling of beam compression flanges, are listed below. The experimental results were originally presented in Ref. 29.

No. 1 - A two-span continuous composite beam with equal span lengths of 3.66 m (12') and composed of a 102 mm (4") deep by 1219 mm (48") wide reinforced concrete slab connected compositely to a W12x27 wide flange beam (Test CB2 - Ref. 29)

No. 2 - A two-span continuous composite beam with equal span lengths of 3.66 m (12') and composed of a 102 mm x 1219 mm (4" x 48") reinforced concrete slab connected compositely to a W10x21 wide flange beam (Test CB3, Ref. 29).

To avoid repetition, as mentioned earlier, only one of these comparisons, No. 1 - Test CB2, will be presented herein.

#### 4.3.1 Example No. 3 - Test CB2

The following experimental results were obtained from one of three tests conducted on composite beams which were reported in a paper by Hamada and Longworth at the University of Alberta (Ref. 29). All of the composite beams in the tests were loaded incrementally until failure. Test beam CB2, was composed of a 102 mm (4") deep by 1219 mm (48") wide reinforced concrete slab connected compositely to a W12x27 steel beam. As shown in Fig. 32a, the composite beam had two equal spans of 3658 mm (144") and two equal loads were placed at the midspan of each span. The material properties for the concrete, reinforcing steel and beam steel are given in Table 6.

Only one-quarter of the structure is discretized due to lines of symmetry in both the longitudinal and transverse direction. The resulting finite element mesh (Fig. 33) is composed of 14 slab elements, 14 beam elements, and 45 node points. The slab and beam layers are defined in Figs. 33a, b, with the respective slab reinforcement and orientation presented in Table 7. In the actual experiment, no reinforcement was provided in the longitudinal direction in the positive moment regions. In the finite element analysis the longitudinal slab reinforcement in this region was modelled by assigning an artificial stiffness of  $1/1000^{\text{th}}$  of the normal values to the modulus of elasticity for the reinforcement. In addition, residual stresses for the steel beam were approximated according to the method developed in Ref. 27.

The analytical and experimental load versus deflection curves for Test CB2 (Fig. 35) do not exhibit perfect correlation; however, considerable similarity in the shapes of the curves does exist. In particular the slope of the inelastic plateau appears to be the same in both the experimental and analytical cases, indicating reasonable agreement exists in the post-elastic region. It should be noted that, in general, much better agreement is obtained when comparing test results on full-size bridge structures and analytical results, than when comparing test results on model-size structures, as in this case, and analytical results (Ref. 27). Thus, some of the differences between the load versus deflection curves may, possibly, be attributed to the size of the structure, and thus the accuracy of the scale model structure in reflecting real life structural response. However, even with the apparent differences the maximum error is only 10%, which is within acceptable limits.

Much better agreement is obtained when comparing the analytical and experimental load versus damage records as reported in Table 8. As can be seen, the actual flange buckling load of 578.3 kN (130 kips) and the finite element prediction of 589.8 kN (132.6 kips) indicates an error of only two percent. In addition, the analytical load for cracking of the slab is only off by 12%. Considering the difficulty during the test to accurately assess the degree of cracking occurring in the slab, such an error is well within reason.

A review of the analytical and experimental results of Test CB3 in Ref. 28, shows the same general trends as shown in the comparison just presented for Test CB2. Based upon these comparisons of load versus deflection diagrams and load versus damage reports, it is justifiable to conclude that the developed method can adequately predict the effects of the torsional flange buckling phenomena. This conclusion becomes more evident if one would consider the results, if flange buckling was excluded from the analysis scheme, i.e. flange buckling ignored.

#### 4.4 Transversely Stiffened Unsymmetrical Plate Girders

A total of eight ultimate load tests were conducted at Lehigh University by Dimitri and Ostapenko (Ref. 20) on three different 914 mm (36") deep transversely stiffened unsymmetrical plate girders, UG1, UG2 and UG3. The top and bottom flanges in each case were 203 mm x 16 mm (8" x 5/8") with a 277 mm x 19 mm (10-1/2" x 3/4") coverplate welded to the bottom flange of all the girders. The web was 914 mm x 3 mm (36" x 1/8") in the center portion of each girder and 914 mm x 5 mm (36" x 3/16") elsewhere. The loading patterns employed were chosen to evaluate the ultimate strength of the girders in pure bending, pure shear, and combined shear and bending (Fig. 36). Since similar results are obtained in each of the different load categories, i.e. shear, bending, or combined, only the results pertaining to girder UG2 (Fig. 37) will be presented, as they are representative of all the tests. A detailed

comparison of all of the tests and analytical results can be found in Ref. 28.

#### 4.4.1 Example 4a, b, c - Tests UG2.1, UG2.2 and UG2.3

Plate girder UG2 and the finite element discretization are shown in Fig. 37. It should be noted that the finite element computer program, BOVAS, requires the existence of a slab, and since the actual plate girder has no slab, the absence of the slab is modelled by a fictitious slab of 610 mm x 25 mm (24" x 1") with stiffness properties equal to 1/10000th of the normal values or about 3.45 MPa (0.5 ksi). With such stiffness values the slab elements have no noticeable influence on any results. The discretization, therefore, contains 14 fictitious slab elements, 14 beam elements, and 45 node points. Due to symmetry in the transverse direction only one-half of the plate girder is discretized with a total of 11 beam layers (Fig. 38). The load placement for girder tests UG2.1, UG2.2 and UG2.3 and the modes of failure expected are given in Figs. 36c, d, e, with the material properties given in Table 9.

The comparison of analytical and experimental load versus deformation curves for test UG2.1 (shear) is presented in Fig. 39. In the analytical model the critical web plate shear panels were assumed to be the two web plate panels to either side of the interior load and one web plate panel to the right of right hand support. As can be seen from the plot, there exists close agreement between the analytical and experimental results. In addition, as

reported in Table 10 the maximum load obtained for the test was 80.1 kN (17.8 kips) while the computer prediction was 81.0 kN (18.0 kips) or only 1% error. Similarly, the actual web buckling load of 11.7 kN (2.6 kips) compares favorably with the BOVAS prediction of 13.5 kN (3.0 kips). While the difference in these two buckling values would appear to be large, a comparison of buckling loads is somewhat questionable due to the qualitative nature of the determination of the actual web buckling load. In addition, it should be noted that while each of the different plate girder tension field models developed, for predicting the plate girder ultimate strength, predicts different loads for the initiation of web buckling, all of the ultimate load predictions, i.e. maximum load predictions, are approximately equal. Thus, while there is great significance attributed to the fact that the plate girder web panel buckles, the actual buckling load is of less significance. This fact is clearly evident in Fig. 39, where the effects of web panel buckling are ignored for the analytical curve labeled, BOVAS no shear panels (i.e. no web plate panels specified in BOVAS). In this case, the first indication of nonlinear behavior does not occur until well outside the graph at a load of 448.7 kN (100.9 kips) and a deflection of 12.8 mm (0.5"). Thus, considerable error can occur by not including the effects of web plate panel buckling.

In Fig. 40 the comparison of analytical and experimental load versus deformation curves for test UG2.2 (combined) is presented. In this case, the buckled panel of test UG2.1 was repaired with a diagonal brace; however, the effect of the repair on the future load versus deflection behavior of the girder is not known. Ideally, the repair would be just sufficient to make the panel behave as if it has never buckled; however, the repaired panel probably would respond somewhat stiffer than the ideal. To model these two possibilities, two analytical studies were conducted: in one case, only the two web plate shear panels to either side of the interior load were considered critical, i.e. the panel stiffer than ideal; and in the second case, the repaired panel was also considered critical, i.e. the panel treated as if nothing had previously occurred. As can be seen in Fig. 40, the two models mentioned above quite effectively bracket the actual test results as would be expected. From Table 10 the maximum loads for the test of 90.9 kN (20.2 kips) and for the ideal case, 3 panels, of 91.4 kN (20.3 kips) indicate an error of only 0.6%. In this case, no test value is given for the web buckling load. Again, when the effects of web plate panel buckling are ignored, i.e. the case of no shear panels, considerable error in estimating the ultimate strength of the plate girder can occur. While in this case the magnitude of the error is less than in the pure shear condition, UG2.1, the magnitude is still quite large.

In test UG2.3 (bending) failure occurred due to lateral buckling of the compression flange. As can be seen in Fig. 41 some discrepancies exist between the experimental and analytical load deflection results. Some of this difference may be attributed to the repairs on the buckled panels. In spite of these differences, however, the comparisons are still reasonably good. It should be noted that two post-buckling curves are given for the analytical results. Referring to Section 2.5.3 one finds that after reaching the critical flange buckling stress, the post-buckling loss of stiffness was modeled in two different ways: first, assuming that only the flange loses stiffness (labeled - BOVAS - in Fig. 41); and second, assuming that both the flange and the web plate panel lose stiffness (labeled - BOVAS - complete failure - in Fig. 41). Considerable improvement in the post-buckling behavior can be noted in Fig. 41 by employing the complete failure assumption; therefore, in all future cases this mode of failure, due to lateral buckling, will be used. The maximum load obtained from Table 10 for the test of 286.7 kN (63.7 kips) compares reasonably well with the predicted value of 315.0 kN (70.8 kips) i.e. 10% error. While the maximum loads are not as close as in the previous examples, they are within acceptable limits, especially considering the behavior when lateral buckling is ignored, i.e. no shear panels.

The comparisons of analytical and experimental results on plate girders indicate: that the analytical model reliably predicts the occurrence of web buckling, lateral flange buckling, and ultimate

load capacity of the girder; that while the analytical model seems to produce a slightly stiffer than normal behavior in the case of bending or combined bending and shear, the overall behavior still reflects the actual girder behavior; and that failure to include these effects can lead to considerable error. Thus, the conclusion can be drawn that BOVAS can reliably predict the response of transversely stiffened plate girders to loads, both in the elastic and inelastic regions.

#### 4.5 Analysis of a Four-Span Continuous Highway Bridge

In Chapter 2, the occurrence of and the effects of flange and web buckling on individual beams and girders was presented. The experimental comparisons of Sections 4.3 and 4.4, however, involved individual beams and girders and not actual steel multi-girder highway bridge superstructures. Thus, in order to fully investigate the applicability of the analytical method to an actual plate girder bridge superstructure, an analysis was conducted on a typical four-span continuous highway bridge. While there are no experimental results which can be used for comparison, the analysis will indicate the expected types of nonlinear behavior and distress when such a bridge is subjected to overload.

#### 4.5.1 FHWA Four-Span Continuous Bridge Superstructure

The bridge to be analyzed comes from the Federal Highway Administration's plans on Typical Continuous Bridges by Load Factor Design (Ref. 67). This bridge superstructure has spans of 30.5 m, (42.7 m, 42.7 m, and 30.5 m (100 ft; 140 ft; 140 ft; and 100 ft) with a 13.4 m (44 ft) roadway width (Figs. 42, 43). The concrete deck averages 229 mm (9") thick and the welded plate girders have web plates 1676 mm x 10 mm (66" x 3/8"). The variation in the girder flange plates is shown in Fig. 44. The girders are braced laterally at the supports by channel sections and at approximately every 7.62 m (25 ft) with steel cross-bracing. The material properties of the concrete, reinforcing steel, and girder steel used in the analysis are outlined in Table 11. The girder web is composed of A36 steel while the girder flanges are composed of either A36 or A441 steel as noted in Fig. 44.

The layered finite element models (Figs. 45, 46) consist of six concrete and four reinforcing layers for the slab, and a total of fifteen steel layers for the girder. It should be noted that, while the transverse slab reinforcement remains constant throughout the slab, the longitudinal reinforcement is increased in the negative moment regions (Table 13). Also, due to the variation in flange thickness along the length of the beam (Fig. 44), certain cross-sections will have layers where theoretically no steel can exist. This fact is modelled by specifying a fictitious material

with effectively no stiffness (Tables 11, 12) in the appropriate areas.

Based upon previous results (Ref. 27), which indicate that the maximum moment envelope of a bridge superstructure can be obtained by a uniform distributed load pattern, a uniformly distributed load pattern will also be applied in this case. While such a loading condition will not necessarily give the worst possible loading condition, the results should effectively exhibit buckling, post-buckling, and any other nonlinear behavior, if any, of conventional bridges.

The uniformly distributed load will be applied over the entire slab surface between girders 1 and 3 (Fig. 43) for the entire length of the superstructure. Due to the symmetry about the center support, Pier 3, only one-half the structure in the longitudinal direction will be discretized. A plan view of the finite element discretization and loading pattern (cross-hatched area) is presented in Fig. 47a, b, where there are a total of 252 nodes, 120 slab elements, and 100 beam elements. A total of six transversely stiffened web plate panels per girder are specified in the analysis. The first four are over the first interior support, Pier 2, with the two to the left of the support having aspect ratios,  $\alpha_p$ , of 0.758, and those to the right with aspect ratios of 0.707. The last two web plate panels are at the center support and have aspect ratios of 0.707. Based upon the lateral bracing, the unbraced lengths of

the web plate panel compression flanges are assumed to be equal to: 7.62 m (300"), 7.11 m (280"), and 7.11 m (280"), respectively. It should also be noted that in this analysis, the fatigue live load stress range feature of program BOVAS is employed. This program feature calculates the live load stress range of specified girder details and compares these values to allowable fatigue stress range values. If the actual stress range at some load level exceeds the allowable value, a warning noting that fact is printed. The complete details of the fatigue stress range check, for this analysis is presented in Section 5.1.2.

The load versus deflection diagram, Fig. 48, indicates the relationship between the maximum static moment at Pier 2 and the maximum deflection of girder 2 at midspan of the second span. On the diagram some key points of failure are noted with capital letters. These capital letters correspond to the maximum moment load levels as reported in the moment versus damage record of Table 12. Perhaps the most significant feature is point A which corresponds to approximately the maximum static moment caused by two HS-20 lane loadings and corresponding point loads, as specified by AASHTO specifications. This moment value was obtained by completing an additional BOVAS analysis of only a few load cycles where the additional concentrated loads were placed at midspan. The preliminary results of that abbreviated analysis indicate that the web plate panel over pier 2 will buckle before reaching load level A; however, the first significant failure for the present

analysis, i.e. no concentrated loads, does not occur until load level B is reached where the first web plate panel over pier 2 buckles.

It should be noted from the load versus deflection plot that the overall structural response is still linear up to load level C, 6055 kN-m (4466 kip-ft), and that the first large deviation from linear behavior does not start until load level E, 2478 kN-m (6352 kip-ft) has been reached. This is particularly important because many of the web plate panels have buckled by the time this load level is reached, but due to the highly redundant nature of the slab-girder structure there is minimum effect on the overall behavior when local failure occurs. Similarly, after lateral buckling of the compression flange at 12928 kN-m (9535 kip-ft), point H, the overall effects of the buckling are still minimal.

And finally, the load level which just causes yielding of the girder steel to begin, does not occur until reaching 19287 kN-m (14225 kip-ft), point J. This corresponds to about 3.4 times the load level at which the first web buckling occurs. Thus, this overload analysis of a continuous multi-girder highway bridge superstructure using program BOVAS, clearly shows its usefulness in being able to predict the occurrence of buckling and post-buckling behavior. The analysis also shows that failure to include the effects of buckling would cause considerable error in the actual results, and that an assessment of the superstructure's resistance to overload is possible through the use of program BOVAS.

To summarize the results of the analysis on the four-span continuous bridge, the following observations can be made:

1. The load versus deflection response is linear up to a load level of 6055 kN-m (4466 kip-ft).
2. Cracking of the slab over the interior support is the first nonlinear form of behavior at 5543 kN-m (4088 kip-ft).
3. Web plate panels over interior support do not buckle until load level 6055 kN-m (4466 kip-ft) is reached.
4. By assuming a total of 12 HS-40 trucks lined up bumper to bumper in each lane, the total load on the bridge would be 7687 kN (1728 kips). Since the total load on the bridge at the first web buckling loads is 7117 kN (1600 kips), it is possible for web buckling to occur in an actual bridge superstructure.
5. Even after considerable web buckling has occurred, the redundancy of the superstructure prevents large changes in the deflection characteristics of the superstructure.
6. A realistic picture of the load versus damage record of the superstructure is available for determining possible serviceability limits of the superstructure.

## 5. FURTHER CONSIDERATIONS

### 5.1 Introduction

In Section 1.5 the major structural response characteristics of steel highway bridges were outlined. In Chapter 2 and 3 the manner in which these response characteristics were included into the analytical model was presented. In addition, the effects of these characteristics on the overall structural response was also studied in Chapter 4 on experimental comparisons. However, two important features of the analytical model, the shear connector stiffness and fatigue, need to be discussed in more detail to fully understand their importance to the overall structural response of beam-slab highway bridges with steel beams. In addition, a study of the effects of torsion of the beams is necessary to fully justify its exclusion from the analytical model at this time. Thus, in this chapter a discussion of these three topics will be presented.

#### 5.1.1 Shear Connector Stiffness

The term  $k_{sc}$  in Eq. 3.26c is the shear connector stiffness per element length (Refs. 27,28,64). By changing the values of  $k_{sc}$  appropriately, the finite element model can successfully simulate varying degrees of composite action between the slab and beam. However, at this time no definitive study has been done to

explicitly define values for  $k_{sc}$ . Thus, the upperbound values used for  $k_{sc}$  in the reported model are those which just produce full composite action (Refs. 27, 28, 64):

$$(k_{sc_{max}}) = \frac{10}{d^2 L^2} (EA_A (e^2) + EB_B (Z_{BB} - e)^2) \quad (5.1)$$

where

$EA_A$  = axial rigidity of the slab

$EA_B$  = axial rigidity of the beam or girder

$Z_{BB}$  = distance from mid-height of slab to centroid of beam or girder

$e = \frac{EA_B \times Z_{BB}}{EA_A + EA_B}$  = centroid of composite section  
with respect to mid-height of slab

$d = Z_{BB}$

$L =$  length of beam element

As was pointed out in Ref. 28, Eq. 5.1 was developed for a different combination of elements than is employed in the present finite element model; thus, the maximum shear connector stiffness equation (Eq. 5.1) should be reformulated. By adding together the appropriate terms of the following matrices,  $[k_{uu}]^e$ ,  $[k_{u\theta}]^e$ ,  $[k_{\theta\theta}]^e$ ,  $[k_B]_b$ ,  $[k_B]_s$ , and  $[k]_d$  from the Appendices of Ref. 27, and then solving for  $k_{sc}$ , the following equation results.

$$\begin{aligned}
(k_{sc})'_{\max} &= \left\{ \frac{12}{L^3} \left[ EI_{oB} + EA_A (e^2) + EI_B (d^2 - e^2) \right] \right. \\
&\quad - 0.75 J_1^2 L (EI_B - EA_B \bar{z}_B^2) \\
&\quad \left. - \left( \frac{1.2}{L} - 0.6 J_1 L + 0.075 J_1^2 L^3 \right) G_{AB} \right\} \\
&\quad \times \frac{1}{\left( \frac{1.2 C_{BA}^2}{L} + 0.6 J_1^2 L^3 C_{BA} C_{TB} + 0.075 J_1^2 L^3 C_{TB}^2 \right)}
\end{aligned}
\tag{5.2}$$

Equation 5.2 is given only to show the degree of complexity for calculating  $(k_{sc})'_{\max}$ . A complete definition of all the terms contained in Eq. 5.2 is, therefore, not necessary. However, a complete description of all of these terms can be found in Ref. 27.

Employing both Eq. 5.1 and Eq. 5.2 to calculate values for  $k_{sc}$ , and then performing an actual analysis indicates that the overall structural response is approximately 3% stiffer when Eq. 5.2 is used. In addition to this fact, it should be noted that:

1. In previous work reliable results have been obtained using Eq. 5.1.

2. In general, finite element models produce a stiffer structure than the actual structure, thus, a reduction in stiffness (i.e. using Eq. 5.1 instead of Eq. 5.2) would be beneficial.
3. Using Eq. 5.1 is far less complicated than using Eq. 5.2.

Based upon the above discussions, Eq. 5.1 is employed in calculating upperbound values for  $k_{sc}$  in the present model; however, should actual shear connector stiffness values become available from future research, then these actual values should be employed instead of Eq. 5.1.

#### 5.1.2 Fatigue

In normal bridge design, the designer accounts for fatigue by checking the live load stress range of particular bridge details and comparing these stress range values to allowable stress range values. The allowable stress range is dependent upon basically three variables:

1. The type of detail
2. The expected number of cycles
3. Type of member (i.e. redundant or non-redundant).

The actual stress range depends basically on the actual live load. In the reported analysis scheme and thus BOVAS, the live load stress ranges of user specified details are automatically calculated and compared to user specified allowable stress ranges at each load level. If the allowable stress range for any detail is exceeded, a warning is printed.

For example, the fatigue stress range checking capabilities of program BOVAS were implemented in analysis of the FHWA four-span continuous bridge analyzed in Section 4.5. The live load stress range of a total of 70 layers were to be checked against the allowable stress range values. The 70 layers correspond to essentially two types of critical details: (1) the groove weld connecting flanges of differing size when reinforcement is not removed (Stress Category C), and (2) transverse stiffener to web or flange welds (Stress Category C\*). Assuming a redundant load path structure and over 2,000,000 cycles as the criteria, the allowable stress ranges become 68.95 MPa (10 ksi) and 82.74 MPa (12 ksi) for Categories C and C\*, respectively.

It was not until a load level where a moment of 12445 kN-M (9179 kip-ft) was reached, that the live load stress range of any detail exceeded the allowable value. In this case, the longitudinal stress in the transverse stiffener detail over pier 2, finally exceeded the extreme life value of 82.74 MPa (12 ksi). Since this load level is extremely high, it is highly unlikely that the structure will ever undergo 2,000,000 cycles at this load level.

In fact, it is doubtful that the structure would experience even a couple hundred cycles at this load level.

However, for more severe details such as Category E, where the extreme life stress range value is 34.47 MPa (5 ksi), the critical load level might be low enough that damage would be more likely. Thus, while the present global analysis performed by BOVAS does not indicate any fatigue problems, this does not mean that fatigue is not a problem with this structure.

Bridge details, where stress concentrations are present due to the severity of the detail, tend to be very susceptible to fatigue failure. Thus, if a very fine finite element discretization is made in the vicinity of an expected area of stress concentration, i.e. the details, then an accurate representation of the local stress distribution can be obtained. Based upon such a local stress distribution a more accurate assessment of the possibility of fatigue failure can be made. The developed analytical method for performing the overload structural analysis of steel bridge superstructures, BOVAS, does not and cannot be extended to predict local high stress gradients, i.e. stress concentrations. However, a reliable fatigue analysis requires an accurate assessment of the true local stress gradient of the area in question. The incorporation of these two methods of analysis into a single analysis scheme is possible, but is considered to be a highly impractical proposition.

Since fatigue is known to be one of the critical issues in steel bridge superstructures, incorporation of a fatigue check, regardless of how approximate, was deemed necessary. In the developed formulation, therefore, stress range checks were performed for predefined details. However, the methodology has been kept sufficiently general to permit the inclusion of other fatigue checks. Further refinements of the present approach can be obtained by using more refined meshes as compared to those reported in this study, and also by the inclusion of other related checks as they are developed.

#### 5.1.3 Torsion of the Beams or Girders

In the finite element model presented in this dissertation the steel beams and/or girders, as well as the entire bridge superstructure, are assumed to fail in essentially a flexural mode. The beam element node points are permitted only major axis bending degrees of freedom: longitudinal displacements,  $U$ ; vertical displacements,  $W$ ; and bending rotations,  $\theta$ . In its present form then the model precludes any consideration of twisting or torsion about the longitudinal axis. Thus, in all the preceding analyses, the effects of torsion in the beam have been completely ignored. To include the effects of torsion would:

1. Require a considerable number of parametric studies to investigate fully the effects of torsion of the beams in the elastic and inelastic regions.

2. Require development of linear and nonlinear finite elements to model this behavior.
3. Require considerable more computer solution time, due to the added degree of freedom.
4. Require extensive alterations in the coding of the developed computer program, BOVAS.
5. In the end, may not improve the results of the analysis, because previous studies with concrete beams have shown negligible effect on the overall bridge response when torsion is considered

(Ref. 44)

However, since steel beams are thin-walled open cross-sections they are more susceptible to the effects of twisting than are concrete beams. Thus, some form of investigation is needed to assess the effects of torsion in a conventional steel bridge superstructure to determine if the assumption of negligible effect is justifiable.

For this purpose, the four-span continuous composite welded steel girder bridge superstructure presented in Section 4.5 is reanalyzed with eccentric loads. The elevational and typical cross-sectional views of this structure are presented in Figs. 42 and 43. It should be noted that the girders are laterally braced at the supports by channel sections and at approximately every 7.62 m (25') with steel truss diaphragms.

In order to determine whether or not the inclusion of a torsional degree of freedom for the beams has a significant effect on overall structural response of this bridge superstructure, a finite element analysis using SAP IV (Ref. 10) was performed where the degree of lateral restraint is varied to study the effects of twisting of the beams. The finite element discretization employed in these analyses is shown in Fig. 49. It should be noted that due to symmetry in the longitudinal direction only one-half of the entire structure is discretized. The finite element model contains 567 nodes, 260 plate elements for the slab, 130 plate elements for the girder webs, 260 beam elements for the girder flanges, 135 beam-slab connector elements, and three different sets of beam and truss elements for the lateral bracing. To simulate the actual support conditions, the vertical displacement of the bottom flange is prevented at the support locations. However, due to the symmetry employed the longitudinal displacements of the slab, top flange, and bottom flange at Pier 3 are also restrained. To prevent instability, the bottom flange of the centermost girder is restricted from moving in the transverse direction at each support. With this minimal amount of restriction an accurate assessment of the effects of the twisting degree of freedom can be made.

The degree of lateral restraint is varied by changing the frequency of lateral bracing along the length of the bridge. If no lateral bracing is present only the slab and the supports are providing lateral and torsional restraint and thus, the effects of

twisting would be the most noticeable. However, since in a real life structure, lateral bracing is always provided at the supports, the finite element model for the least amount of lateral restraint has cross-bracing only at the supports. In the actual structure the design calls for additional cross-bracing between the girders at approximately every 7.62 m (25'). In the model this condition is considered as the basis because it most accurately reflects the actual structure. If the structure was braced all along the length, twisting of the beams would not occur at all. It should be noted that this corresponds to the analytical model presented in this report. This condition can be simulated effectively by providing bracing at approximately every 3.05 m (10') in the structure. By applying the same eccentric load to the above different models, the effects of the varying degrees of lateral restraint on the stresses and deflections of the superstructure can be investigated.

For this investigation two different loading patterns were applied to the three differently braced structures discussed above to give a total of six separate analyses. It should be noted that the loads applied must realistically simulate actual traffic loads, i.e. only vertical downward loads are applied to the structure. In the first loading condition a uniform live load is placed midway between girder 1 and girder 2, exterior and interior girders (Fig. 43), to cause the worst possible torsional type loading condition due to gravity loads. In the second loading condition the same live load is split in half with each half applied directly

over girders 1 and 2. This last loading condition also approximates the condition of no consideration of twist because the load is applied directly over the girders.

In the first three load cases A, B, and C a uniform line load is placed between the girders. Then the degree of lateral restraint for each case is: A - at the supports only; B - at the supports and at every 7.62 m (25'); and C - at the supports and at every 3.05 m (10'). Likewise, for the last three load cases, D, E, and F, two equal line loads with one-half the magnitude of the line load for cases A, B, and C are placed directly over the exterior and interior beams. Also, the degree of lateral restraint of cases D, E, and F is the same as A, B, and C, respectively. Since load case B reflects most accurately the actual structure, it is used as the basis in the comparisons. In Table 15, the percent difference between the maximum stress in the critical girder of load case B, i.e. the basis, and of the other load cases is presented. Likewise Table 16 presents the percent difference in maximum deflection between the basis and the other load cases. As can be noted in these tables the maximum percent difference is 5% for stress and 4% for deflection. More importantly, however, when comparing the basis to load case C, which most accurately reflects the results of the analytical method presented in this dissertation because there is almost complete lateral restraint, the maximum percent difference is only 1.4%. This suggests that the probable error introduced into the present analysis technique by ignoring

the twisting degree of freedom in the elastic range is about 1.4%. Of course, many more comparisons would be required to completely confirm that the error is only around 1.5%, but sufficient justification exists to continue to neglect the twisting degree of freedom for the beam.

## 6. SUMMARY AND CONCLUSIONS

### 6.1 Summary

In Section 1.4 it was noted that previous research by Peterson and Kostem led to the development of a finite element model which could successfully predict the complete overload response of beam-slab highway bridges, made of prestressed or reinforced concrete beams and a reinforced concrete slab (Refs. 54 and 55). That finite element model could not, however, perform a reliable overload analysis on beam-slab highway bridges made with steel beams (girders) and a reinforced concrete slab. In the same section it was also noted that another finite element model for analyzing steel bridges was developed by Tumminelli and Kostem (Ref. 64). This model, while including the effects of slip between the beam and the slab and the effects of shear deformation in the beams, was limited to the elastic response of the structure. By "integrating" the works of Peterson and Kostem, and also, Tumminelli and Kostem, and introducing the additional nonlinear response characteristics mentioned at the end of this section (6.1), a new analytical model (presented in this report) was developed for performing an accurate overload analysis of steel beam-concrete slab highway bridges.

This new method of analysis gives a solution for the response of the structure to overloads in terms of displacements, stresses, cracking and crushing of concrete, yielding and strain

hardening of steel, and buckling of flanges and webs. Once serviceability limits, in terms of damage, stress, or deflection have been firmly established, then a check of these limits can be made at various load levels by employing the response information. The solution process is applicable up to the complete collapse of the structure.

In the reported analytical technique the following nonlinearities, which were taken from the previously noted research, are considered in the analysis:

1. Nonlinear and linear stress-strain behavior of the slab concrete.
2. Elastic-plastic stress-strain relationships for the beam (girder) steel and reinforcing bar steel.
3. Cracking and crushing of slab concrete.
4. Yielding of steel.

In addition to the above phenomena, the following nonlinear response characteristics have been included in the analysis for the first time:

1. Post-plastic stress-strain relationships for the beam (girder) steel.
2. Strain hardening of steel.
3. Buckling of beam compression flanges and plate girder webs and compression flanges.
4. Post-buckling response of the flanges and webs.

In the analytical model a piecewise linear solution process is used, in which solutions are obtained for each load increment up to the collapse of the structure. The total solution for a particular load level is obtained by summing up all the previous solution increments. While two different tangent stiffness solution techniques were available for the analyses; the incremental-iterative method or the incremental method; only the incremental-iterative method was employed in the research presented in this dissertation. In this method the tangent stiffness matrix is continually updated within each load increment, thus, providing a more reliable solution than the incremental process where no updating within the increment occurs.

The predicted response of two bridges, two bridge models, two composite beams, and eight plate girder tests have been compared with corresponding experimental results (Refs. 27, 28). The two bridges, one of the composite beams, and three of the plate girder tests have been presented in this report. In all cases adequate agreement was obtained in the comparisons. Experimental and analytical load versus deformation curves were compared for all problems, as were load versus damage records, where applicable.

The additional considerations of shear connector stiffness, fatigue, and torsion of the beams have been investigated. While the shear connector stiffness calculation and fatigue stress range check are included in the analysis, the effect of torsion of the beams was determined to still be of minor importance and not included in the analysis. Besides neglecting the effects of torsion

in the analysis, the following phenomena are also neglected in the analysis scheme:

1. Dynamic and impact effects.
2. Shear punching failure of the slab.
3. Minor axis bending of the beams.

## 6.2 Conclusions

Based upon the comparisons between the experimental results and the analytical results, the following observations and conclusions can be noted:

1. The overload structural response of steel beam concrete slab highway bridges, composite beams, and plate girder structures, in terms of stresses, deflections, and damages, can be adequately predicted by the developed analytical method.
2. In continuous beam-slab bridge superstructures the first failure is the cracking of the concrete slab in the negative moment region.
3. In all the continuous structures analyzed the negative moment regions of the structures appeared to suffer the greatest amount of damage.
4. The effects of cross-bracing on the overall structure response are negligible.

5. Based upon the experimental and analytical results studied so far, it would appear that web plate panel buckling would be more likely to occur than that of torsional buckling of the beam compression flange.
6. The failure to include the effects of web plate panel buckling in plate girder structures can lead to considerable error in results.
7. The occurrence of slip between the slab and the beam and, thus, the effects of the shear connector stiffness,  $k_{sc}$ , appear to be of minimal importance (i.e. an assumption of full composite action is very reasonable).

### 6.3 Suggestions for Future Research

The observations and conclusions presented in Section 6.2 are those which were clearly evident in the examples studied as part of this research. It would be expected that further analytical results would confirm these conclusions. However, because the results already obtained come from only a limited number of tests, the following recommendations are made for future research:

1. Conduct an extensive parametric study on many different beam-slab bridge superstructures and loading patterns using program BOVAS. This study would more firmly establish overload response characteristics.

2. Conduct further studies on the effects of torsion in the beams to more fully justify its exclusion from the analytical model.
3. Investigate the feasibility of including cross beams in the analytical model so that superstructures with stringer and floor beam systems can be analyzed using BOVAS.
4. Investigate the variation in the overall response of bridge superstructures when the shear connector stiffness is varied from 100% full composite action to approximately 50% full composite action.
5. Determine, if possible, through experimental data, field observations and analytical studies made with BOVAS, appropriate serviceability limits for frequent and infrequent overloads.

If all of this research is conducted, a more complete understanding of the overload response characteristics of steel multi-girder bridge superstructures will be established. Thus, the bridge engineer should then have an even better capacity for making an accurate assessment of the resistance of any superstructure to overloads.

## NOMENCLATURE

|                              |  |
|------------------------------|--|
| $A_j$                        | = layer area   |
| $A_{SB}$                     | = effective shear area of beam   |
| $A_W$                        | = cross-sectional area of beam web   |
| $C, D$                       | = curve parameters of concrete stress-strain relationship                                    |
| $C, R, S$                    | = parameters of tension field stress equation  |
| $C_1$                        | = reduction factor   |
| $E, E_t$                     | = tangent modulus and inelastic tangent  |
| $EA_A, EA_B$                 | = axial rigidity ( $E \times A$ )  |
| $E_c$                        | = initial modulus of elastic   |
| $E_i$                        | = initial modulus of elasticity, steel   |
| $E_j$                        | = tangent modulus beam layer   |
| $E_p$                        | = peak modulus concrete  |
| $E_{pb}, G_{pb}$             | = post-buckling tangent modulus and shearing modulus of web plate panel                      |
| $E_{st}$                     | = initial strain hardening modulus of elasticity   |
| $E_{1b}, E_{2b}$             | = tangent moduli for principal stress directions of slab                                     |
| $\hat{E}_{1b}, \hat{E}_{2b}$ | = tangent moduli for principal stress directions of slab employed in formulating $[\bar{D}]$ |
| $G, G_t$                     | = shearing modulus and inelastic shearing modulus  |

NOMENCLATURE (continued)

|                          |   |
|--------------------------|---|
| $I_j$                    | = beam layer moment of inertia  |
| $I_w$                    | = warping constant  |
| $K_T$                    | = St. Venant's constant   |
| $L$                      | = length of beam element  |
| $L/n$                    | = half wave length of compression flange buckle                                   |
| $U_B, U_A$               | = axial displacement for beam or in-plane<br>displacement for x-direction of slab |
| $V$                      | = shear force or volume of finite element   |
| $V_A$                    | = in-plane displacement for y-direction of slab                                   |
| $V_{TC}, V_{OC}, V_{TH}$ | } = shear in web plate panel  |
| $W$                      | = displacement in z-direction   |
| $Z_{BB}$                 | = distance between midheight of slab and centroid<br>of beam                      |
| $a_p, b_p$               | = slab element half lengths   |
| $a$                      | = plate girder web plate panel length   |
| $b$                      | = flange half width   |
| $d$                      | = beam web depth or distance between midheight<br>of slab and centroid of beam    |
| $e$                      | = eccentricity of beam and slab   |
| $f'_c$                   | = uniaxial compressive strength of concrete                                       |
| $f_t$                    | = tensile strength of concrete  |

NOMENCLATURE (continued)

|                               |  |
|-------------------------------|--|
| $k_s, k_b, k_c$               | = stiffness coefficients web panel buckling          |
| $k_{sc}, k_{max}$             | = stiffness of shear connector                       |
| $k_v, k_t$                    | = stiffness parameters torsional flange buckling     |
| $l_b$                         | = unbraced length compression flange                 |
| $m, n$                        | = Ramberg-Osgood curve parameters                    |
| $s$                           | = interface shear flow                               |
| $t$                           | = thickness of flange                                |
| $x, y, z$                     | = local cartesian coordinates                        |
| $x_n, y_n$                    | = nodal point coordinates                            |
| $w$                           | = thickness of web                                   |
| $z'$                          | = vertical direction web panel                       |
| $z_i$                         | = vertical distances from reference planes           |
| $\alpha, \alpha_1, \alpha_2$  | = stress ratios                                      |
| $\alpha_b, \beta_b, \gamma_b$ | = curve parameters post-plastic region steel         |
| $\alpha_p$                    | = ratio of web panel length-to-depth                 |
| $\gamma, \dot{\gamma}$        | = shear strain and shear strain increment            |
| $\gamma_B$                    | = shear strain in beam                               |
| $\delta$                      | = curve parameter tension field equation             |
| $\epsilon, \dot{\epsilon}$    | = strain and strain increment in principal direction |
| $\epsilon_{st}$               | = limiting strain plastic region of steel            |
| $\epsilon_t$                  | = total strain in steel layer                        |
| $\theta$                      | = angle which defined principal stress directions    |

NOMENCLATURE (continued)

|                             |  |
|-----------------------------|--|
| $\theta_x, \theta_y,$       |  |
| $\theta_A, \theta_B$        | = rotations about x and y axes and slab and beam element rotations |
| $\lambda, \lambda_\ell$     | = nondimensional parameters  |
| $\nu, \nu_1, \nu_2$         | = Poisson's ratio and Poisson's ratio in principal directions      |
| $\sigma, \dot{\sigma}$      | = a principal stress and stress increment                          |
| $\sigma_b, \sigma_{bcr}$    | = bending buckling stresses web plate panel                        |
| $\sigma_{bc}$               | = combined buckling stress web plate panel                         |
| $\sigma_{cc}, \sigma_{ccr}$ | = compressive buckling stresses web plate panel                    |
| $\sigma_{cr}, \sigma_{av}$  | } = compression flange buckling stresses                           |
| $\sigma_{cr}, \sigma_{in}$  |  |
| $\sigma_{\ell cr}$          | = lateral buckling stress  |
| $\sigma_p, \epsilon_p$      | = peak stress and peak strain                                      |
| $\sigma_{tc}$               | = tension field stress   |
| $\sigma_y$                  | = yield stress or stress in y direction                            |
| $\sigma_{yw}$               | = web yield stress   |
| $\sigma_u, \epsilon_u$      | = ultimate stress and corresponding strain                         |
| $\tau, \dot{\tau}$          | = shear stress and stress increment                                |
| $\tau_c, \tau_{ccr}$        | = shear buckling stresses web plate panel                          |
| $\phi, \phi_c, \phi_{co}$   | = direction of action of tension field                             |

NOMENCLATURE (continued)

Matrices

- [B] = strain-displacement matrices
- [C],[C1]  
[C2] = matrices relating element nodal point  
displacements to polynomial coefficients
- [C]<sup>-1</sup>  
[CC CX]  
[CA],[CB]  
[CW],[CD] } = coefficient displacement matrices
- [D],[D̄] = element elasticity matrices of slab
- [D<sub>i</sub>] = elasticity matrix layer i
- [E<sub>B</sub>],[G<sub>B</sub>] = beam element elasticity matrices (flexure and shear)
- [E<sub>j</sub>],[G<sub>j</sub>] = beam layer rigidity and shear matrices
- {F} {F}<sup>e</sup> = global and element force vectors
- {Ḟ} = incremental force vector
- {f} = vector of shape functions
- [K],[k]<sup>e</sup> = global and element stiffness matrices
- [N] = shape function matrix
- [P(x,y)] = polynomial function matrix
- [Q] = connectivity matrix
- [T] = transformation matrix

NOMENCLATURE (continued)

Matrices

|                                    |   |
|------------------------------------|---|
| $\{\epsilon\}, \{\dot{\epsilon}\}$ | = strain and incremental strain vectors             |
| $[\Gamma]$                         | = matrix differential operator                      |
| $\{\delta\}, \{\dot{\delta}\}$     | = displacement and incremental displacement vectors |
| $\{\zeta\}$                        | = polynomial coefficients vector                    |
| $\{\sigma\}, \{\dot{\sigma}\}$     | = stress and incremental stress vectors             |
| $\{\bar{\sigma}_i\}$               | = integrated average stress vector                  |

Notes:

1. The use of subscripts  $u$ ,  $\phi$ ,  $b$ ,  $s$ , and  $d$  on matrices indicates that the matrix is derived from the consideration of in-plane deformations ( $u$ ), bending deformations ( $\phi$ ), axial and bending deformations ( $b$ ), shear deformations ( $s$ ), and slip ( $d$ ).
2. The use of the subscripts  $uu$ ,  $u\phi$ , and  $\phi\phi$  on matrices indicates that the matrix is derived from the consideration of in-plane deformations ( $uu$ ), coupling deformations ( $u\phi$ ), and bending deformations ( $\phi\phi$ ).
3. The use of the subscripts  $A$  and  $B$  used alone indicates the parameter is associated with either the plate ( $A$ ) or the beam ( $B$ ).

NOMENCLATURE (continued)

4. The use of L or M as a subscript indicates that the quantity is at node L or M.
5. The use of ('), primes, indicates quantities expressed in skew coordinates.
6. The use of superscript, e, on vectors or matrices indicates that the quantities are applicable to the element.
7. The use of 1, 2 as subscripts indicates that the quantities are with respect to the directions of principle stress.
8. A (·) dot used over any term indicates an incremental quantity.
9. The subscripts x,y,z,xy denote the direction of action in local coordinates.

TABLE 1A SLAB REINFORCEMENT AND ORIENTATION

EXAMPLE 1 (AASHTO - 3B)

| <u>Centroidal Location<br/>(Positive Downward)</u> | <u><math>\theta_x</math><br/>(degrees)</u> | <u>Thickness</u>        | <u>Size/Spacing</u>       |
|--|--|-------------------------|---------------------------|
| - 36.4 mm<br>(- 1.435 in)                          | - 90                                       | 1.575 mm<br>(0.0620 in) | 5 @ 127 mm<br>(5 @ 5 in)  |
| - 23.7 mm<br>(- 0.934 in)                          | 0  | 1.397 mm<br>(0.0550 in) | 3 @ 508 mm<br>(3 @ 20 in) |
| 23.7 mm<br>(0.935 in)                              | 0  | 1.397 mm<br>(0.0550 in) | 3 @ 508 mm<br>(3 @ 20 in) |
| 36.4 mm<br>(1.435 in)                              | - 90                                       | 1.575 mm<br>(0.0620 in) | 5 @ 127 mm<br>(5 @ 5 in)  |

TABLE 1B SLAB REINFORCEMENT AND ORIENTATION

EXAMPLE 2 (UNIV. TENN)

| <u>Centroidal Location<br/>(Positive Downward)</u> | <u><math>\theta_x</math><br/>(degrees)</u> | <u>Thickness</u>         | <u>Size/Spacing</u>        |
|--|--|--------------------------|----------------------------|
| 43 mm<br>(-1.6875 in)                              | - 90                                       | 1.432 mm<br>(0.05636 in) | 5 @ 140 mm<br>(5 @ 5.5 in) |
| 27 mm<br>(-1.0625 in)                              | 0  | 0.984 mm<br>(0.03875 in) | 5 @ 203 mm<br>(5 @ 8 in)   |
| 27 mm<br>( 1.0625 in)                              | 0  | 0.984 mm<br>(0.03875 in) | 5 @ 203 mm<br>(5 @ 8 in)   |
| 43 mm<br>(1.5625 in)                               | - 90                                       | 1.432 mm<br>(0.05636 in) | 5 @ 140 mm<br>(5 @ 5.5 in) |

TABLE 2 MATERIAL PROPERTIES - EXAMPLE 1 (AASHTO - 3B)

| Property  | Material             | Actual                           | BOVAS                   |
|---|----------------------|----------------------------------|-------------------------|
| $f'_c$  | Slab<br><br>Concrete | 39.58 MPa<br>(5.74 ksi)          |                         |
| $f_t$   |                      | —                                | 3.17 MPa<br>(0.459 ksi) |
| $E_c$   |                      | 35852 MPa<br>(5200 ksi)          |                         |
| $\sigma_y$  | Reinforcing          | 422.0 MPa<br>(61.2 ksi)          |                         |
| $E_i$   | Steel                | 198,569 MPa<br>(28,800 ksi)      |                         |
| $\sigma_y$ , flange                               | Beam<br><br>Steel    | 242.0 MPa<br>(35.1 ksi)          |                         |
| $\sigma_y$ , web                                  |                      | 275.1 MPa<br>(39.9 ksi)          |                         |
| $\sigma_y$ , cover-plate                          |                      | 268.1 MPa<br>(38.9 ksi)          |                         |
| $E_i$   |                      | 206,842 MPa<br>(30,000 ksi)      |                         |
| $E_{st}, \epsilon_{st}$<br>$\sigma_u, \epsilon_u$ |                      | NOT EMPLOYED IN<br>THIS ANALYSIS |                         |

TABLE 3 LOAD VERSUS DAMAGE RECORD - EXAMPLE 1 (AASHTO - 3B)

| Load<br>kN-M<br>(kip-ft) | Damage - Test  | Load<br>kN-M<br>(kip-ft) | Damage - BOVAS  |
|--------------------------|--|--------------------------|---|
|                          |  | 1033<br>(762)            | Yielding of exterior beam bottom flange at midspan  |
|                          |  | 1228<br>(906)            | Yielding of interior beam bottom flange at midspan  |
|                          |  | 1436<br>(1059)           | Yielding of coverplate of exterior beam at midspan  |
|                          |  | 1567<br>(1156)           | Yielding of exterior and interior beam bottom flange at end of coverplate   |
| 1807<br>(1333)           | Yielding of bottom flange near ends of coverplate  | 1849<br>(1364)           | Complete yielding of exterior beam coverplate. 85% of exterior beam bottom flange has yielded   |
| 2024<br>(1493)           | Almost complete yielding of bottom flange except near supports, extensive coverplate yielding  | 1973<br>(1455)           | Complete yielding of interior beam coverplate. 85% of interior beam bottom flange has yielded   |
|                          |  | 2253<br>(1662)           | Bottom layer of slab has a transverse crack all the way across at midspan   |
|                          |  | 2553<br>(1883)           | The web of exterior beam has yielded over 70% of its depth  |
| 2712<br>(2000)           | Web yielding is clearly evident  | 2602<br>(1919)           | The web of interior beam has yielded over 70% of its depth  |
| 3087<br>(2277)           | Extensive web yielding and tension cracks in slab halfway through depth in coverplated section | 3113<br>(2296)           | The slab has a transverse crack through 50% of its depth at midspan and 33% through depth in coverplated section. The web has yielded through 86% of depth at midspan |

TABLE 4 MATERIAL PROPERTIES - EXAMPLE 2 (UNIV. TENNESSEE)

| Property  | Material    | BOVAS                            |
|---|-------------|----------------------------------|
| $f'_c$  | Concrete    | 47.37 MPa<br>(6.87 ksi)          |
| $f_t$   |             | 3.38 MPa<br>(0.49 ksi)           |
| $E_c$   |             | 32,929 MPa<br>(4,776 ksi)        |
| $\sigma_y$  | Reinforcing | 275.8 MPa<br>(40 ksi)            |
| $E_i$   | Steel       | 199,948 MPa<br>(29,000 ksi)      |
| $\sigma_y$  | Beam        | 275.8 MPa<br>(40 ksi)            |
| $E_i$   |             | 212,014 MPa<br>(30,750 ksi)      |
| $E_{st}, \epsilon_{st}$<br>$\sigma_u, \epsilon_u$ | Steel       | Not employed in<br>this analysis |

TABLE 5 LOAD VERSUS DAMAGE RECORD - EXAMPLE 2 (UNIV. TENNESSEE)

| Load<br>kN<br>(kip) | Damage - Test  | Load<br>kN<br>(kip) | Damage - BOVAS   |
|---------------------|--|---------------------|--|
|                     |  | 1154<br>(259.5)     | Up to this point there has only been longitudinal cracking of the slab in the bottom layers at the centerline of the bridge under or near the load |
|                     |  | 1790<br>(402.5)     | The first transverse cracks appear in the top layer of the slab near first pier  |
|                     |  | 1987<br>(446.7)     | Transverse cracks appear in the top of slab near the second pier   |
|                     |  | 2475<br>(556.4)     | First yielding begins in bottom flange of interior beams in area under the load  |
|                     |  | 2628<br>(590.9)     | First yielding begins in bottom of web of interior beams in areas under the load   |
| 2758<br>(620)       | First yielding of steel appears to occur at this load - shortly after yielding started the bridge "lifted off" the abutment nearest the load | 2782<br>(625.5)     | The transverse crack over the first pier is now through 50% of the slab depth  |
| 2891<br>(650)       | Tension cracks visible in deck slab over first pier  |                     |  |
| 3114<br>(700)       | Tension cracks which extend across the slab and through the curb at second pier are visible  | 3160<br>(710.4)     | The first transverse crack in the bottom of the slab in the area under the load now appears  |

TABLE 5 LOAD VERSUS DAMAGE RECORD - EXAMPLE 2 (UNIV. TENNESSEE)

(continued)

| Load<br>kN<br>(kip) | Damage - Test | Load<br>kN<br>(kip) | Damage - BOVAS  |
|---------------------|---------------|---------------------|---|
|                     |               | 3370<br>(757.5)     | The slab over first pier is now completely cracked longitudinally through the complete depth, however, the reinforcement is still functional  |
|                     |               | 3415<br>(767.8)     | The slab over second pier is now cracked completely through the depth in the longitudinal direction   |
|                     |               | 3644<br>(819.3)     | Yielding of the bottom flange of the exterior beams in the area of the load has started   |
|                     |               | 3788<br>(851.6)     | The slab between the interior and exterior beam at the second pier is now also cracked through 60% of its depth in the longitudinal direction |
|                     |               | 4116<br>(925.4)     | The bottom transverse reinforcement in the slab in the area of the load has now yielded in tension  |
|                     |               | 4411<br>(991.6)     | Yielding in compression of the bottom flange of interior beam at first pier   |
|                     |               | 4577<br>(1029.2)    | The transverse crack in the bottom of the slab under the load is now halfway through the slab depth in the area near the center of the bridge |

TABLE 5 LOAD VERSUS DAMAGE RECORD - EXAMPLE 2 (UNIV. TENNESSEE)

(continued)

| Load<br>kN<br>(kip) | Damage - Test   | Load<br>kN<br>(kip) | Damage - BOVAS   |
|---------------------|---|---------------------|--|
|                     |   | 4771<br>(1072.6)    | The web of interior beam under the load is now fully yielded   |
|                     |   | 4982<br>(1119.9)    | First crushing of slab at load point   |
|                     |   | 5348<br>(1202.3)    | Yielding in compression of top transverse slab reinforcement in area under load. Yielding in tension of top longitudinal slab reinforcement near the first pier. Yielding in tension of bottom longitudinal slab reinforcement in area under the load. |
|                     |   | 5432<br>(1221.2)    | The interior beam in the area under the load has now fully yielded forming a plastic hinge in the beam   |
| 5627<br>(1265)      | Maximum load reached. Compression failure of curb section | 5581<br>(1254.7)    | The web of exterior beam under point of loading has now fully yielded  |

TABLE 6 MATERIAL PROPERTIES - TEST BEAM CB2

| Property        | Material             | BOVAS                       |                             |
|-----------------|----------------------|-----------------------------|-----------------------------|
| $f'_c$          | Concrete<br><br>Slab | 37.65 MPa<br>(5.46 ksi)     |                             |
| $f_t$           |                      | 3.01 MPa<br>(0.44 ksi)      |                             |
| $E_c$           |                      | 29,355 MPa                  | (4258 ksi)                  |
| $\sigma_y$      | Reinforcing          | # 3 Bars                    | # 5 Bars                    |
|                 |                      | 364.8 MPa<br>(52.9 ksi)     | 346.8 MPa<br>(50.3 ksi)     |
| $E_i$           | Steel                | 199,948 MPa<br>(29,000 ksi) |                             |
| $\sigma_y$      | Beam                 | Web                         | Flange                      |
|                 |                      | 338.5 MPa<br>(49.1 ksi)     | 311.6 MPa<br>(45.2 ksi)     |
| $E_i$           | Steel                | 208,221 MPa<br>(30,200 ksi) | 215,806 MPa<br>(31,300 ksi) |
| $E_{st}$        |                      | 6,895 MPa<br>(1,000 ksi)    | 7,998 MPa<br>(1,160 ksi)    |
| $\epsilon_{st}$ |                      | 0.0226 mm/mm<br>(in/in)     | 0.0104 mm/mm<br>(in/in)     |
| $\sigma_u$      |                      | 459.9 MPa<br>(66.7 ksi)     | 465.4 MPa<br>(67.5 ksi)     |
| $\epsilon_u$    |                      | 0.120 mm/mm<br>(in/in)      | 0.120 mm/mm<br>(in/in)      |

TABLE 7 SLAB REINFORCEMENT - ORIENTATION CB2

| Test Beam | Centroidal Distance from midheight + down) | $\theta_x$ (orientation w.r.t. x axis) | Thickness               | Size/Spacing                 |
|-----------|--|--|-------------------------|------------------------------|
| CB2       | 0.00                                       | 0°                                     | 1.64 mm<br>(0.06458 in) | #5 @ 122 mm<br>(#5 @ 4.8 in) |
|           | 0.00                                       | 90°                                    | 0.62 mm<br>(0.02444 in) | #3 @ 114 mm<br>(#3 @ 4.5 mm) |

TABLE 8 LOAD VERSUS DAMAGE RECORD - CB2

| Load<br>kN<br>(kip)                  | Damage - Test                                      | Load<br>kN<br>(kip) | Damage - BOVAS  |
|--------------------------------------|--|---------------------|---|
|                                      |  | 110.3<br>(24.8)     | Slab completely cracked in transverse direction over interior support                           |
|                                      |  | 348.7<br>(78.4)     | First yielding of beam, tension flange under the load and compression web over interior support |
|                                      |  | 470.2<br>(105.1)    | Web under load starts to yield  |
|                                      |  | 478.2<br>(107.5)    | Tension flange over interior support yields   |
|                                      |  | 521.8<br>(117.3)    | Slab in vicinity of load completely cracked   |
| 533.8<br>(120.0)                     | Initial flange buckling load                       |                     |   |
|                                      |  | 560.5<br>(126.0)    | Strain hardening begins in tension flange under load  |
| 578.3<br>(130.0)                     | Complete flange buckling                           |                     |   |
|                                      |  | 581.4<br>(130.7)    | Strain hardening begins in compression flange over interior support                             |
|                                      |  | 589.8<br>(132.6)    | Compression flange buckles  |
| 591.6-<br>605.0<br>(133.0-<br>136.0) | Crushing failure of slab in positive moment region |                     |   |

TABLE 9 MATERIAL PROPERTIES - TEST GIRDER UG2

| Property                  | Top Flange               | Bottom Flange           | Cover Plate             | Web                     |
|---------------------------|--------------------------|-------------------------|-------------------------|-------------------------|
| $\sigma_y$ (actual)       | 253.0 MPa<br>(36.7 ksi)  | 248.9 MPa<br>(36.1 ksi) | 244.8 MPa<br>(35.5 ksi) | 299.2 MPa<br>(43.4 ksi) |
| E (assumed)               | 203,400 MPa (29,500 ksi) |                         |                         |                         |
| $E_{st}$ (assumed)        | 5,500 MPa (800 ksi)      |                         |                         |                         |
| $\epsilon_{st}$ (assumed) | 0.014 mm/mm (in/in)      |                         |                         |                         |
| $\sigma_u$ (assumed)      | 403.3 MPa (58.5 ksi)     |                         |                         |                         |
| $\epsilon_u$ (assumed)    | 0.120 mm/mm (in/in)      |                         |                         |                         |

TABLE 10 BUCKLING LOADS FOR TEST UG2.1 → UG2.3

| TEST   | WEB BUCKLING LOAD (P) |                       | FLANGE+ BUCKLING LOAD (P) | ULTIMATE LOAD LOAD (P)  |                         |
|--------|-----------------------|-----------------------|---------------------------|-------------------------|-------------------------|
|        | TEST                  | BOVAS                 | BOVAS                     | TEST                    | BOVAS                   |
| UG2.1  | 11.7 kN<br>(2.6 kips) | 13.5 kN<br>(3.0 kips) | --                        | 80.1 kN<br>(17.8 kips)  | 81.0 kN<br>(18.0 kips)  |
| UG2.2* | --                    | 13.1 kN<br>(2.9 kips) | --                        | 90.9 kN<br>(20.2 kips)  | 91.4 kN<br>(20.3 kips)  |
| UG2.3  | --                    | --                    | 294.8 kN<br>(65.5 kips)   | 286.7 kN<br>(63.7 kips) | 315.0 kN<br>(70.0 kips) |

\* 3 Panels

+ No test results

**TABLE 11 MATERIAL PROPERTIES - FHWA FOUR-SPAN**

| Property            | Material             | BOVAS  |                         |                       |
|---------------------|----------------------|--|-------------------------|-----------------------|
| $f'_c$              | Concrete<br><br>Slab | 37.9 MPa (5.5 ksi)                               |                         |                       |
| $f_t$               |                      | 3.0 MPa (0.44 ksi)                               |                         |                       |
| $E_c$               |                      | 29,462.0 MPa (4273 ksi)                          |                         |                       |
| $\sigma_y$<br>$E_i$ | Reinforcing Steel    | 413.7 MPa (60 ksi)<br>203,395.0 MPa (29,500 ksi) |                         |                       |
|                     |                      | A36  | A441                    | Fictitious*           |
| $\sigma_y$          | Beam<br><br>Steel    | 248.0 MPa<br>(36 ksi)                            | 317.0 MPa<br>(46 ksi)   | 248 MPa<br>(36 ksi)   |
| $E_i$               |                      | 203,395 MPa<br>(29,500 ksi)                      |                         | 21 MPa<br>(3 ksi)     |
| $E_{st}$            |                      | 5515 MPa<br>(800 ksi)                            | 4826 MPa<br>(700 ksi)   | 0.6 MPa<br>(0.08 ksi) |
| $\epsilon_{st}$     |                      | 0.014 mm/mm<br>(in/in)                           | 0.0215 mm/mm<br>(in/in) | 140 mm/mm<br>(in/in)  |
| $\sigma_u$          |                      | 403 MPa<br>(58.5 ksi)                            | 462 MPa<br>(67.0 ksi)   | 403 MPa<br>(58.5 ksi) |
| $\epsilon_u$        |                      | 0.120 mm/mm<br>(in/in)                           | 0.120 mm/mm<br>(in/in)  | 1200 mm/mm<br>(in/in) |

\*In the layered finite element model, the number of layers must remain constant; however, since the width and thickness of the flanges changes from section to section, certain layers (Table 12) are given fictitious material properties to model the non-existence of material for that section.

TABLE 12 TOP AND BOTTOM FLANGE CROSS-SECTIONS

TOP FLANGE CROSS-SECTIONS

| Section | Layer | Width ( $b_t$ )   | Material |
|---------|-------|-------------------|----------|
| 1       | 1     | 305 mm<br>(12 in) | *        |
|         | 2     |                   | *        |
|         | 3     |                   | A36      |
| 2       | 1     | 406 mm<br>(16 in) | *        |
|         | 2     |                   | A441     |
|         | 3     |                   | A441     |
| 3       | 1     | 305 mm<br>(12 in) | *        |
|         | 2     |                   | *        |
|         | 3     |                   | A36      |
| 4       | 1     | 406 mm<br>(16 in) | A441     |
|         | 2     |                   | A441     |
|         | 3     |                   | A441     |

BOTTOM FLANGE CROSS-SECTION

| Section | Layer | Width ( $b_b$ )   | Material |
|---------|-------|-------------------|----------|
| 1       | 12    | 406 mm<br>(16 in) | A36      |
|         | 13    |                   | *        |
|         | 14    |                   | *        |
|         | 15    |                   | *        |
| 2       | 12    | 406 mm<br>(16 in) | A441     |
|         | 13    |                   | A441     |
|         | 14    |                   | A441     |
|         | 15    |                   | *        |
| 3       | 12    | 406 mm<br>(16 in) | A36      |
|         | 13    |                   | A36      |
|         | 14    |                   | *        |
|         | 15    |                   | *        |
| 4       | 12    | 457 mm<br>(18 in) | A441     |
|         | 13    |                   | A441     |
|         | 14    |                   | A441     |
|         | 15    |                   | A441     |

\* Fictitious Material - See Table 11

TABLE 13 SLAB REINFORCEMENT - FHWA FOUR-SPAN

| For Slab Elements       | Centroidal Location from midheight (+ downward) | $\theta_x$ orientation w.r.t. x axis) | Thickness             | Size/Spacing                |
|-------------------------|---|---------------------------------------|-----------------------|-----------------------------|
| 1-36<br>and<br>61-102   | - 55.6 mm<br>(-2.1875 in)                       | - 90°                                 | 1.57 mm<br>(0.062 in) | #5 @ 127 mm<br>#5 @ 5 in)   |
|                         | - 41.3 mm<br>(-1.625 in)                        | 0°                                    | 0.87 mm<br>(0.034 in) | #5 @ 229 mm<br>#5 @ 9 in)   |
|                         | 66.7 mm<br>(2.625 in)                           | 0°                                    | 0.78 mm<br>(0.031 in) | #5 @ 165 mm<br>#5 @ 5 in)   |
|                         | 81.0 mm<br>(3.1875 in)                          | - 90°                                 | 1.57 mm<br>(0.062 in) | #5 @ 127 mm<br>#5 @ 5 in)   |
| 37-60<br>and<br>103-120 | - 55.6 mm<br>(-2.1875 in)                       | - 90°                                 | 1.57 mm<br>(0.062 in) | #5 @ 127 mm<br>#5 @ 5 in)   |
|                         | - 41.3 mm<br>(-1.625 in)                        | 0°                                    | 1.75 mm<br>(0.069 in) | #5 @ 114 mm<br>#5 @ 4.5 in) |
|                         | 66.7 mm<br>(2.625 in)                           | 0°                                    | 0.78 mm<br>(0.031 in) | #5 @ 165 mm<br>#5 @ 65 in)  |
|                         | 81.0 mm<br>(3.1875 in)                          | - 90°                                 | 1.57 mm<br>(0.062 in) | #5 @ 127 mm<br>#5 @ 5 in)   |

TABLE 14 MOMENT VERSUS DAMAGE RECORD

FHWA FOUR-SPAN

| Maximum Static Moment,<br>kN-M, (kips-ft) | Damage   |
|---|--|
| 4095<br>(3020)                            | A Maximum Static Moment<br>corresponding to two lanes of<br>uniform live load for HS-20<br>loading plus concentrated loads   |
| 5543<br>(4088)                            | First cracking of slab in trans-<br>verse direction over interior<br>supports  |
| 5616<br>(4142)                            | B Web plate panel of girder 2<br>over Pier 2 buckles   |
| 6055<br>(4466)                            | C Web plate panel of girder 2<br>over Pier 3 buckles, first<br>significant deviation from<br>linear load versus deflection<br>behavior noted                               |
| 6310<br>(4654)                            | All six web plate panels of<br>girder 2 have now buckled   |
| 6799<br>(5015)                            | D Web plate panel of girder 1<br>over Pier 3 buckles   |
| 7500<br>(5532)                            | All six web plate panels<br>of girder 2 have now buckled   |
| 8478<br>(6253)                            | E First web plate panels buckle<br>for girder 3, and first cracking<br>of slab in longitudinal direction,<br>large derivation in load versus<br>deflection behavior starts |
| 9256<br>(6827)                            | All six web plate panels of<br>girder 3 have now buckled   |

TABLE 14 MOMENT VERSUS DAMAGE RECORD

FHWA FOUR-SPAN (continued)

| Maximum Static Moment,<br>kN-M, (kips-ft) | Damage   |
|---|--|
| 11,630<br>(8578)                          | F Slab completely cracked over girder 2 at interior supports   |
| 12,445<br>(9179)                          | G Maximum deflection allowed by AASHTO of 1/1000 of span length exceeded. Also the longitudinal live load stress range for transverse stiffener detail exceeds allowance for over 2,000,000 cycles of 82.74 MPa (12 ksi) |
| 12,928<br>(9535)                          | H Web plate panel compression flange for girder 2 over Pier 2 buckles laterally.   |
| 13,461<br>(9928)                          | I Web plate panel compression flange for girder 2 over Pier 3 buckles laterally  |
| 19,287<br>(14,225)                        | J First yield of girder flange at midspan second span for girder 2   |

TABLE 15 STRESS COMPARISON OF TORSION STUDY

| Load Case | <u>Percent Difference from Basis</u> |                            | Ratio Maximum<br>Exterior to Interior<br>Girder Stress |
|-----------|--------------------------------------|----------------------------|--|
|           | <u>Exterior<br/>Girder</u>           | <u>Interior<br/>Girder</u> |  |
| A         | 1.7                                  | 2.9                        | 1.36   |
| B         | 0.0                                  | 0.0                        | 1.37   |
| C         | - 0.6                                | - 1.4                      | 1.38   |
| D         | 5.2                                  | - 4.0                      | 1.50   |
| E         | 1.7                                  | - 3.8                      | 1.45   |
| F         | 0.5                                  | - 3.9                      | 1.44   |

TABLE 16 DEFLECTION COMPARISON OF TORSION STUDY

| Load Case | <u>Percent Difference from Basis</u> |                            | Ratio Ext. Def.<br>to Int. Def. |
|-----------|--------------------------------------|----------------------------|---------------------------------|
|           | <u>Exterior<br/>Girder</u>           | <u>Interior<br/>Girder</u> |                                 |
| A         | 1.8                                  | 1.5                        | 1.40                            |
| B         | 0.0                                  | 0.0                        | 1.40                            |
| C         | - 0.8                                | - 1.4                      | 1.41                            |
| D         | 4.3                                  | - 3.0                      | 1.50                            |
| E         | 1.2                                  | - 2.4                      | 1.45                            |
| F         | - 0.2                                | - 2.5                      | 1.43                            |

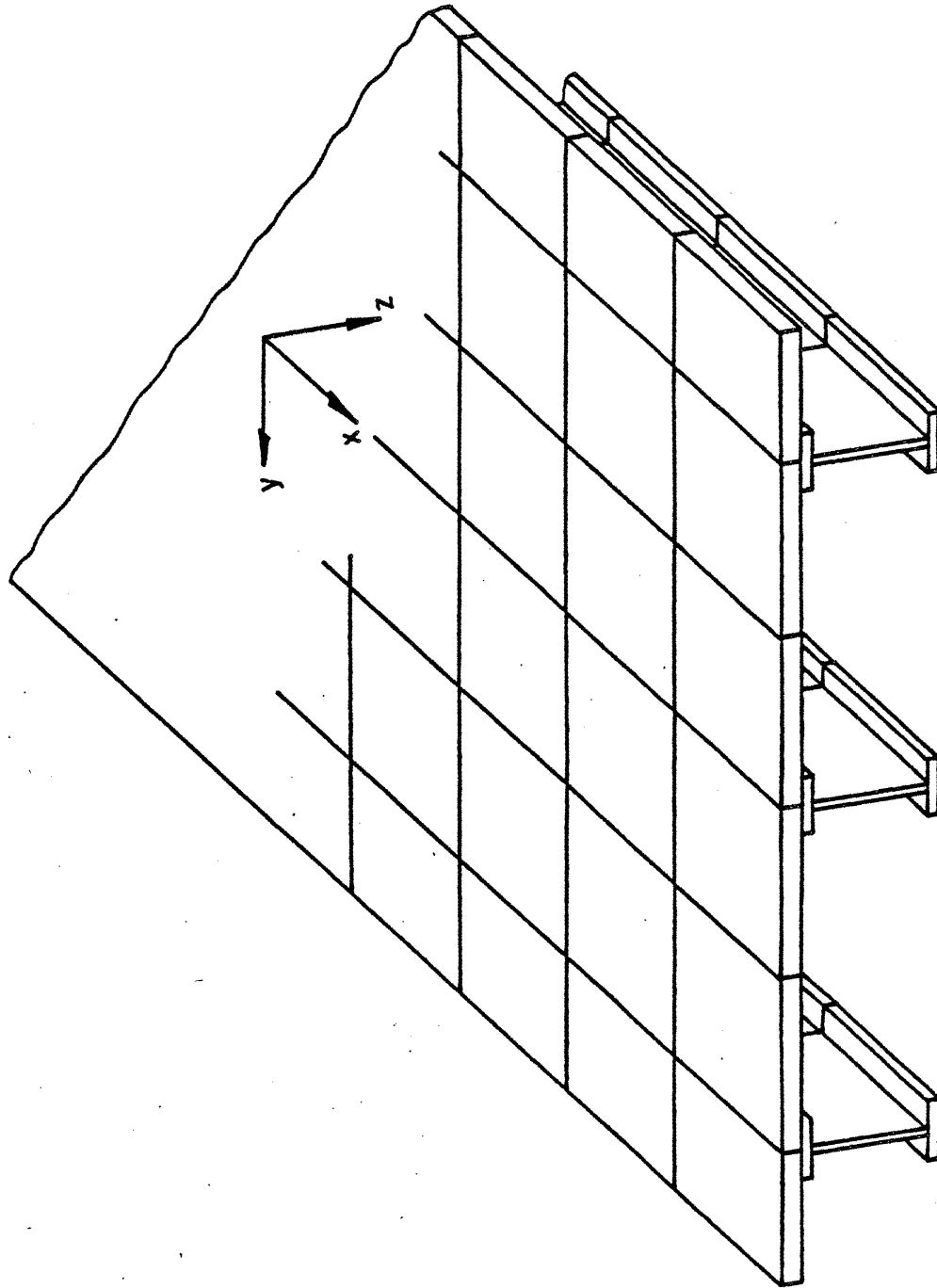


Fig. 1 Typical Slab-Girder Highway Bridge Finite Element Discretization

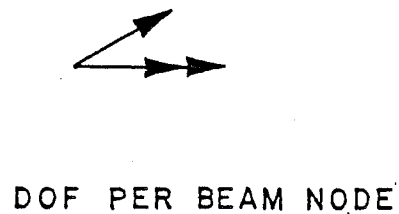
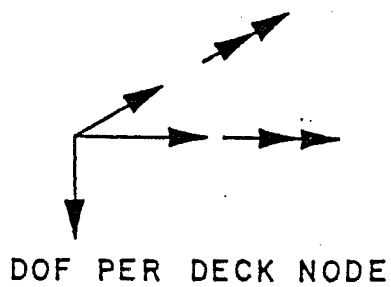
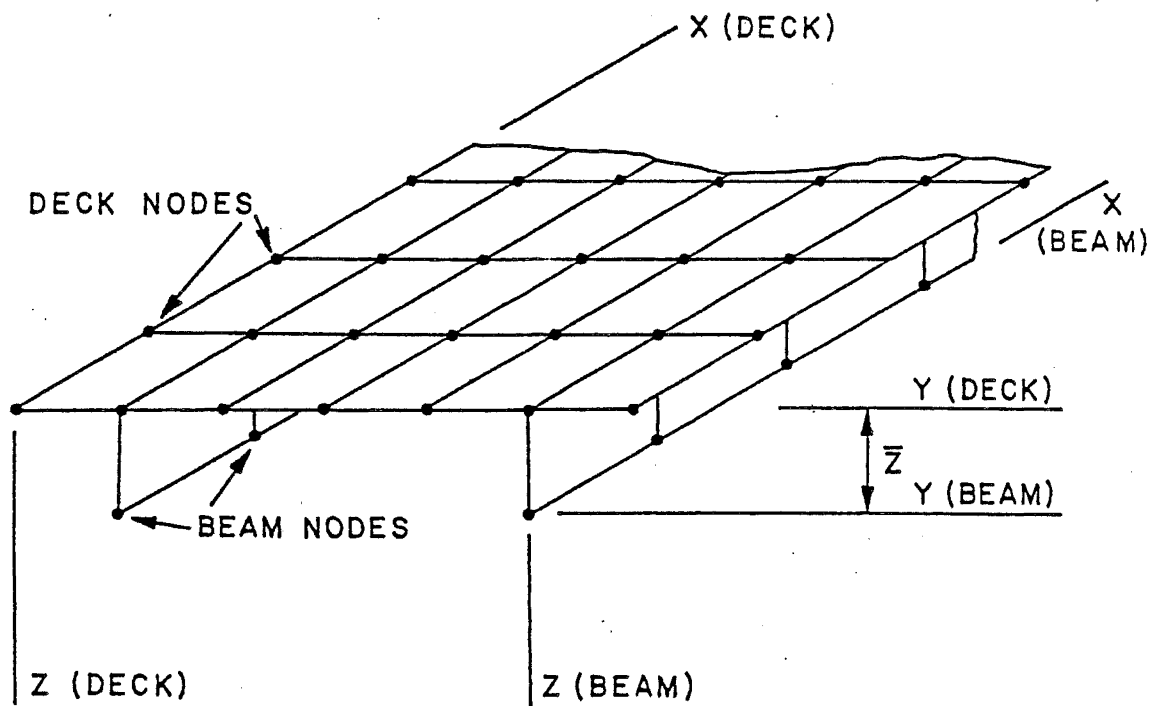


Fig. 2 Beam and Slab Node Point Arrangement

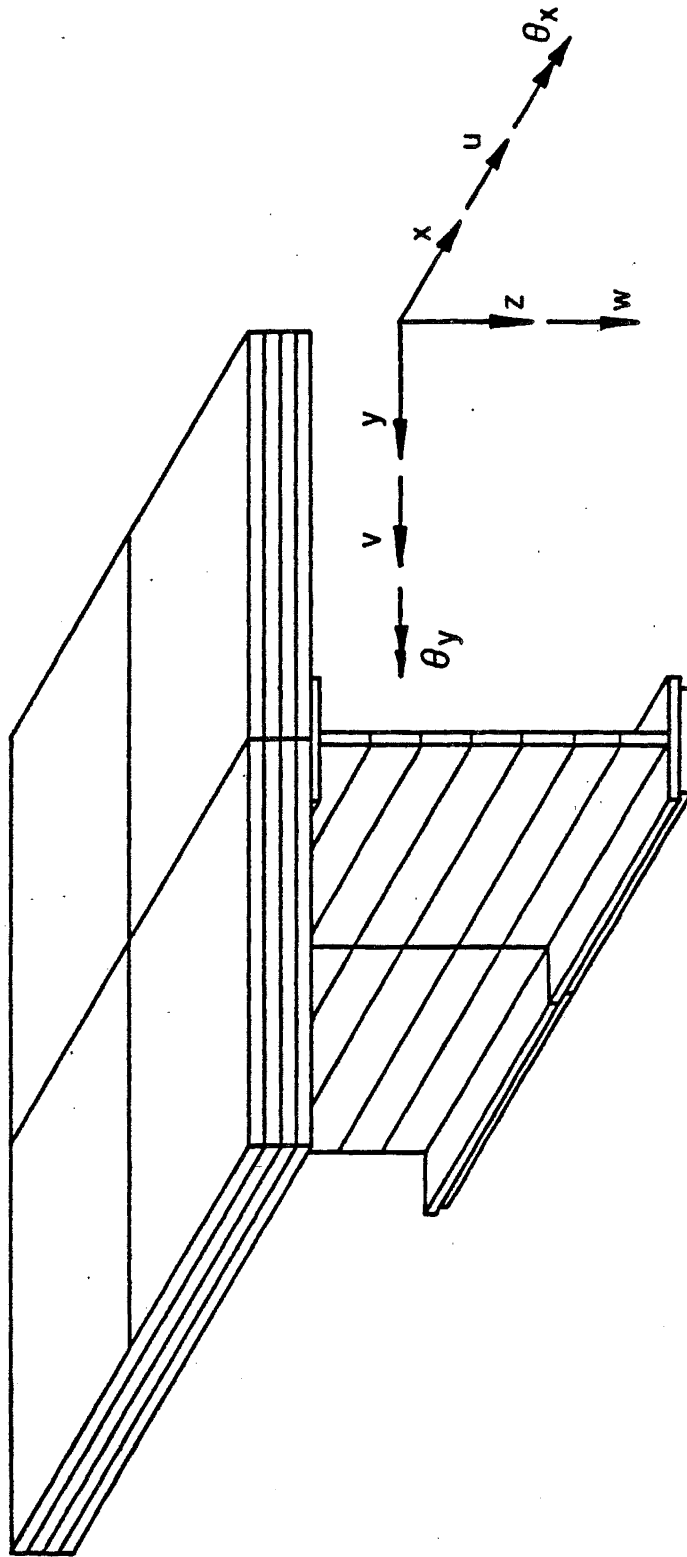


Fig. 3 Slab and Girder Layering

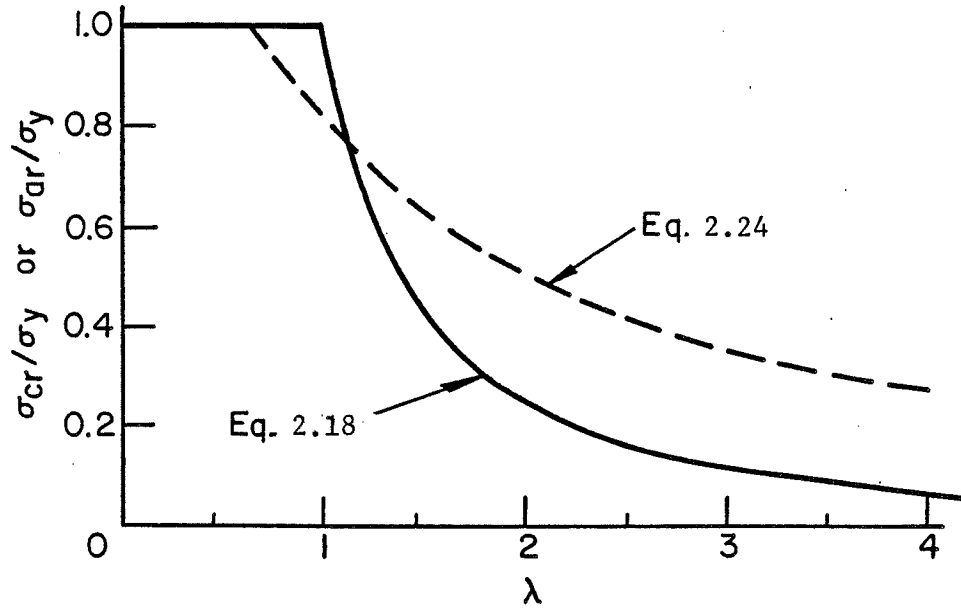


Fig. 4 Torsional Buckling Curves

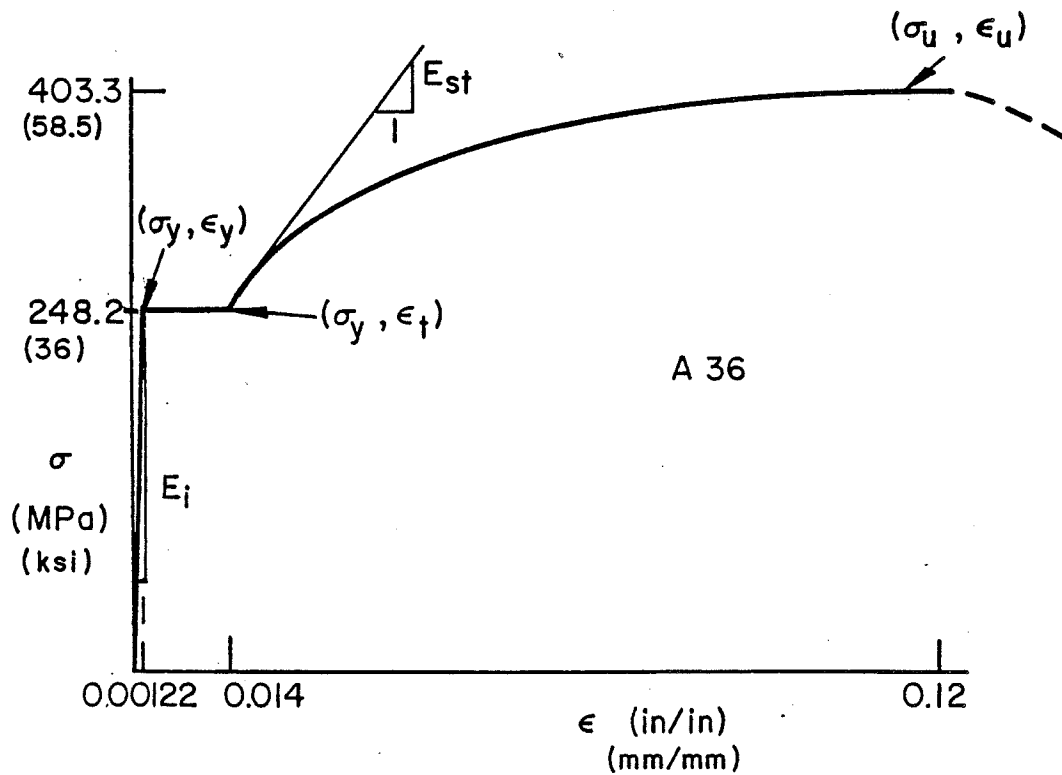


Fig. 5 Idealized Stress-Strain Relationship for Steel

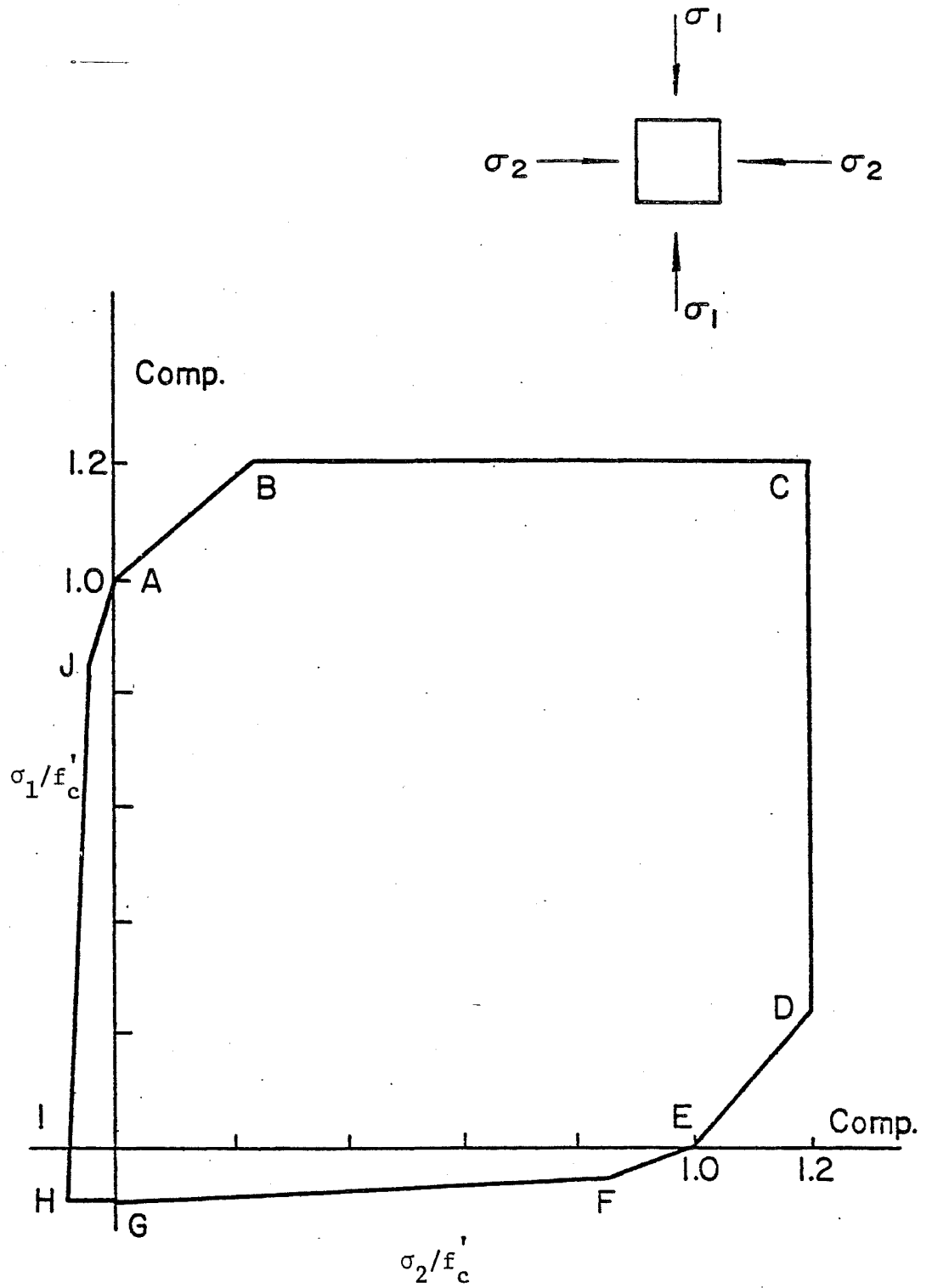


Fig. 6 Idealized Biaxial Failure Envelope with Characteristic Points

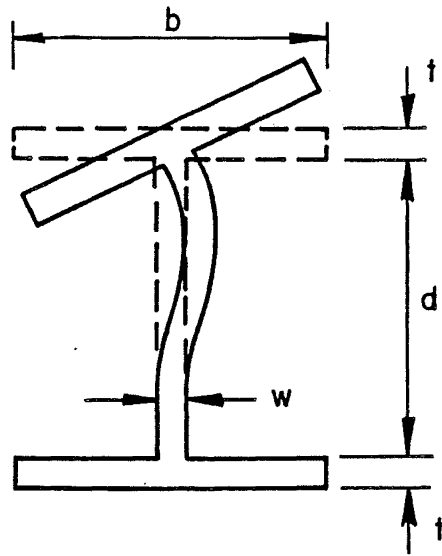


Fig. 7 Torsional Buckling of Compression Flange - Deformed Shape

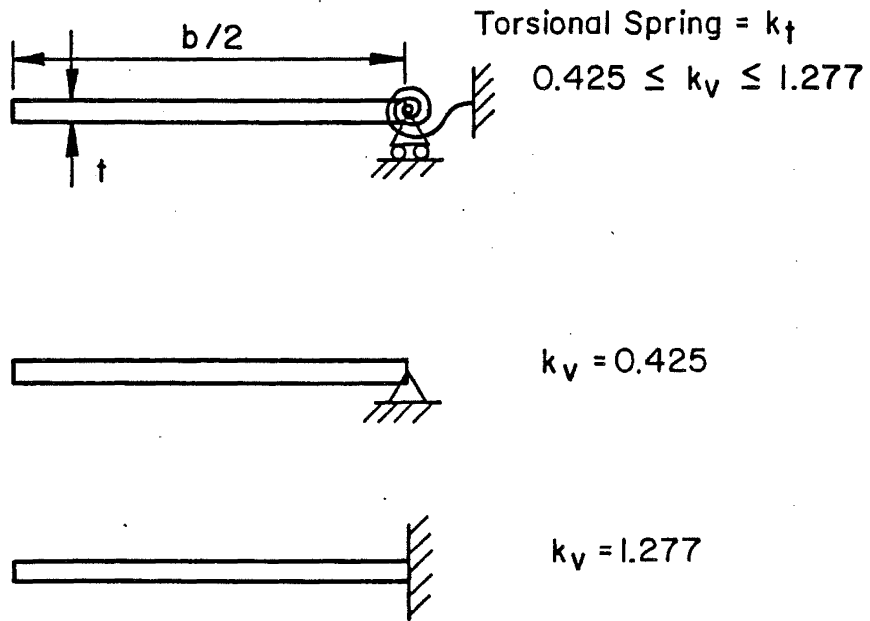


Fig. 8 Torsional Buckling Coefficient  $k_v$

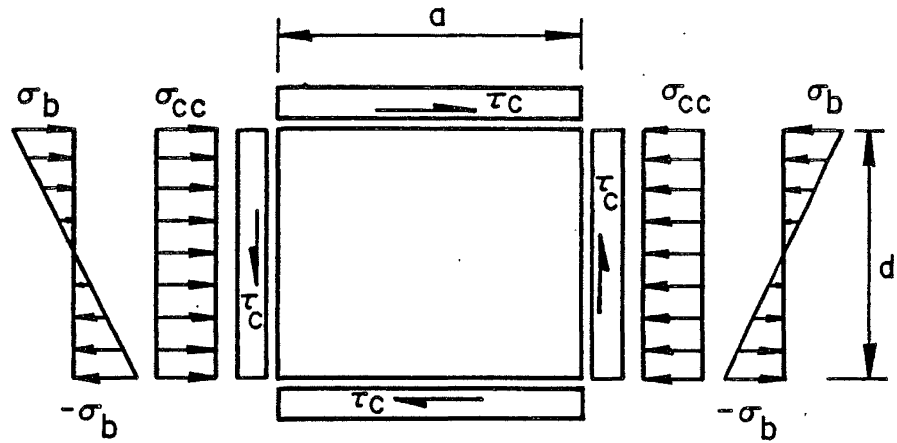


Fig. 9 Stress Distribution in Web Plate Panel at Critical Buckling Load

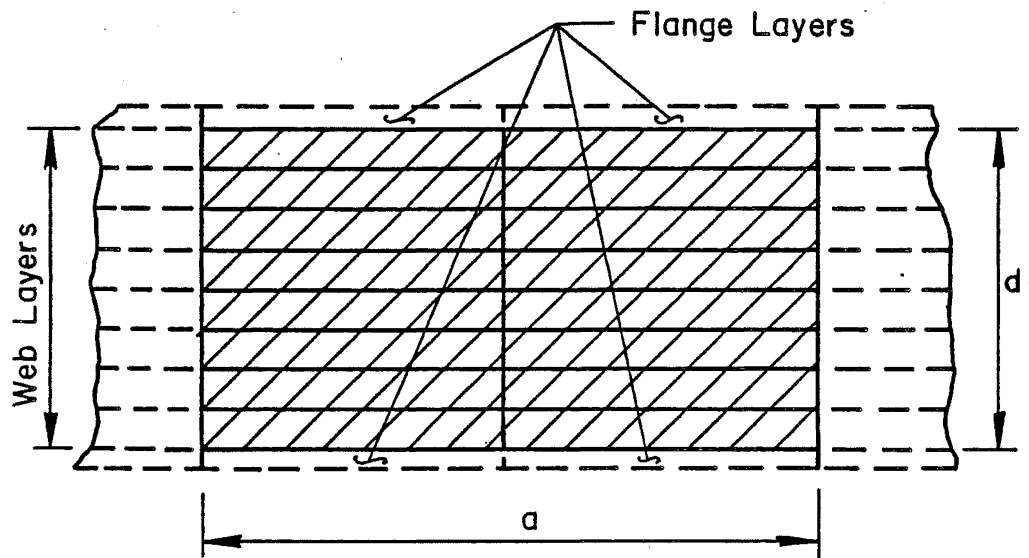


Fig. 10 Finite Element Idealization of Web Plate Panel

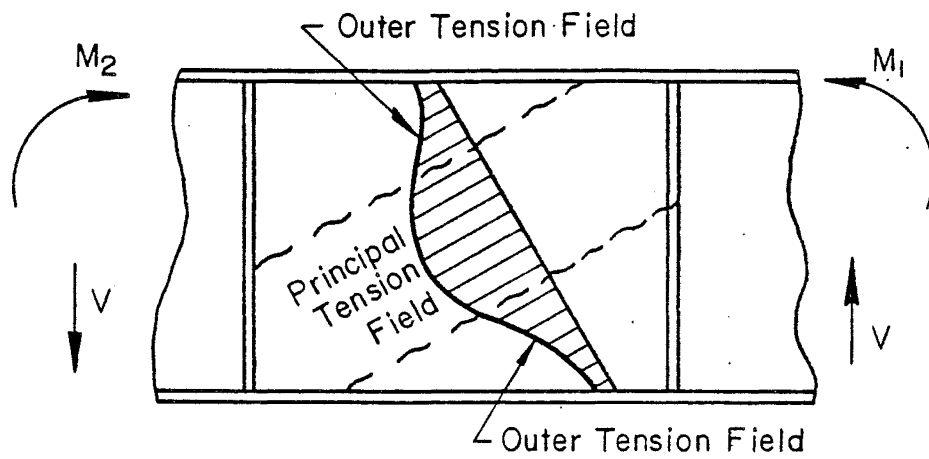


Fig. 11 Typical Transversely Stiffened Plate Girder Web Plate Panel Under Combined Moment and Shear

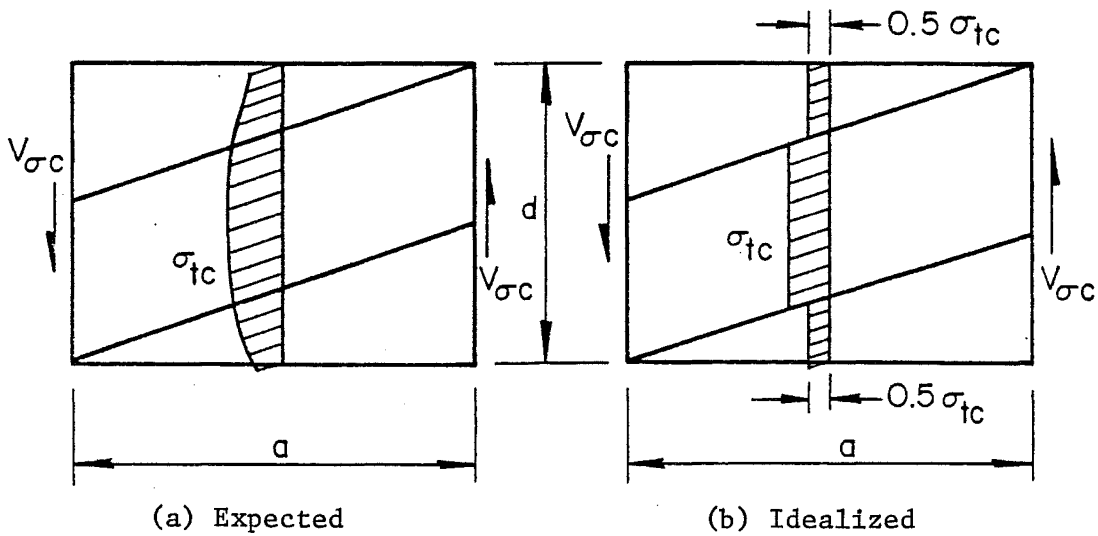


Fig. 12 Tension Field of Web Plate Panel

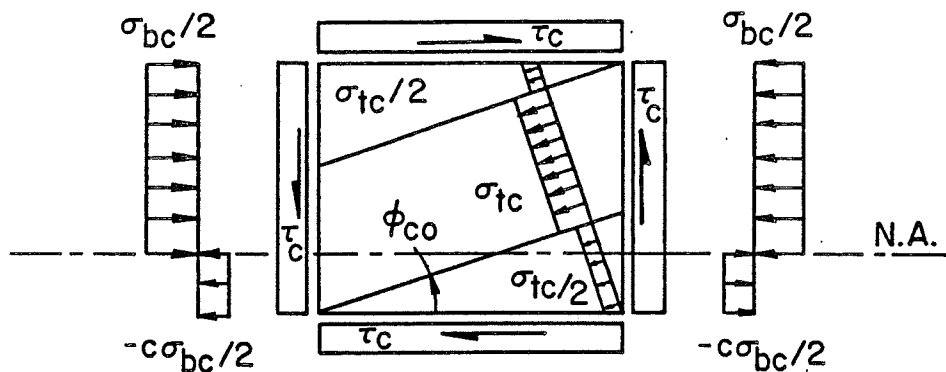


Fig. 13 Combined Buckling Stress State and Tension Field Stress State

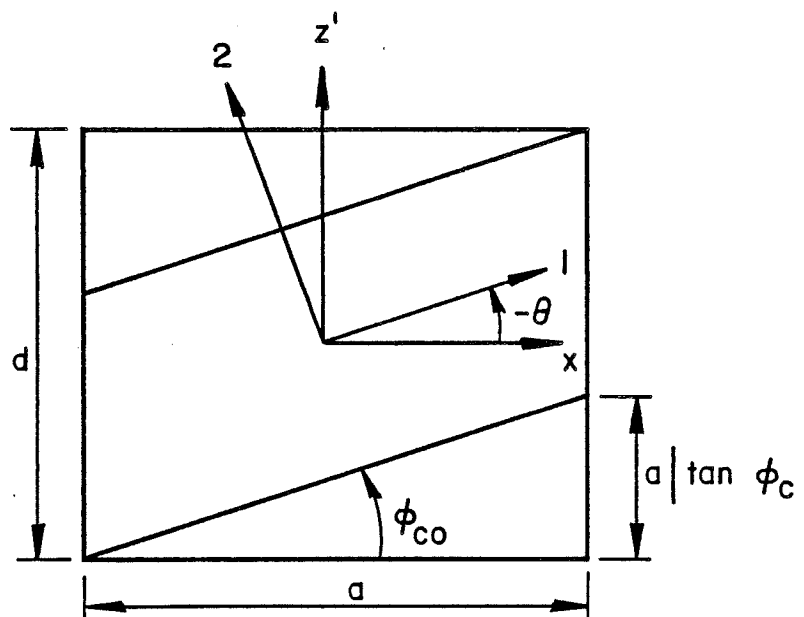


Fig. 14 Local Coordinate Axes and Tension Field Axes for Web Plate Panel

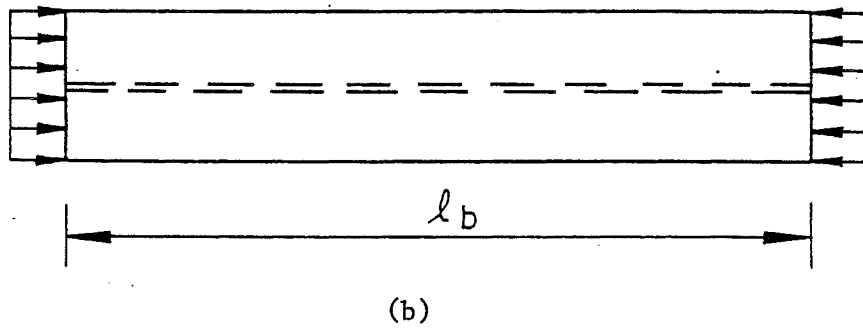
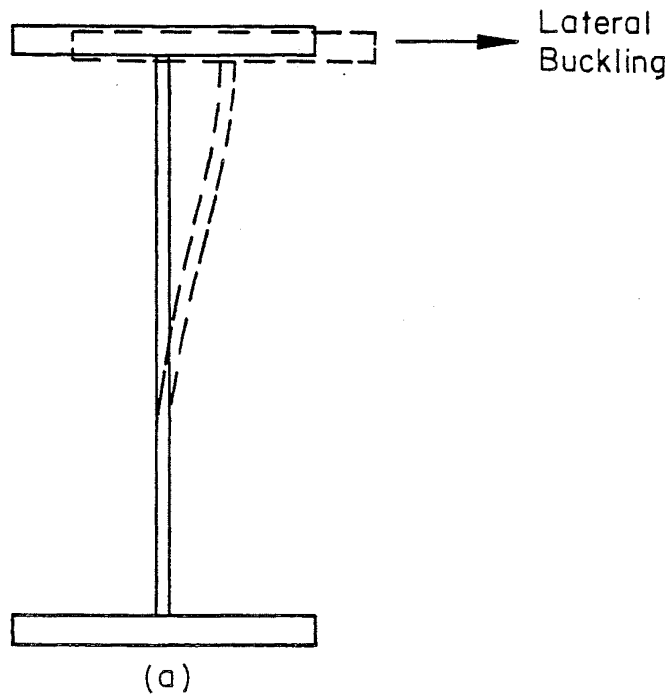


Fig. 15 Lateral Buckling of Plate Girder  
Compression Flanges

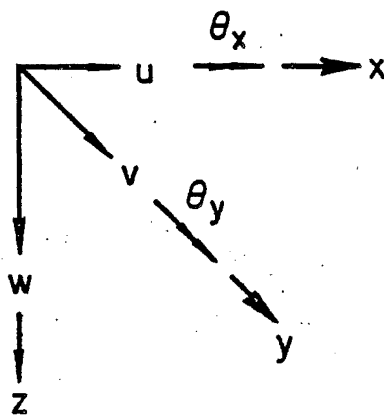
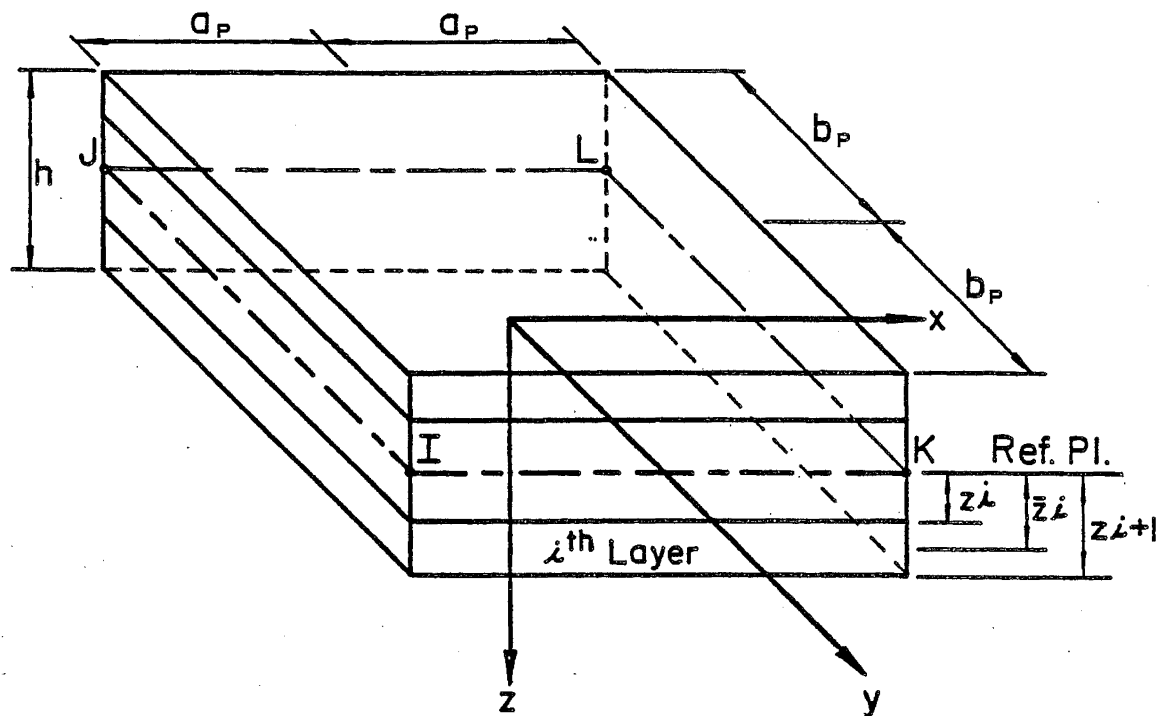


Fig. 16 Rectangular Slab Finite Element:  
Layering and Coordinate System

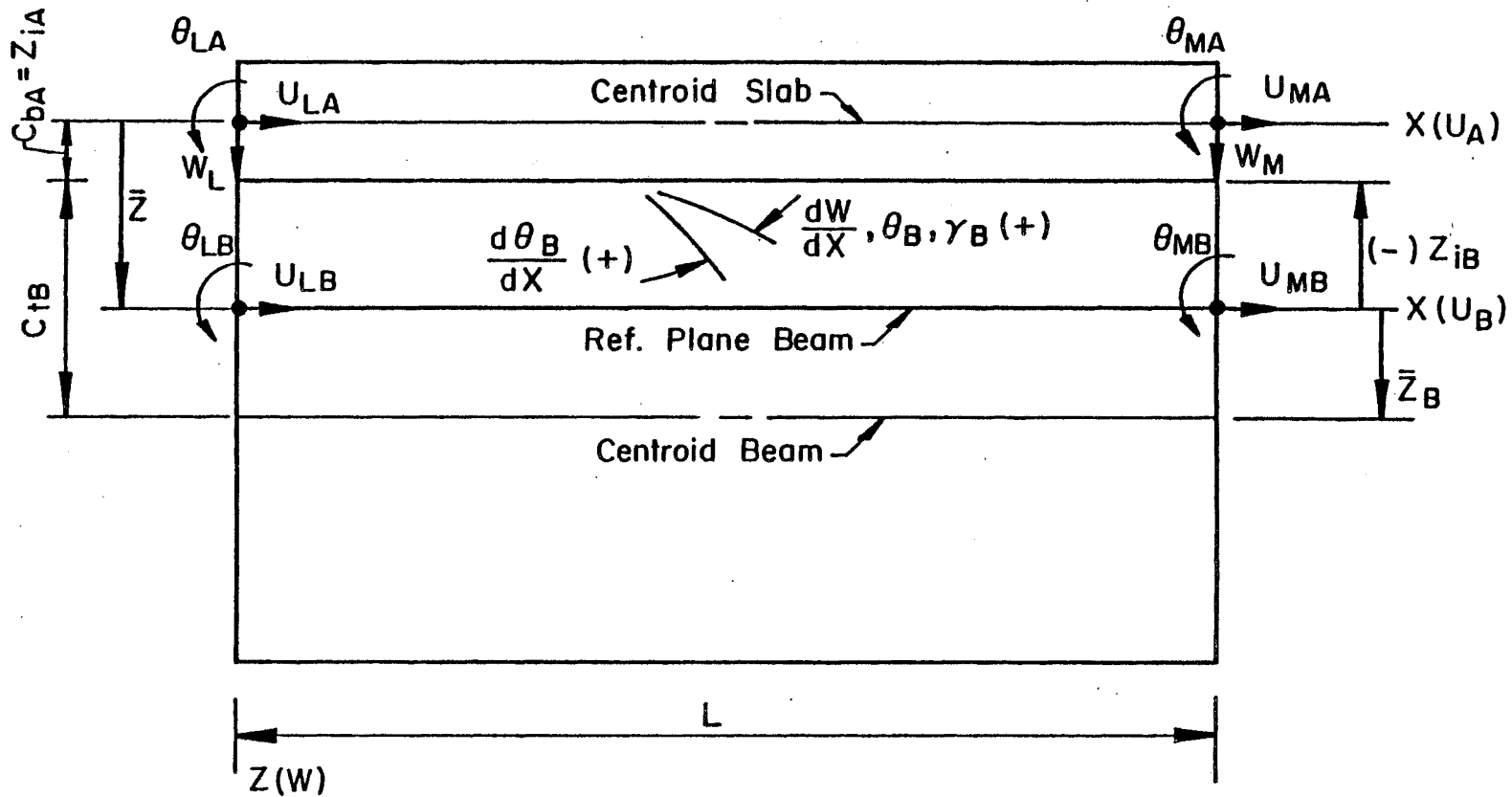


Fig. 17 Beam and Slab Element Node Point Deformations and Sign Conventions

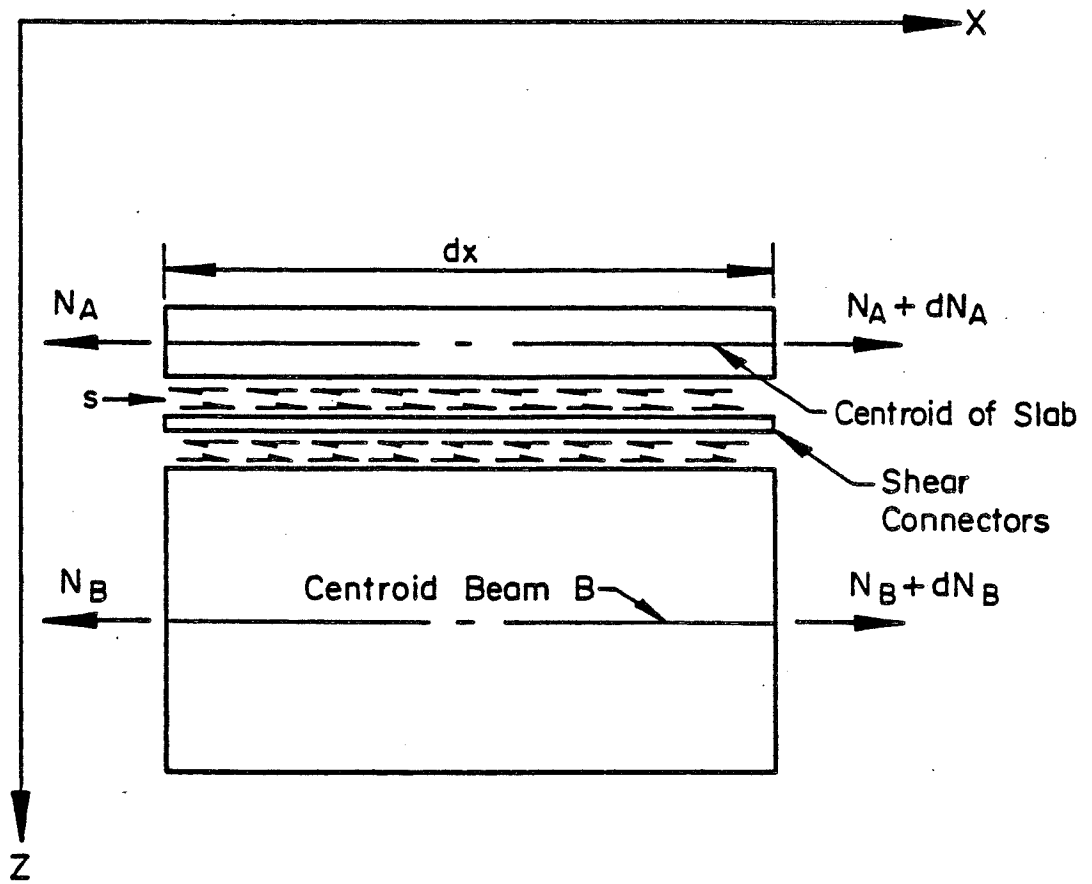


Fig. 18 Shear-Flow Equilibrium Diagram

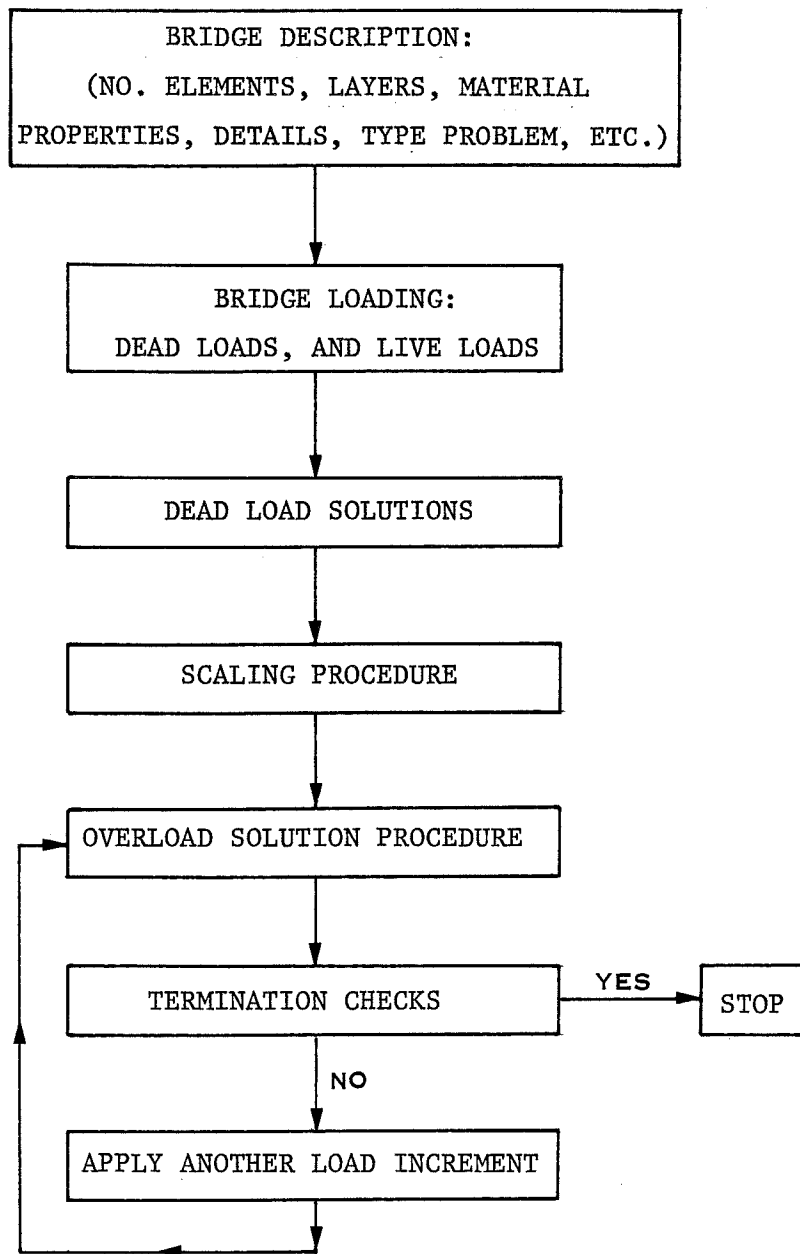


Fig. 19 Flow Chart BOVAS Solution Scheme

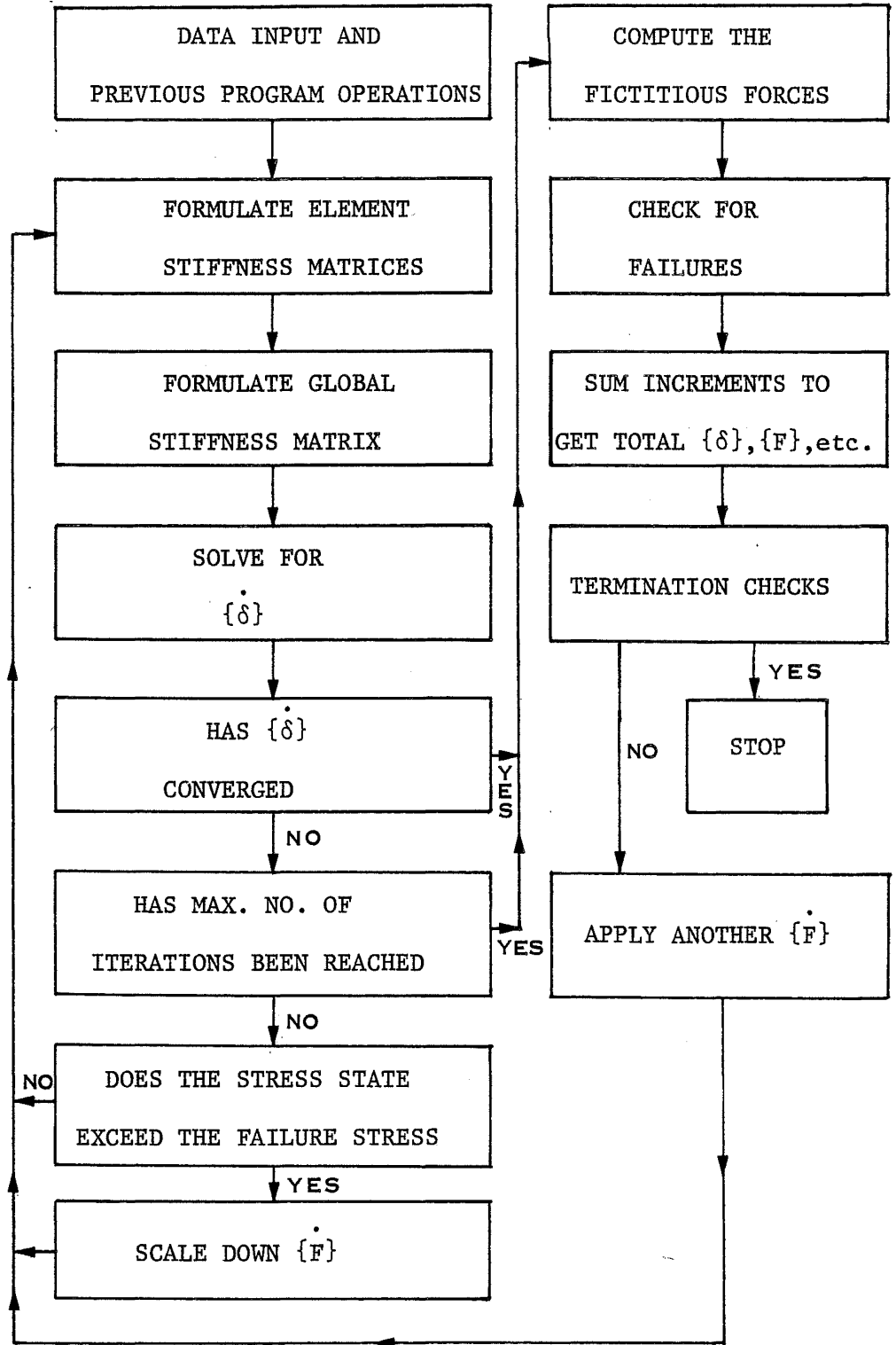


Fig. 20 Flow Chart BOVAS Overload Solution Process

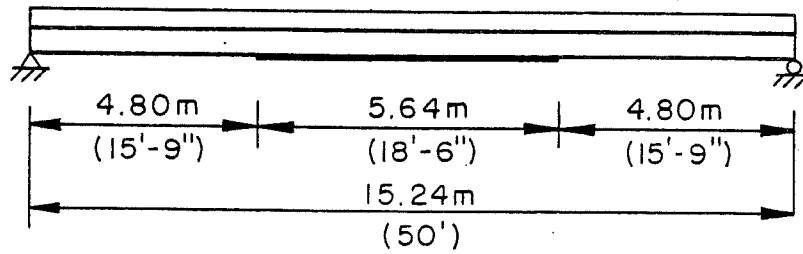


Fig. 21 Example No. 1 - Bridge 3B - Elevation

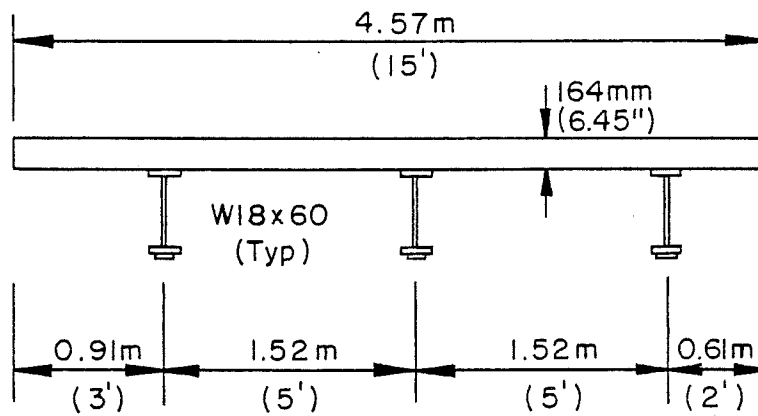


Fig. 22 Example No. 1 - Bridge 3B - Cross-section

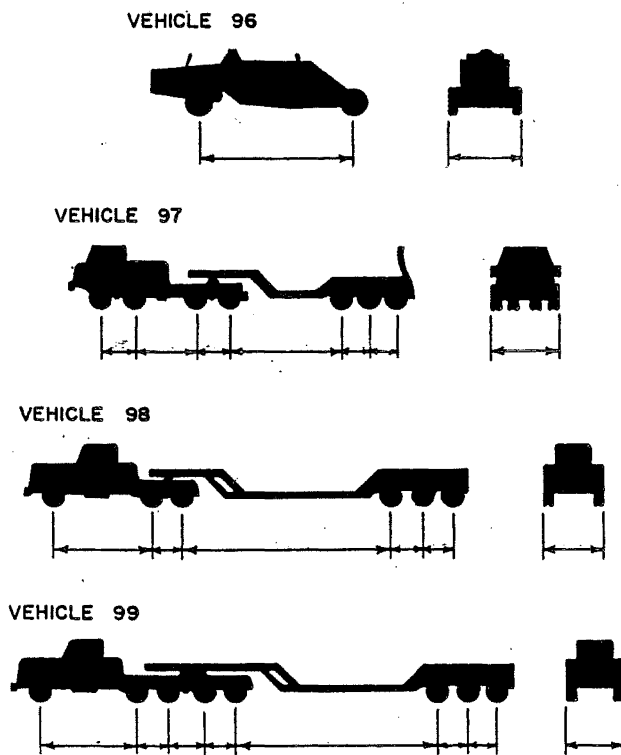


Fig. 23 Overloaded Test Vehicles - Example  
No. 1 (AASHTO Bridge 3B)

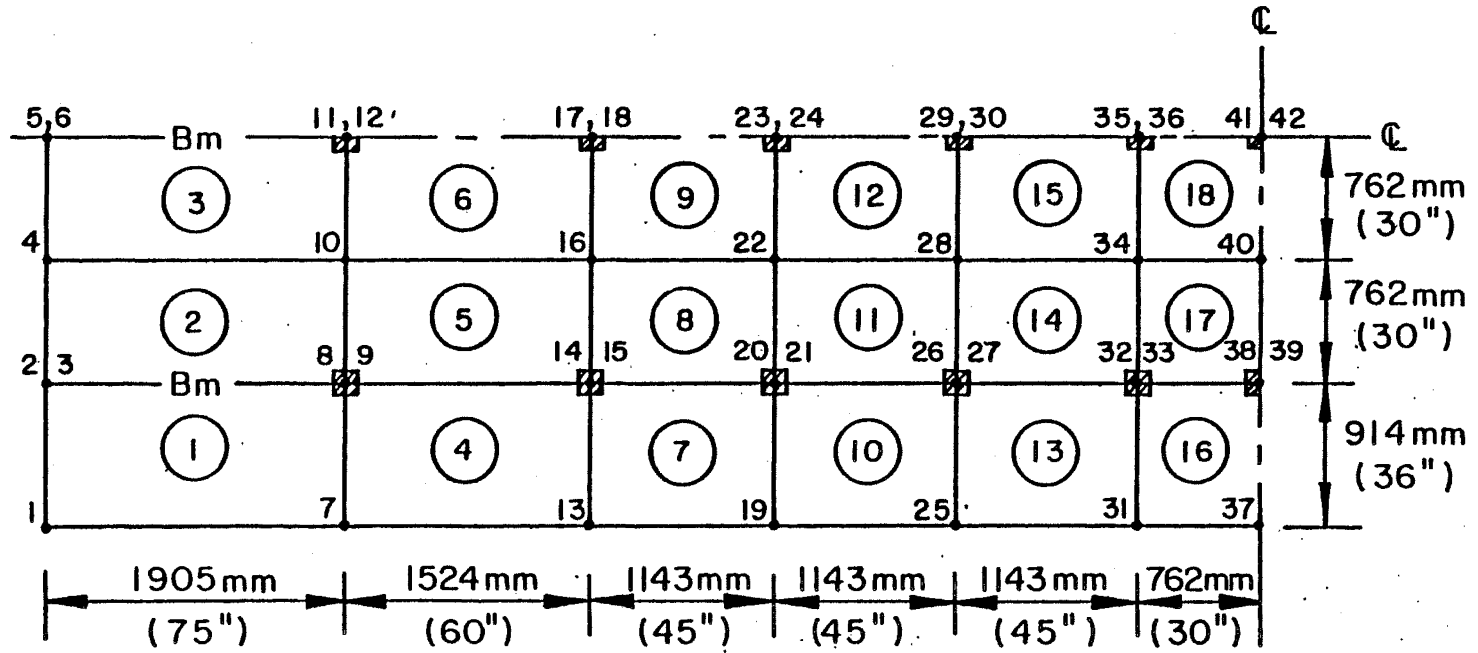


Fig. 24 Example No. 1 (AASHTO - Bridge 3B) - Finite Element Discretization



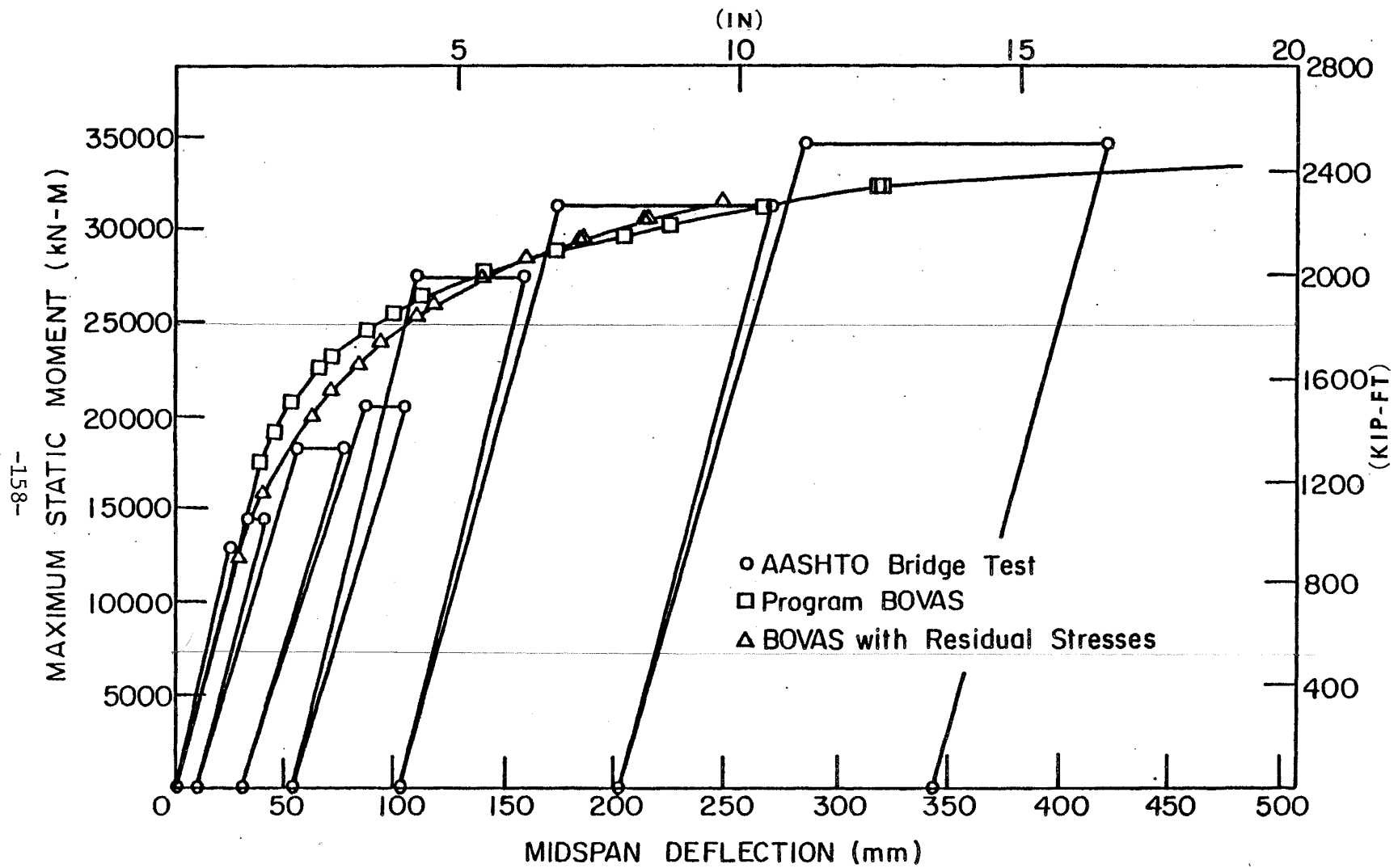
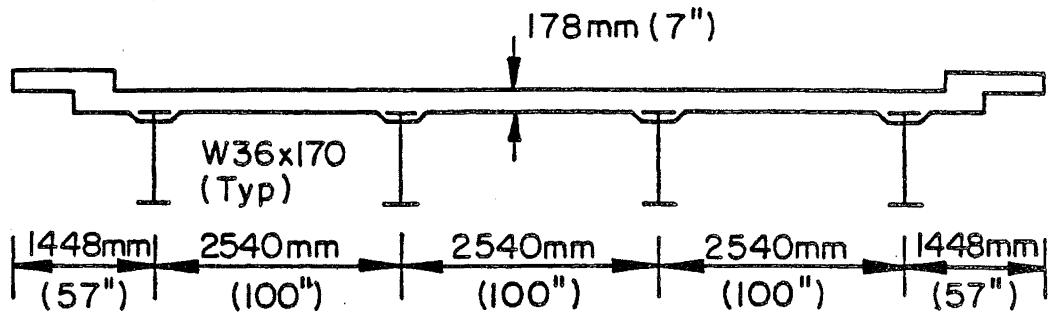
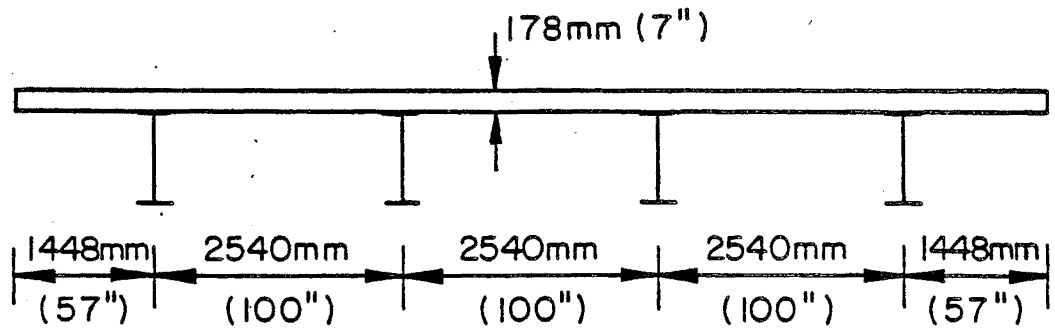


Fig. 26 Example No. 1 (AASHTO, Bridge 3B) - Moment versus Deflection Diagram

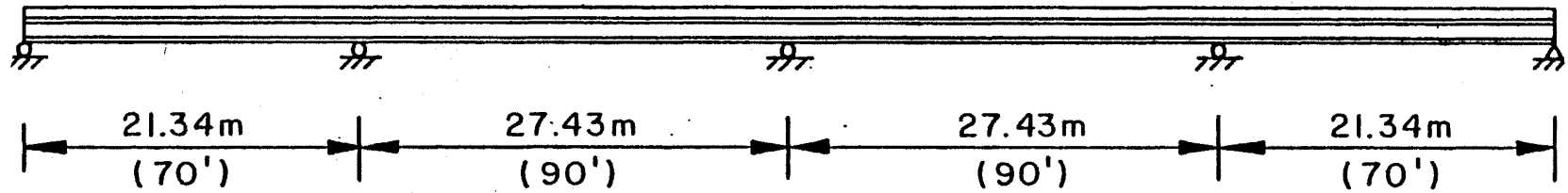


(a) Example No. 2 Actual Cross Section

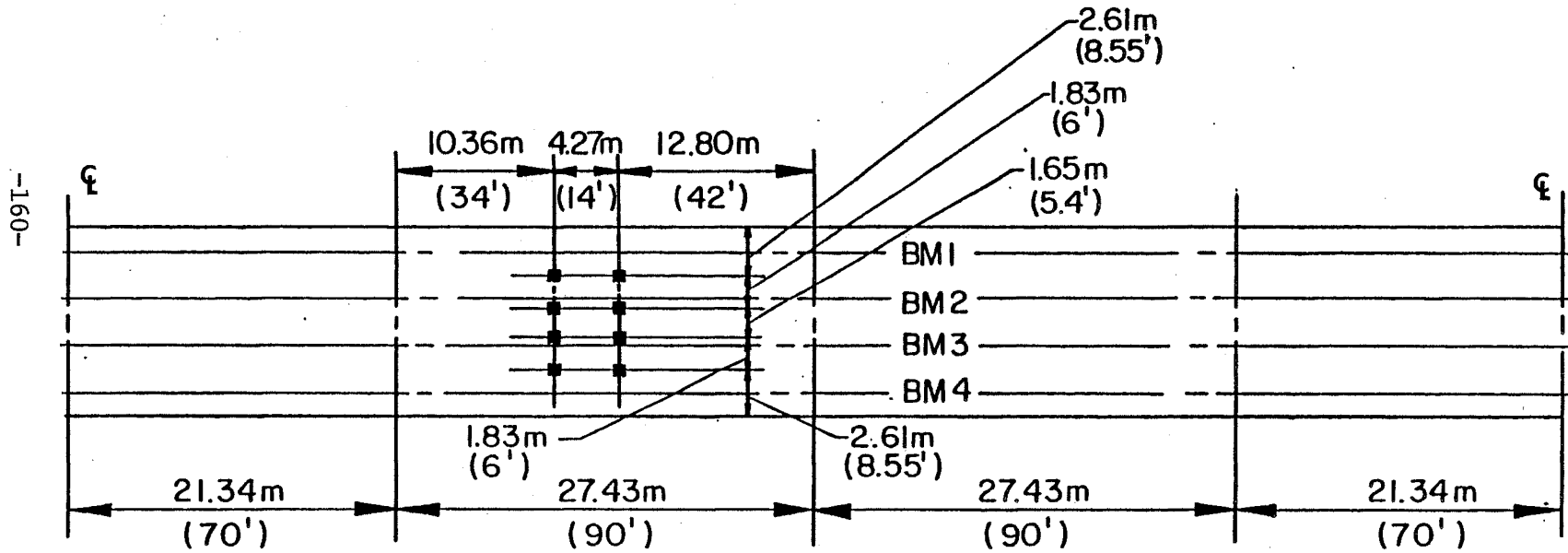


(b) Example No. 2 Idealized Cross Section

Fig. 27 Example No. 2 - Actual Cross-Section and Idealized Cross-Section



(a) Example No. 2 Elevation



(b) Example No. 2 Plan and Loading

Fig. 28 Example No. 2 - Elevation and Plan Views

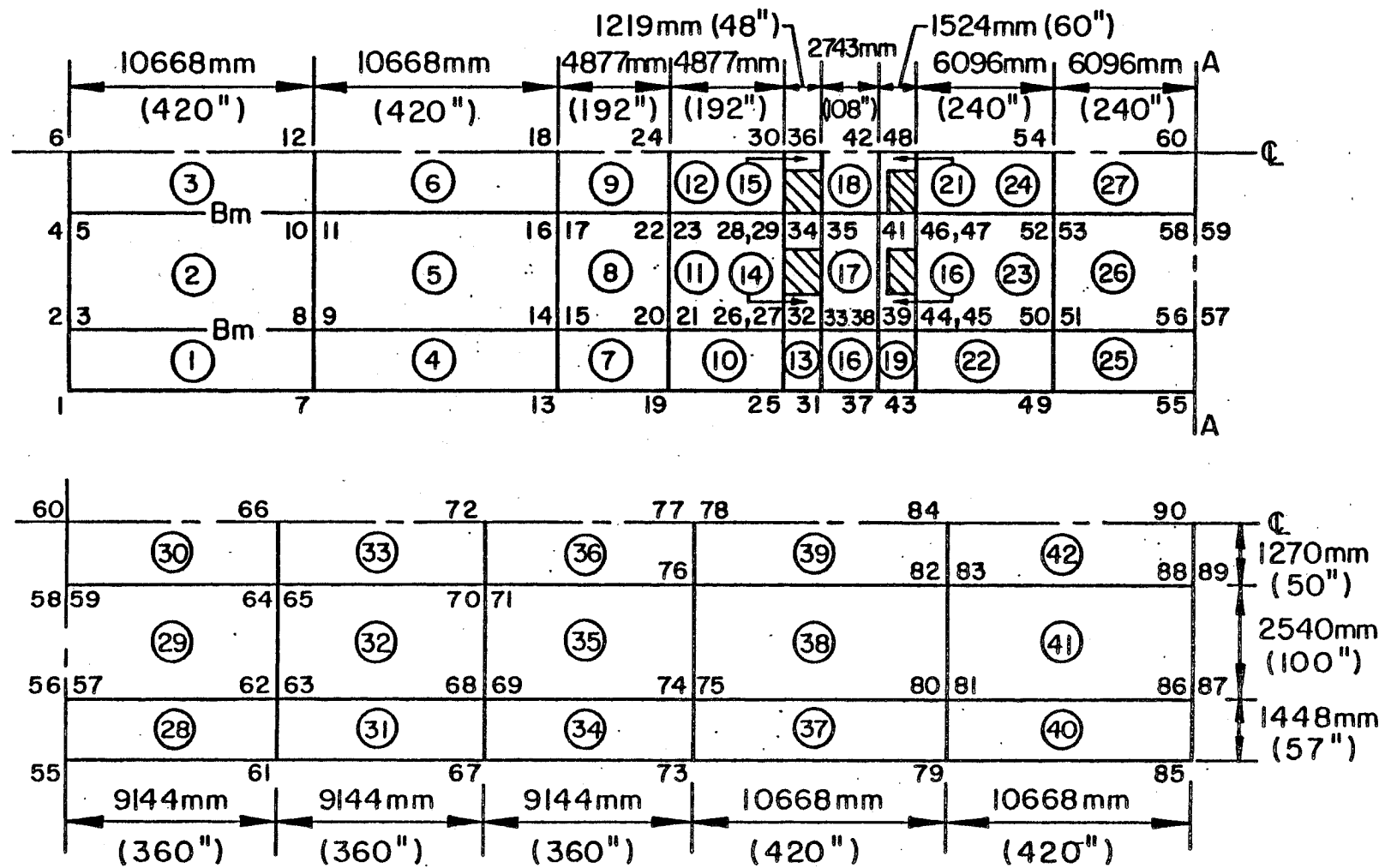


Fig. 29 Example No. 2 (University of Tennessee) - Finite Element Discretization

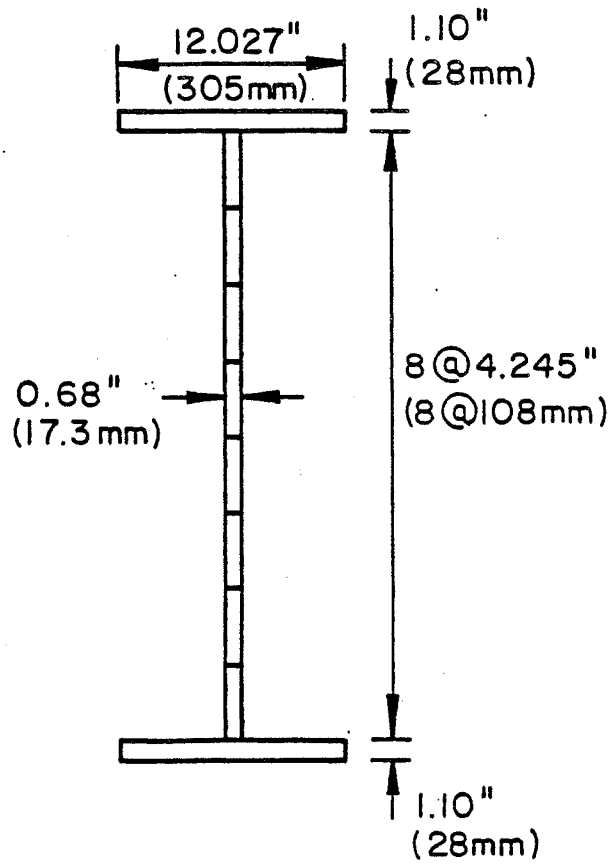
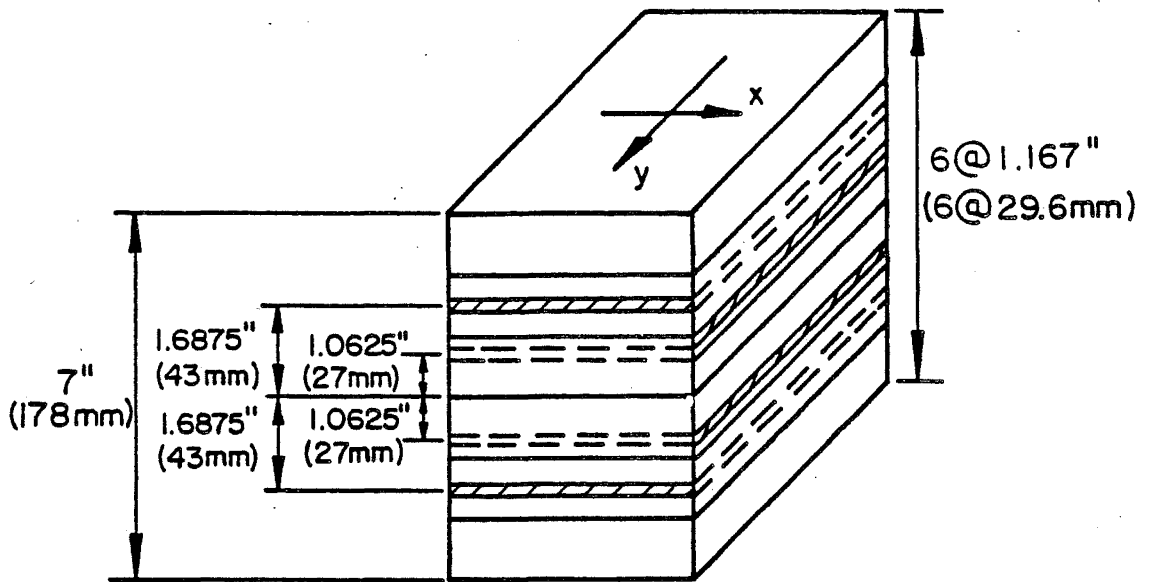


Fig. 30 Example No. 2 (University of Tennessee)  
 Slab and Beam Layering

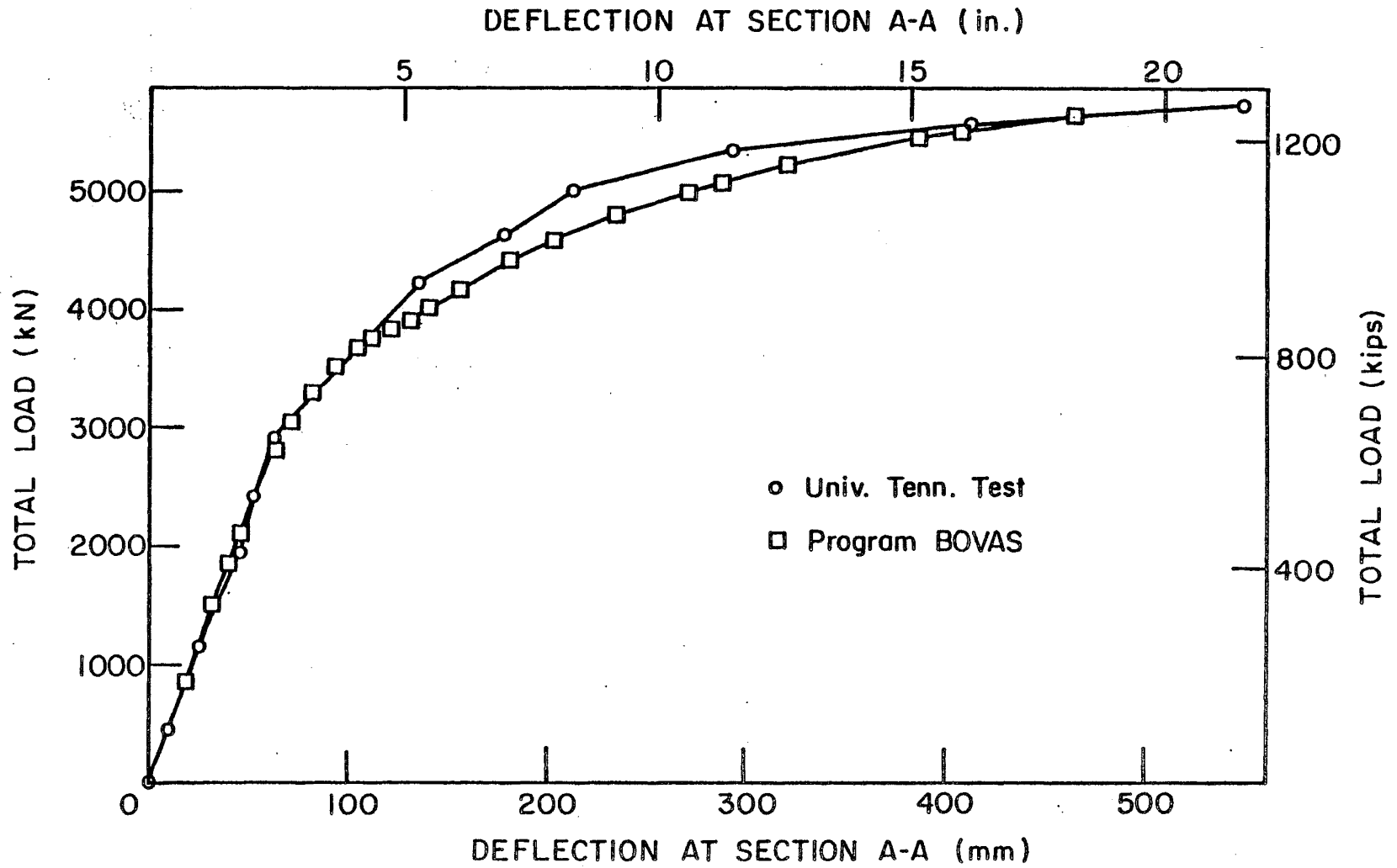
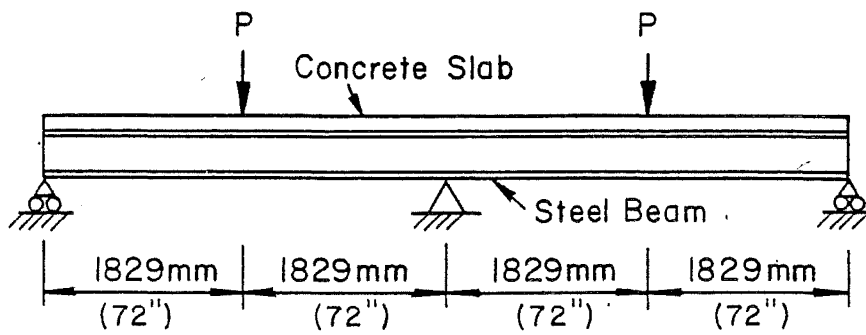
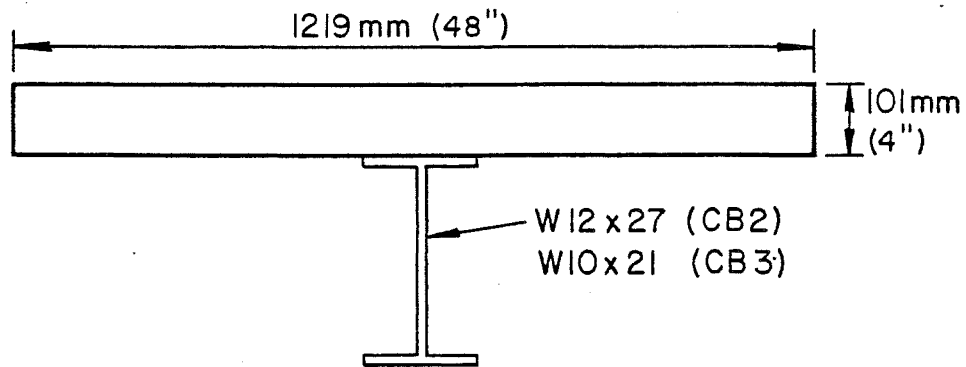


Fig. 31 Example No. 2 (University of Tennessee) - Load versus Deflection Curve



(a) Elevation



(b) Cross-section

Fig. 32 Example No. 3 - Test CB2 - University of Alberta

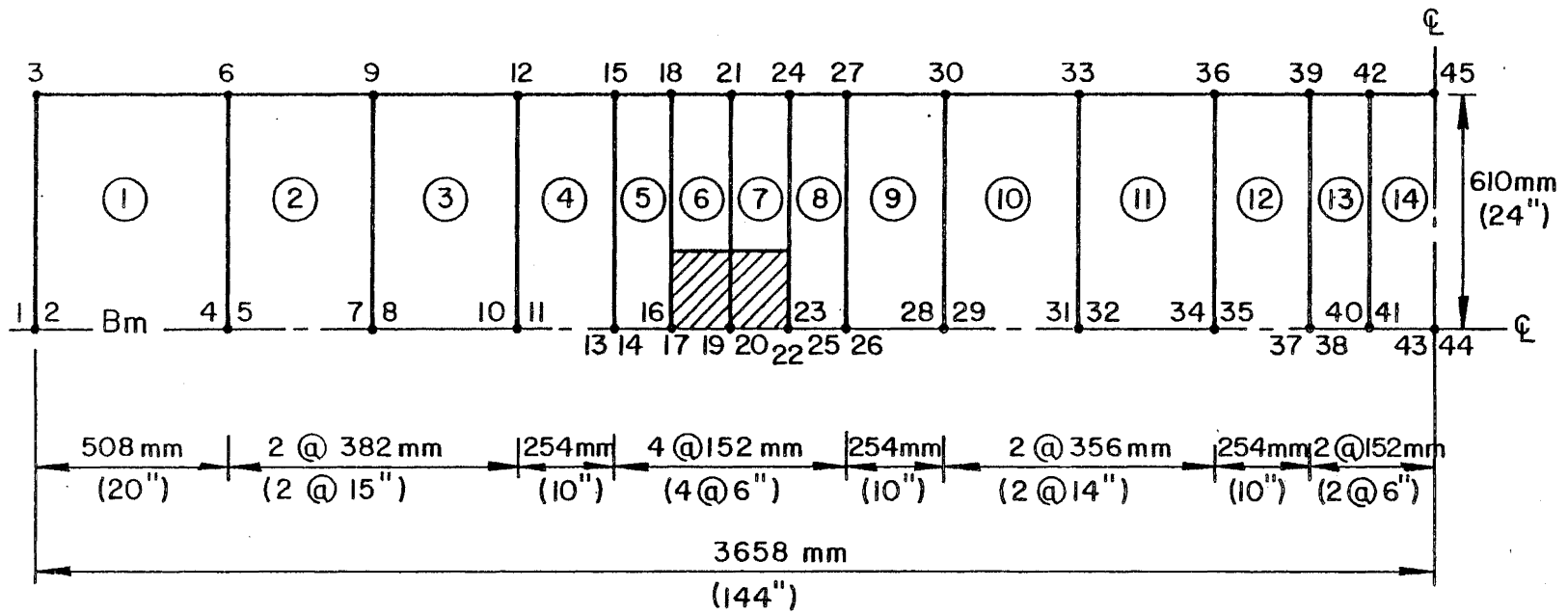


Fig. 33 Example No. 3 - Test CB2 - Finite Element Discretization

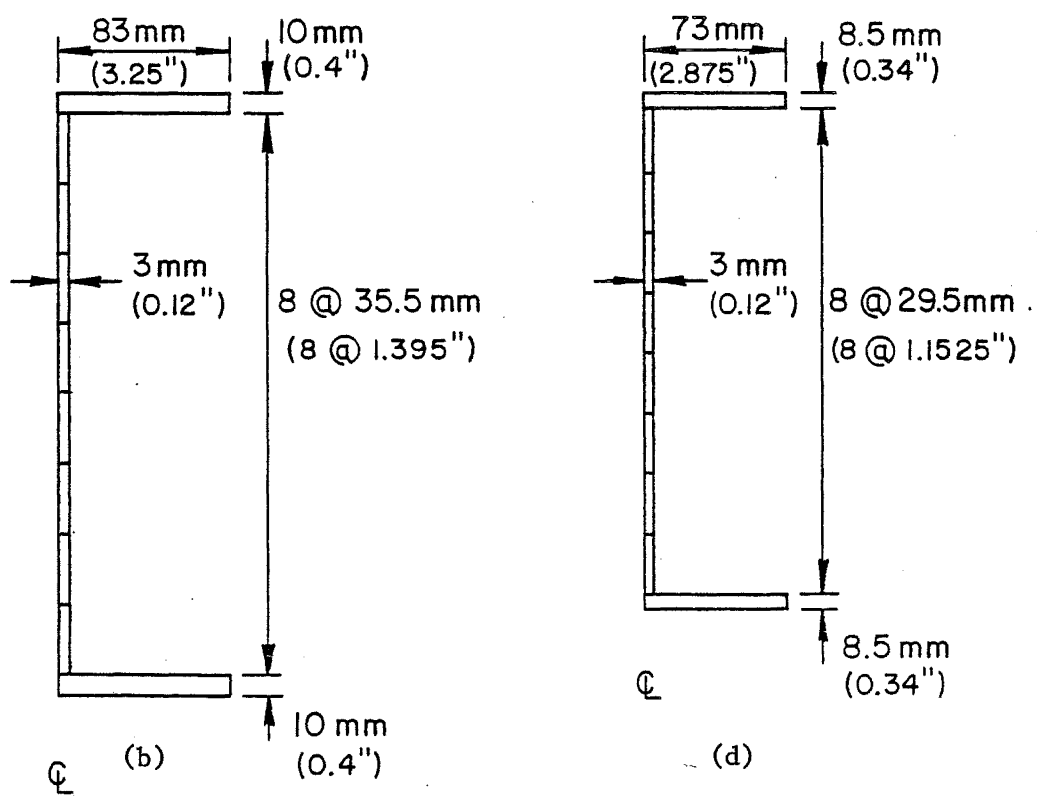
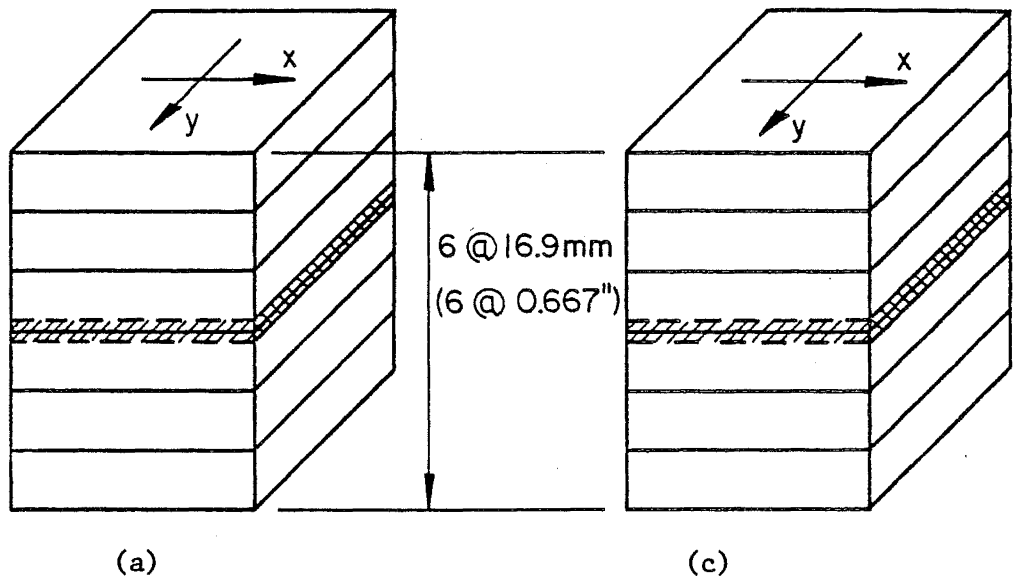


Fig. 34 Slab and Beam Layering - Test Beams CB2 and CB3

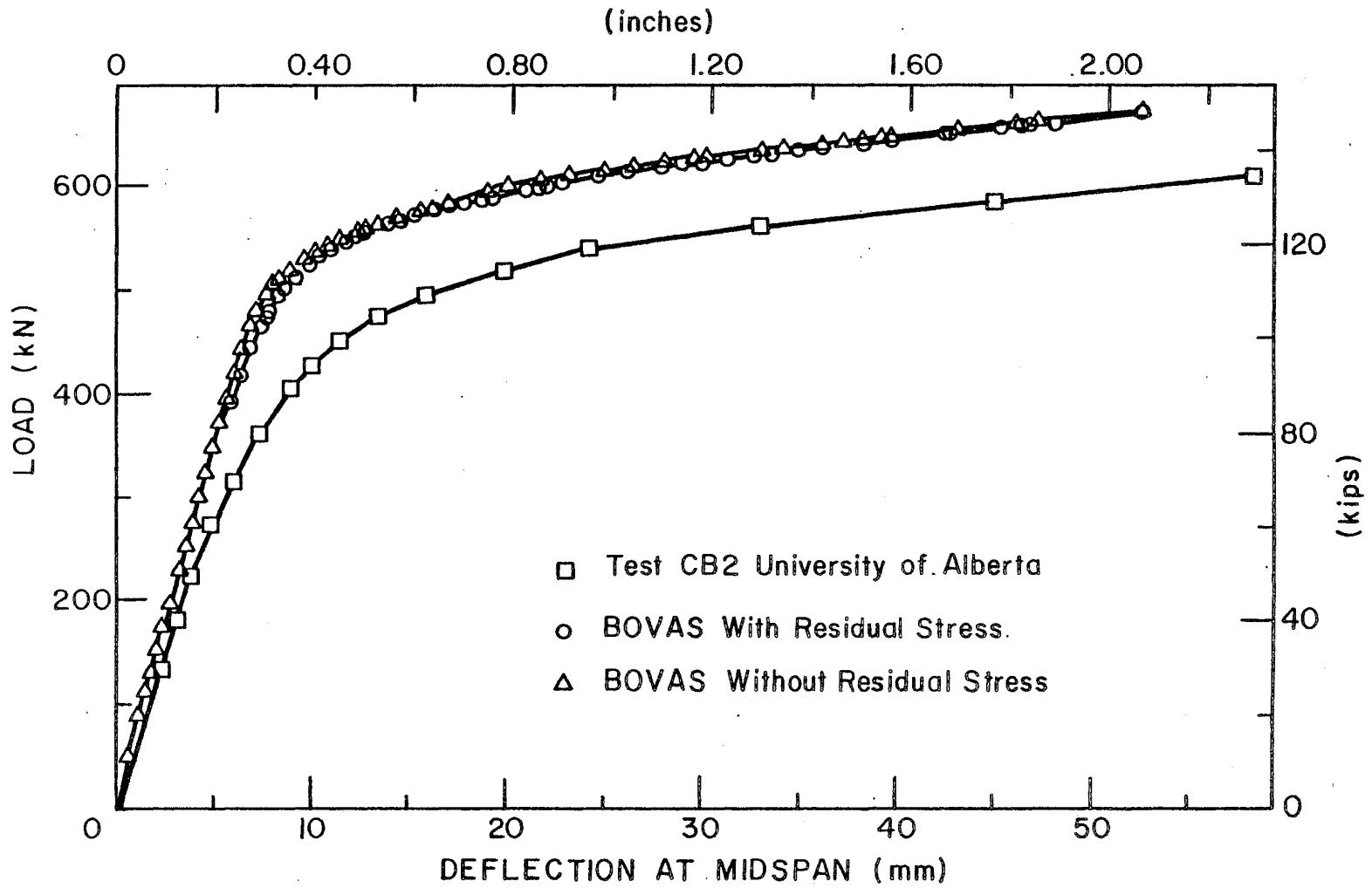


Fig. 35 Load versus Deflection Diagram Test CB2

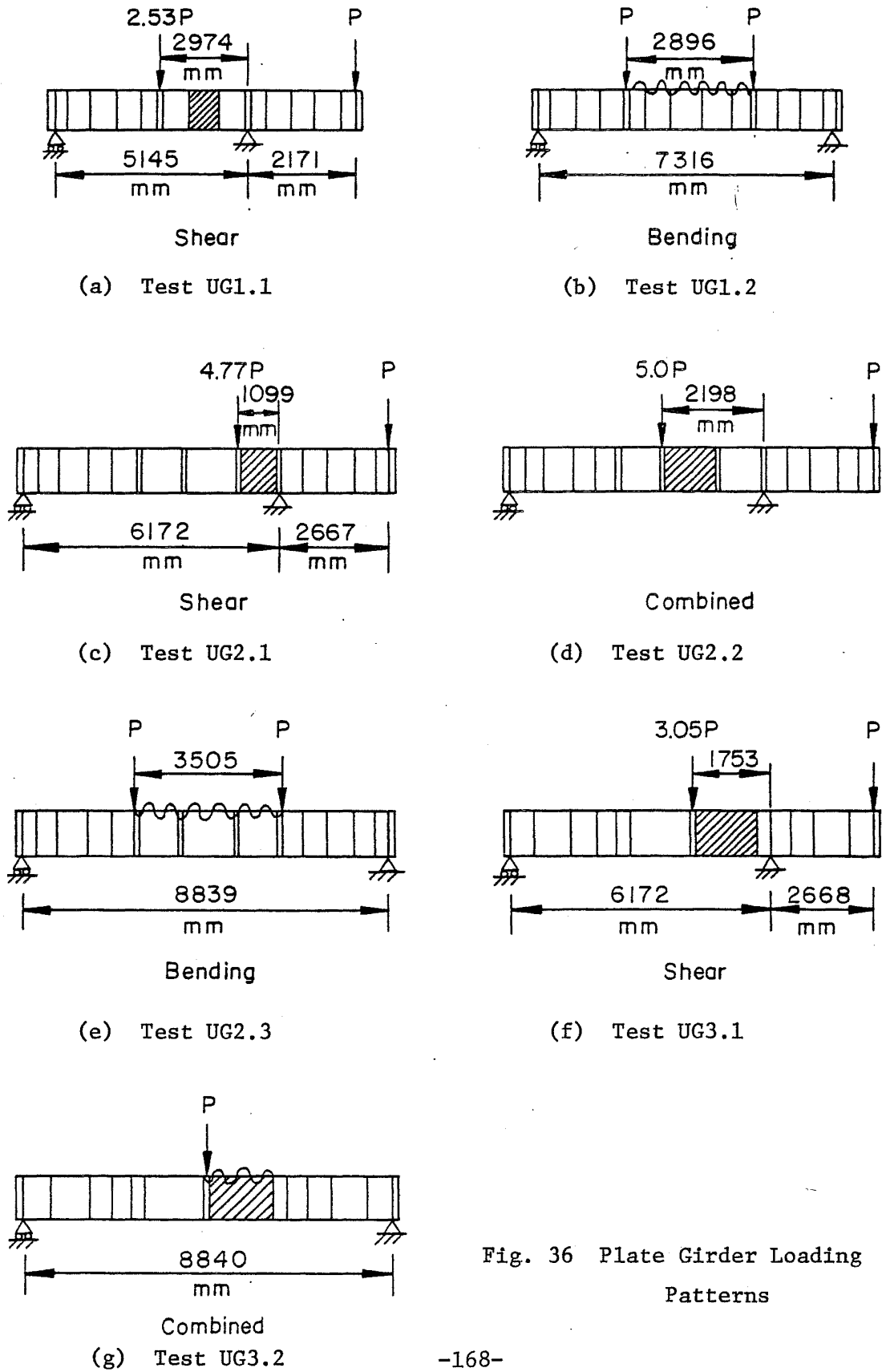
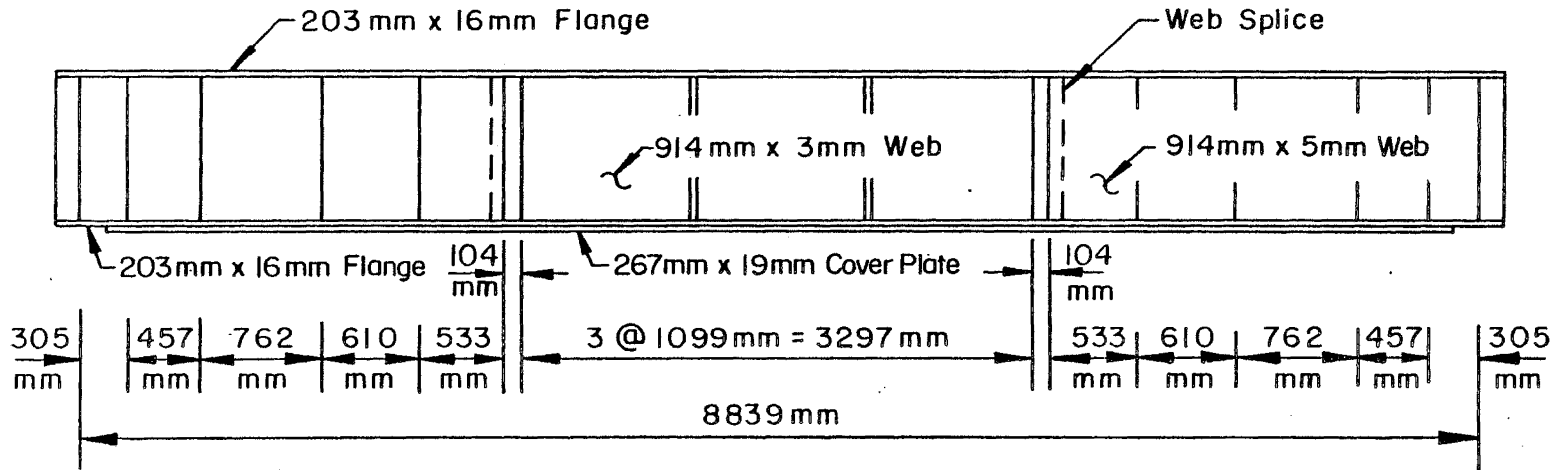
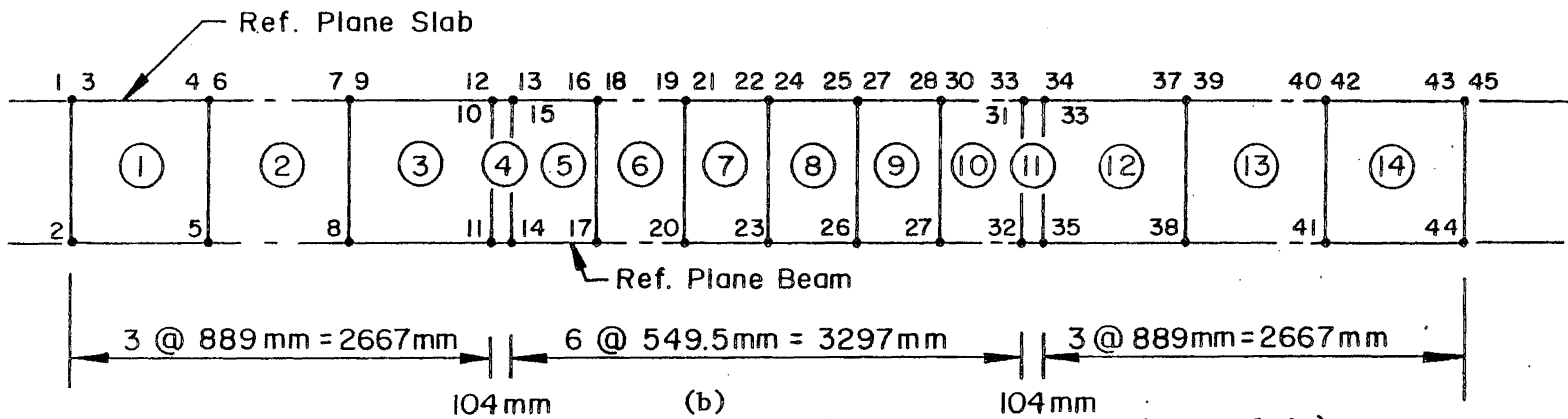


Fig. 36 Plate Girder Loading Patterns



(a)



(b)

Fig. 37 Test Girder UG2 and Finite Element Discretization (Note: 25.4 mm = 1 in)

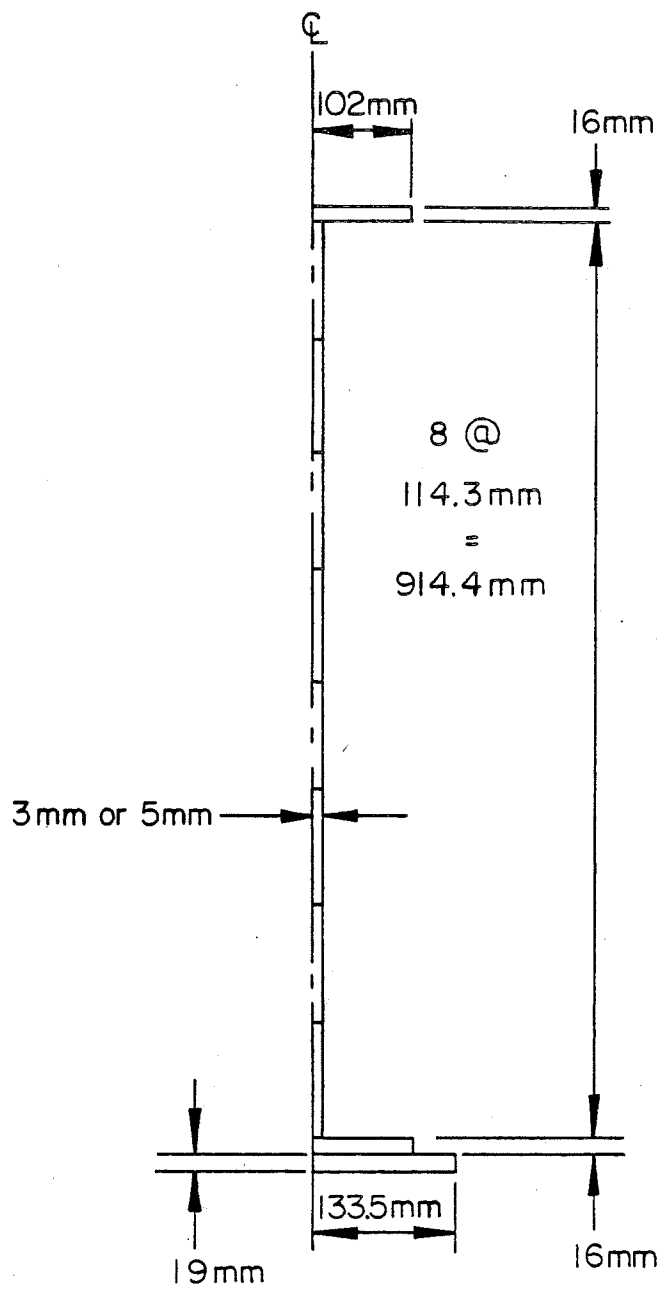


Fig. 38 Girder UG2 Beam Layering

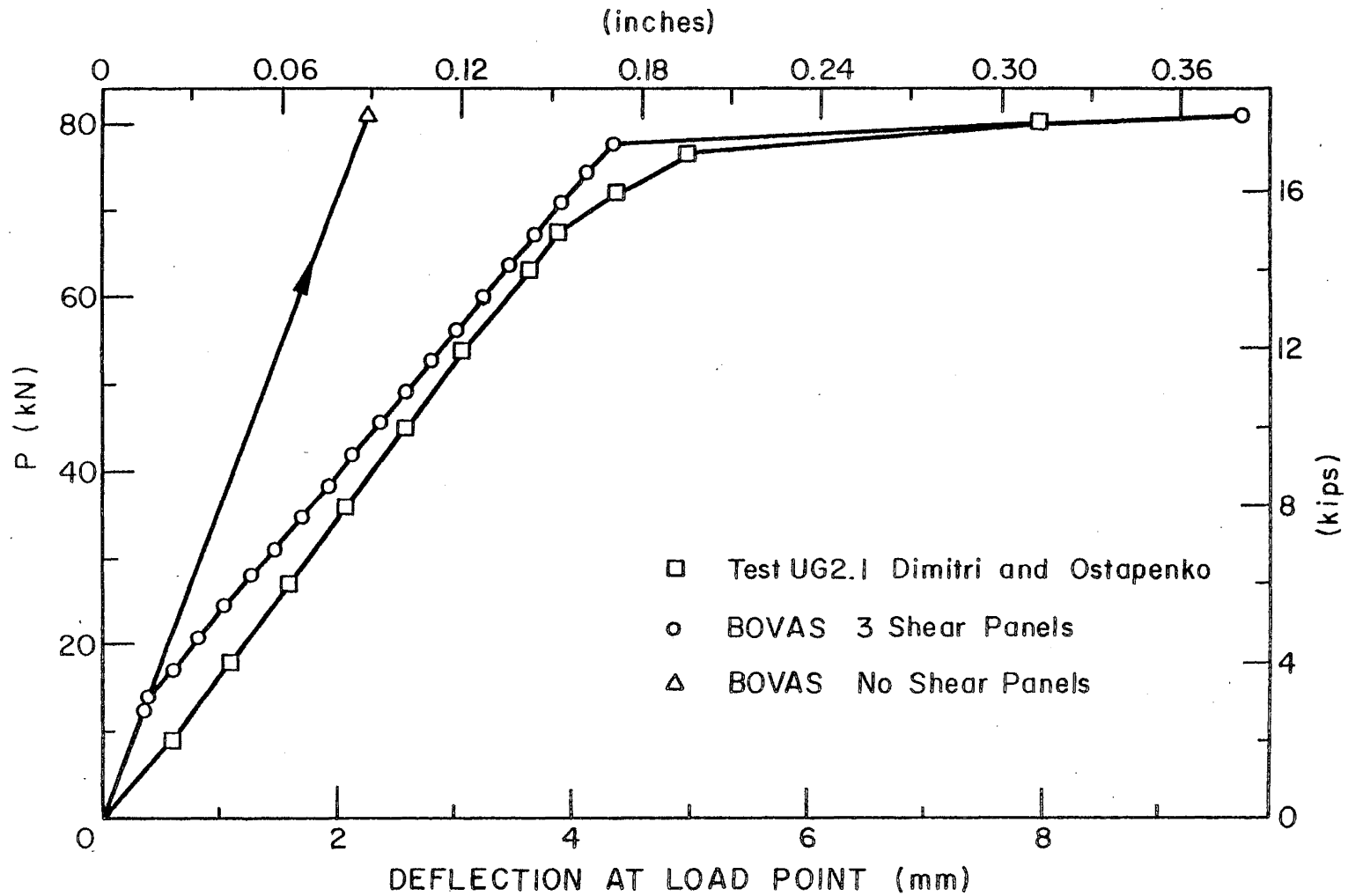


Fig. 39 Load versus Deflection Diagram - Test UG2.1 (Note: No Shear Panel Curve is Linear to 448.7 kN and 12.8 mm)

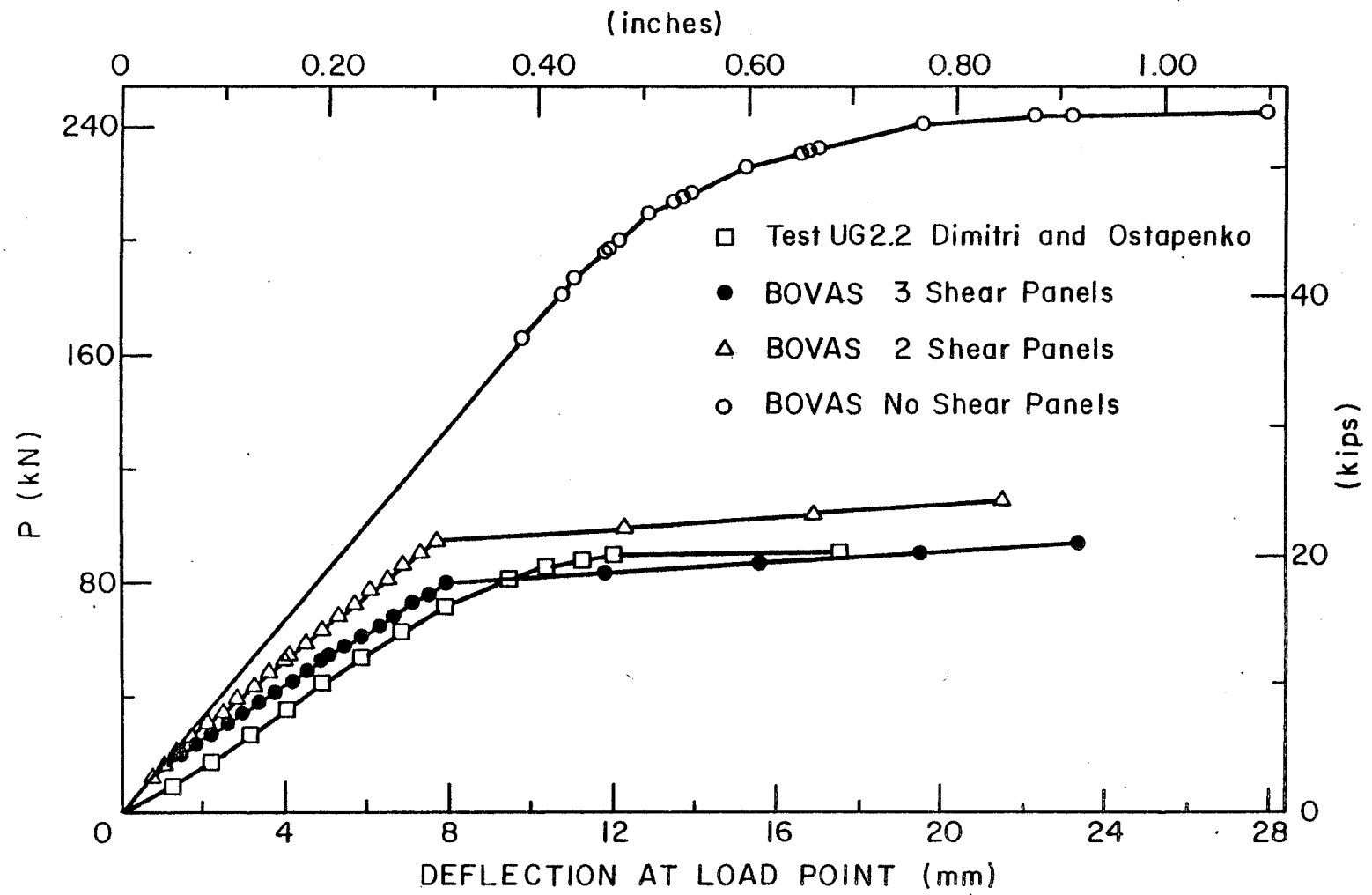


Fig. 40 Load versus Deflection Diagram - Test UG2.2

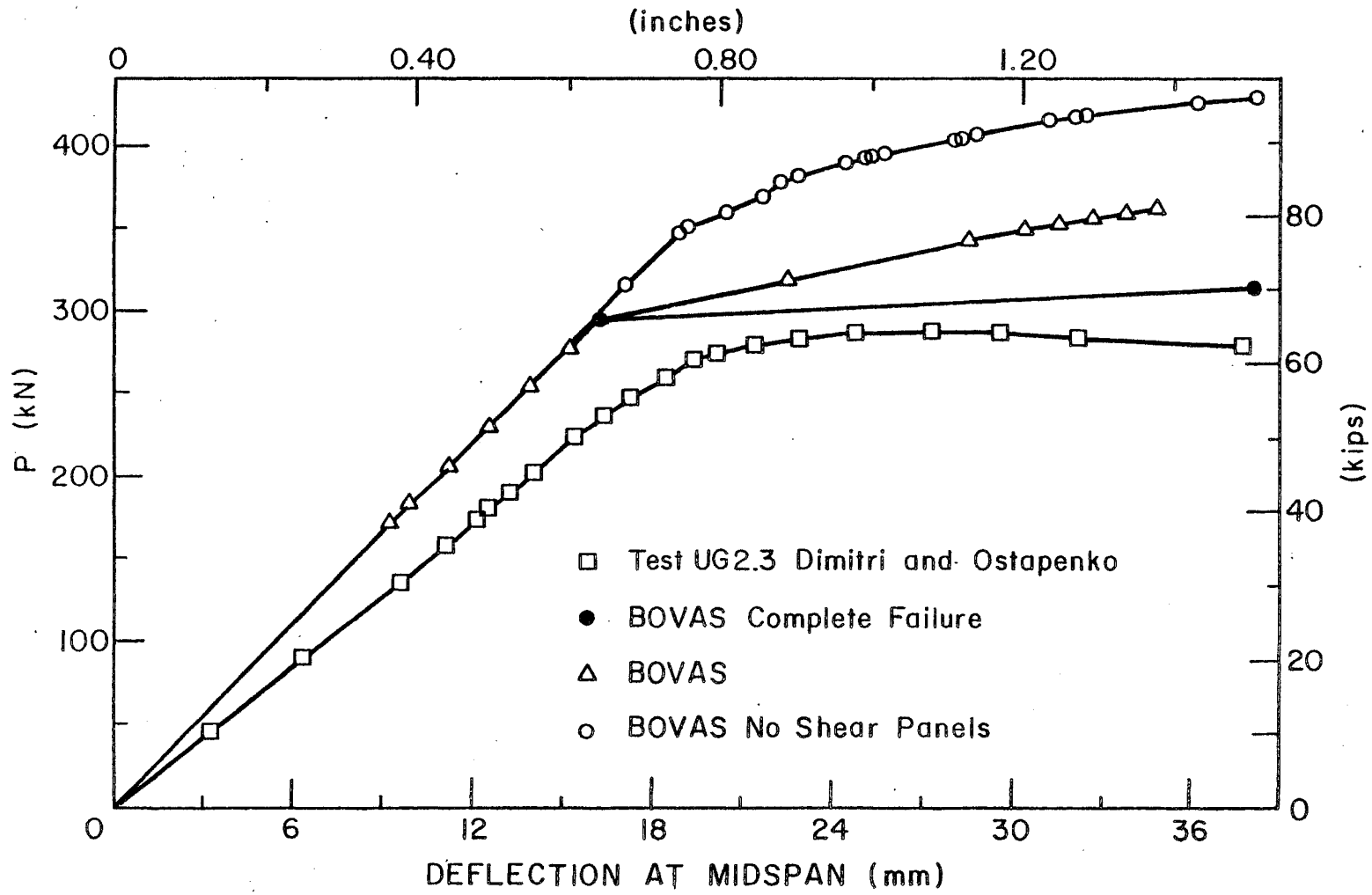
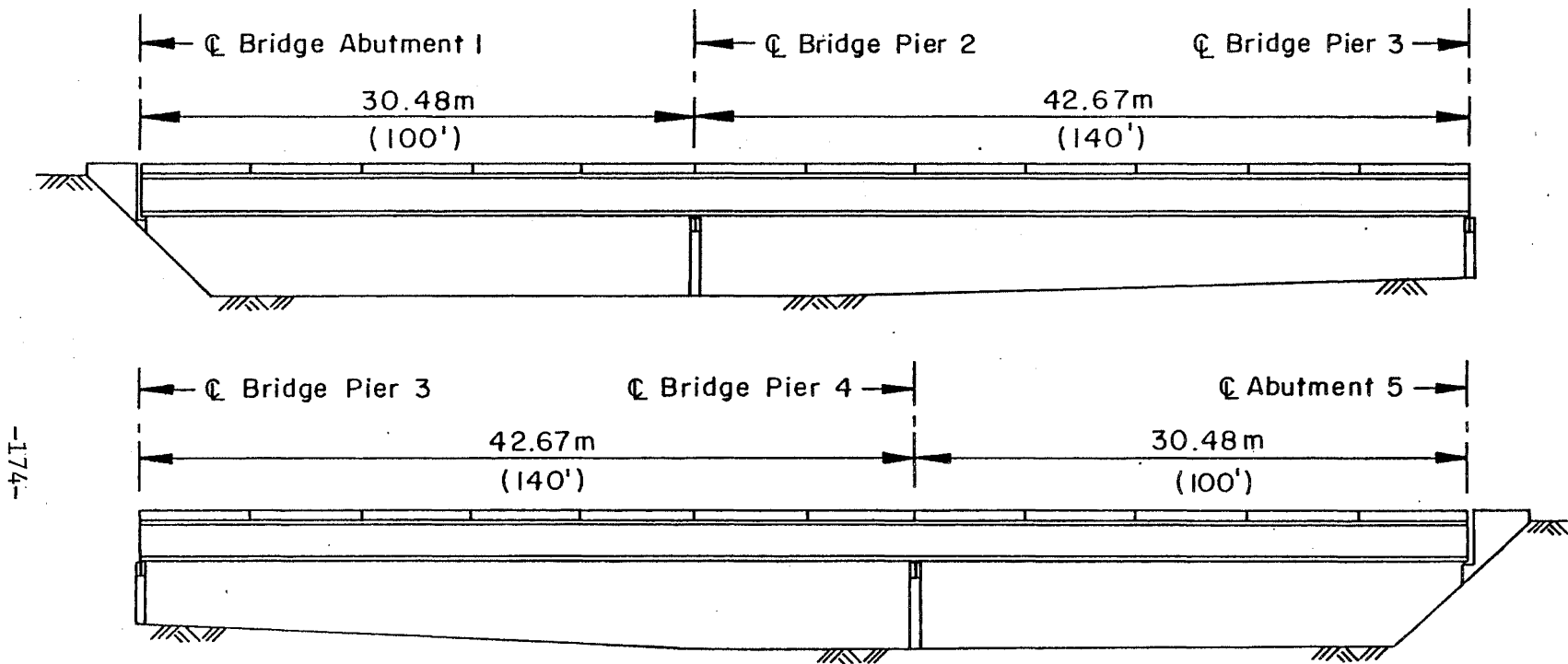


Fig. 41 Load versus Deflection Diagram - Test UG2.3



-174-

Fig. 42 FHWA Four-Span Continuous Plate Girder Bridge - Elevation

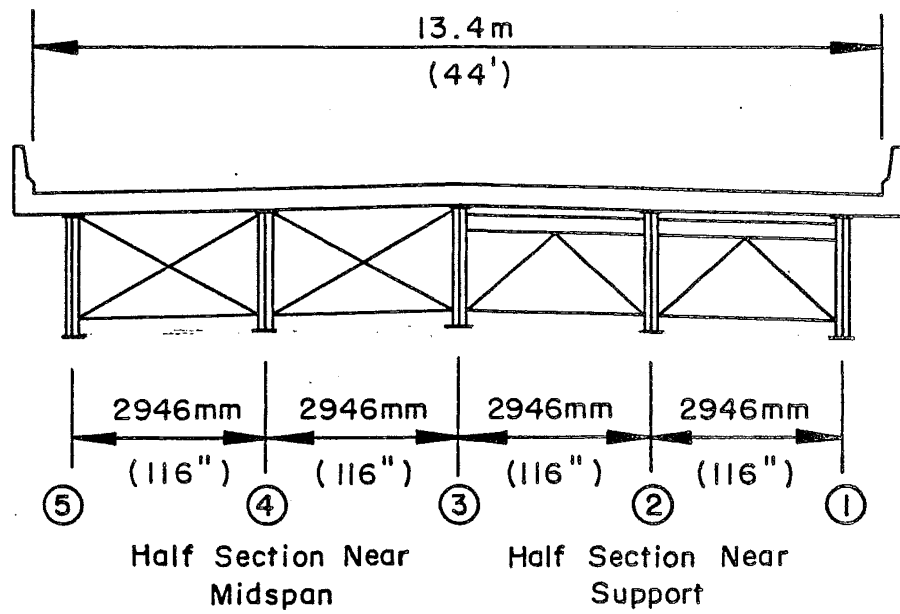


Fig. 43 FHWA Four-Span Cross-Section

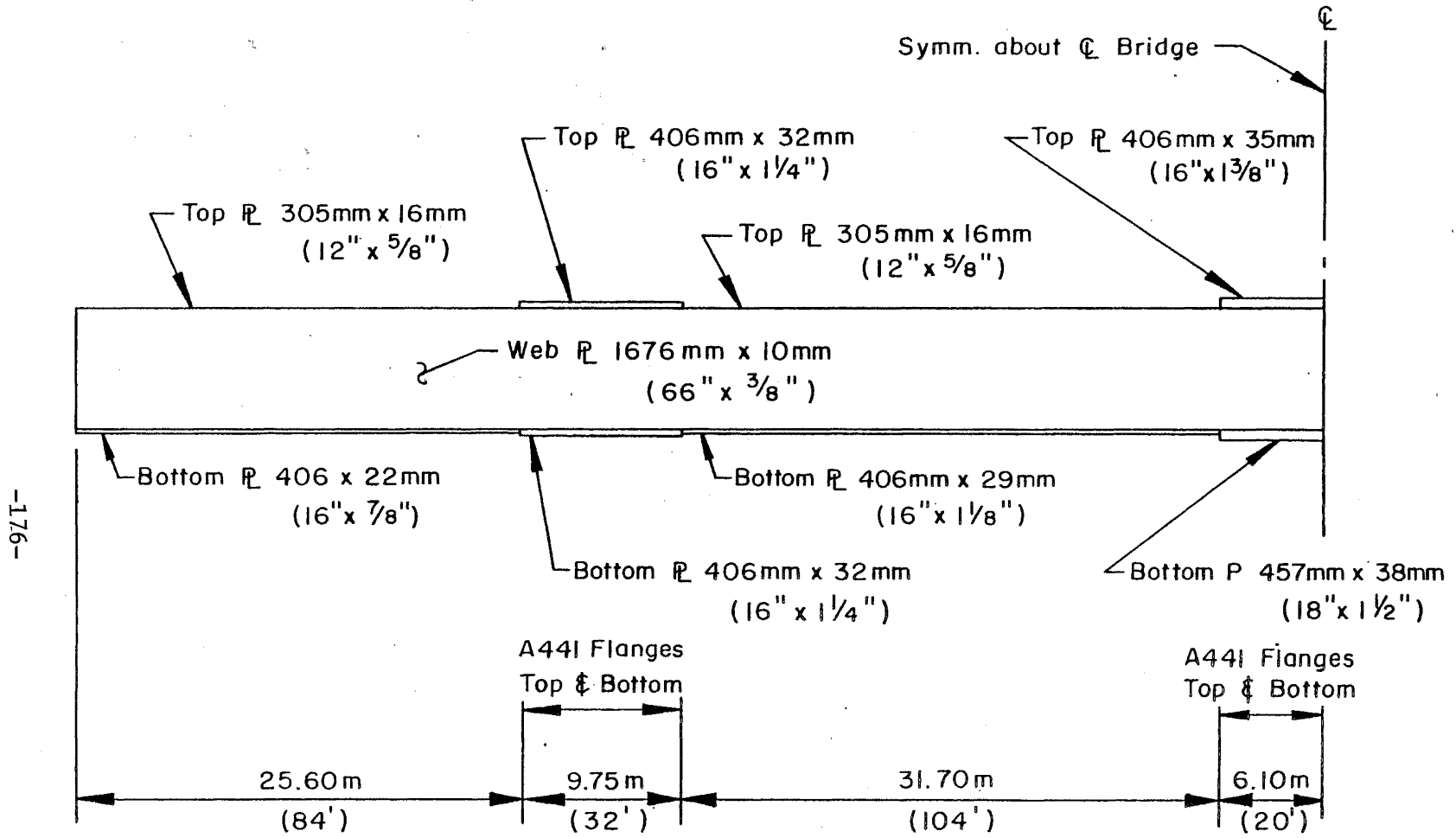


Fig. 44 FHWA Four-Span Plate Girder - Elevation

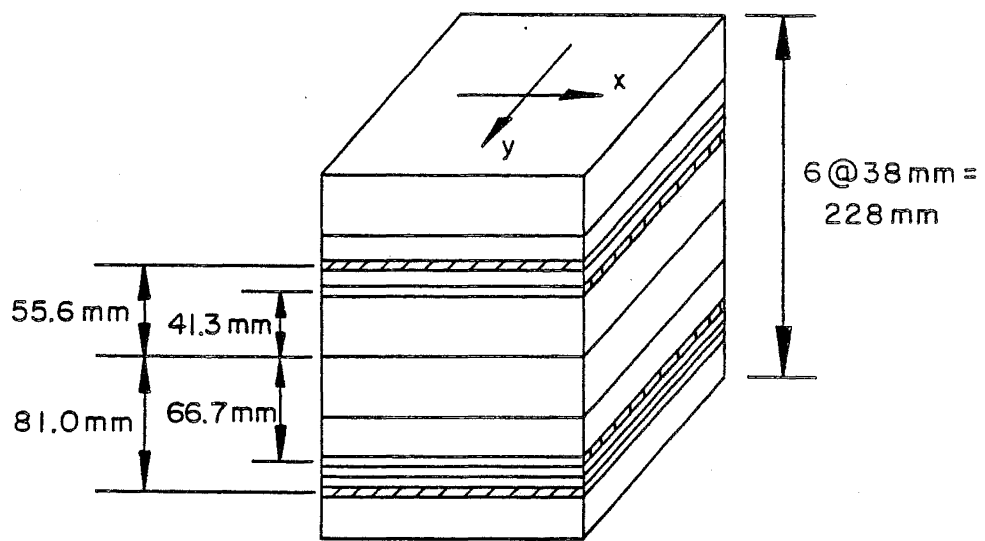


Fig. 45 FHWA Four-Span - Slab Layering

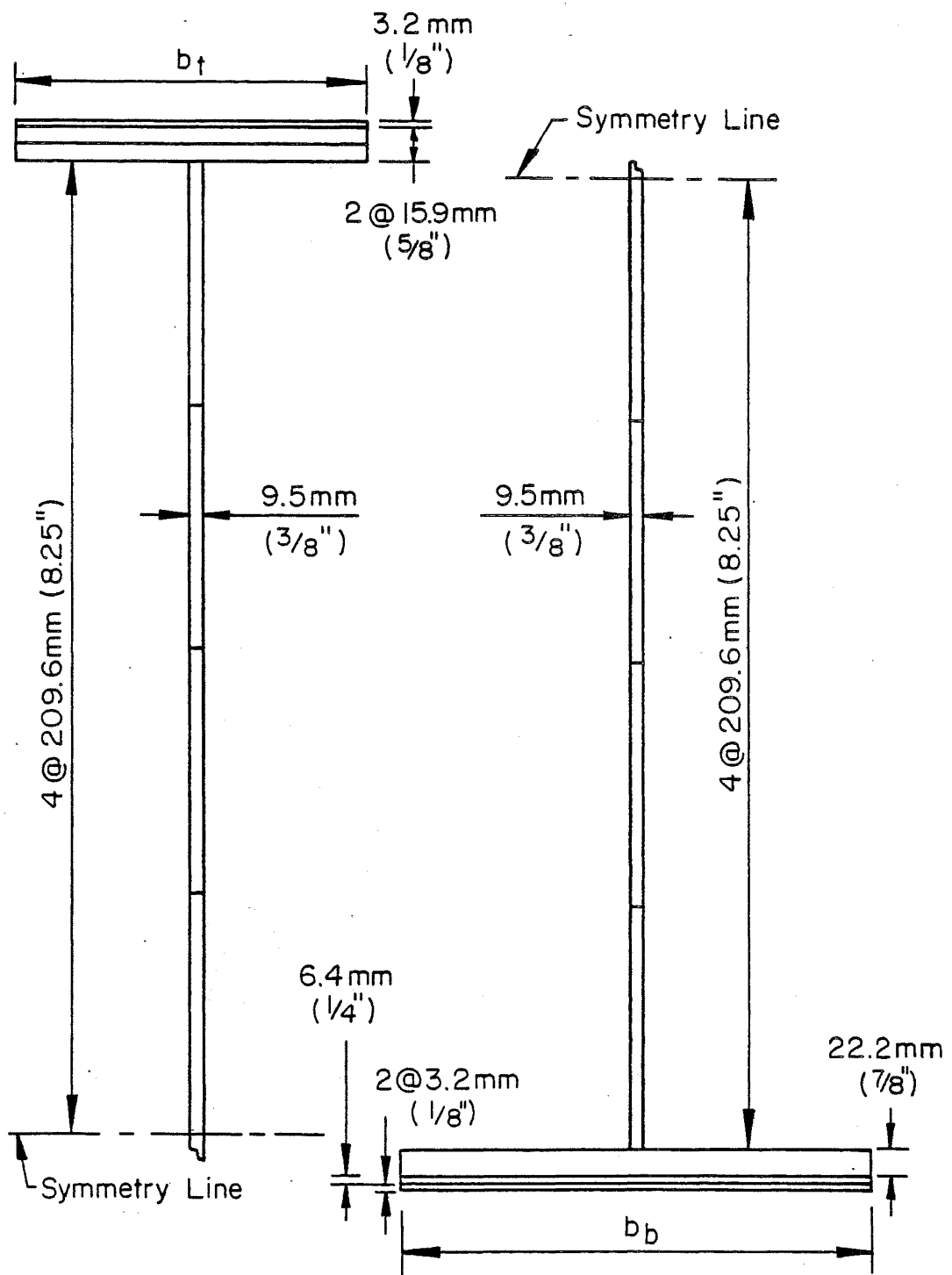


Fig. 46 FHWA Four-Span - Beam Layering

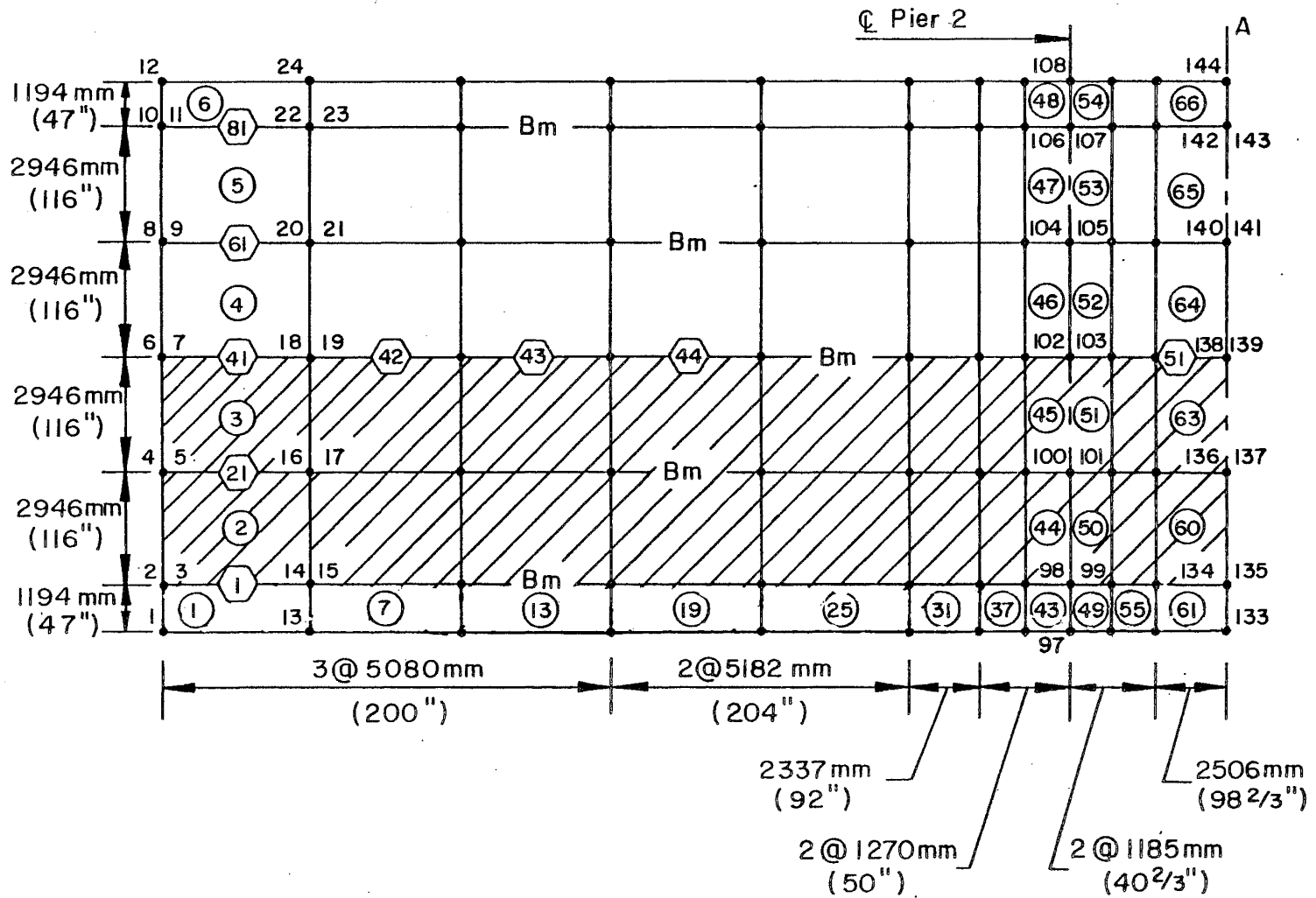


Fig. 47a FHWA Four-Span - Finite Element Discretization

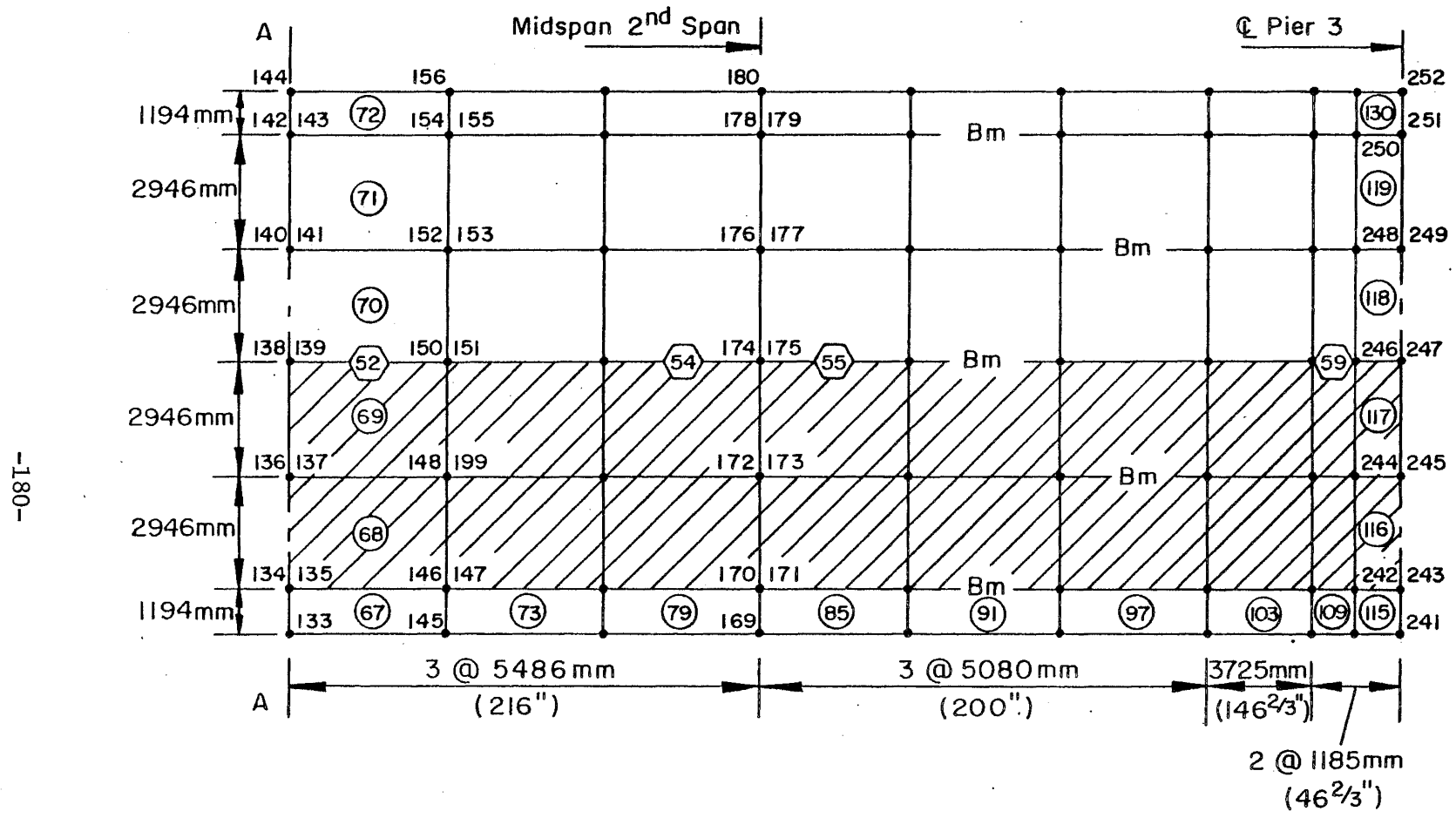


Fig. 47b FHWA Four-Span - Finite Element Discretization (continued)

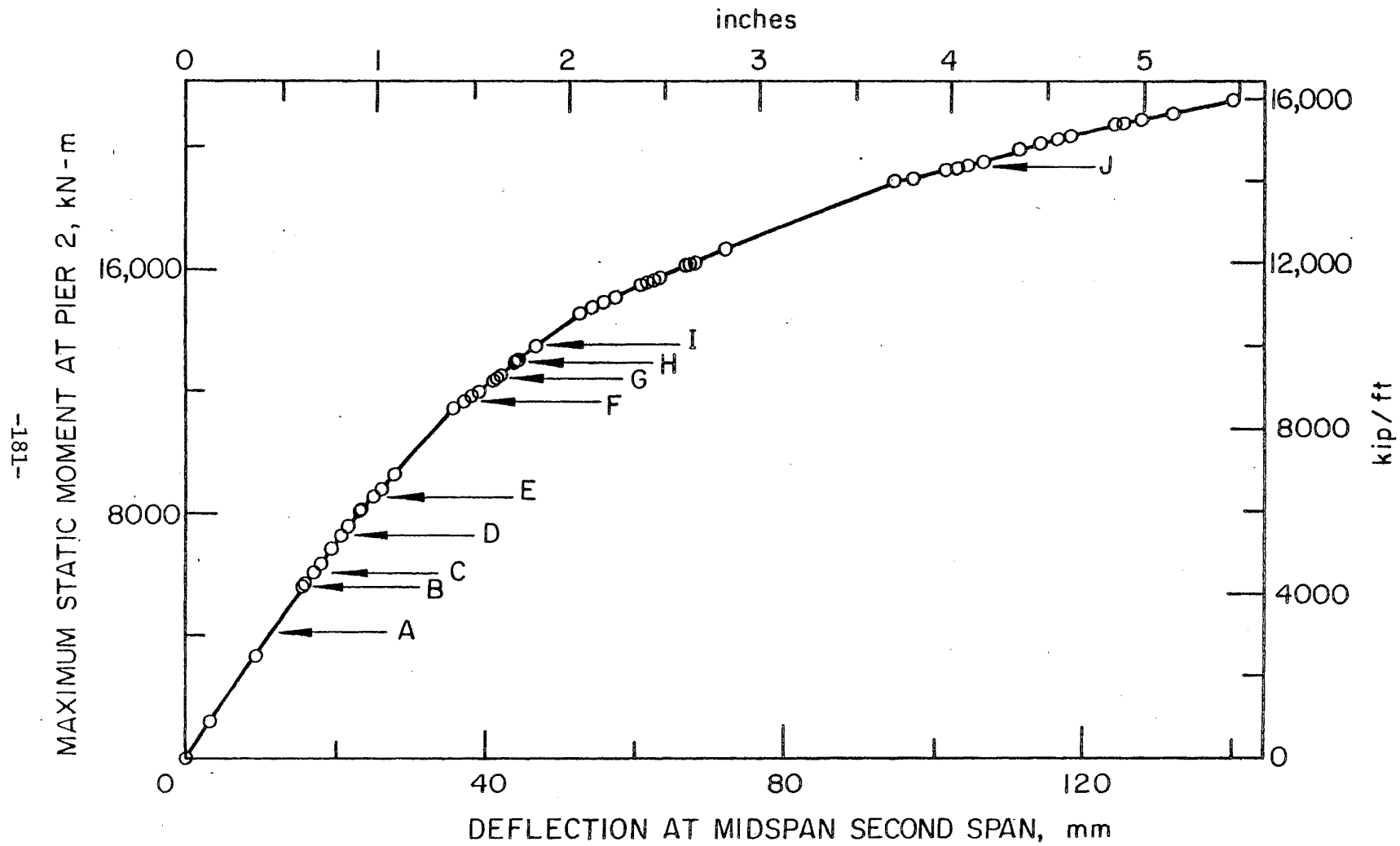


Fig. 48 FHWA Four-Span Load versus Deflection Diagram

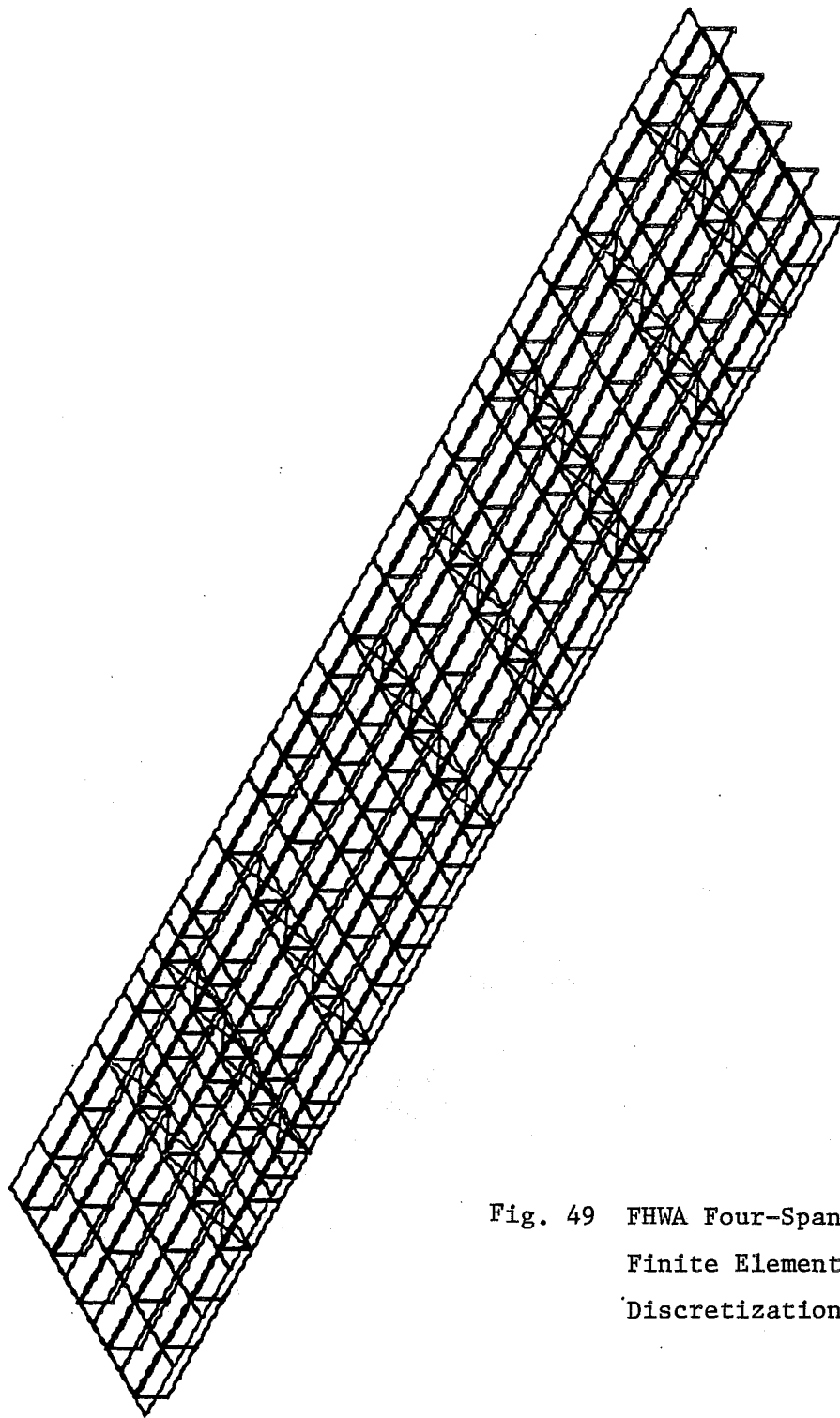


Fig. 49 FHWA Four-Span SAPIV  
Finite Element  
Discretization

## REFERENCES

1. Adini, A. and Clough, R. W.  
ANALYSIS OF PLATE BENDING BY THE FINITE ELEMENT METHOD,  
Report submitted to the National Science Foundation,  
Grant G7337, University of California, Berkeley,  
California, 1960.
2. American Association of State Highway Transportation  
Officials,  
STANDARD SPECIFICATIONS FOR HIGHWAY BRIDGES,  
Washington, D. C., 1974.
3. American Society of Civil Engineers  
COMPOSITE STEEL-CONCRETE CONSTRUCTION, Report of the  
Sub-committee on the State-of-the-Art Survey of the  
Task Committee on Composite Construction of the  
Committee on Metals of the Structural Division,  
Journal of the Structural Division, ASCE, Vol. 100,  
ST5, May 1974.
4. Armen, H. Pifko and Levine. H. S.  
FINITE ELEMENT ANALYSIS OF STRUCTURES IN PLASTIC RANGE,  
NASA Contractor Report NASA CR-1649, National Aero-  
nautics and Space Administration, Washington, D. C.,  
1971.
5. Baldwin, J. W., Jr., Henry, J. R. and Sweeney, C. M.  
STUDY OF COMPOSITE BRIDGE STRINGERS, PHASE II,  
University of Missouri, Columbian May 1965.
6. Barnard, P. R.  
RESEARCHES INTO THE COMPLETE STRESS-STRAIN CURVE FOR  
CONCRETE, Magazine of Concrete Research, Vol. 16, No.  
49, December 1964.
7. Basler, K. and Thurlimann, B.  
STRENGTH OF PLATE GIRDERS IN BENDING,  
Journal of the Structural Division, ASCE, Vol. 87, No.  
ST6, August 1961.
8. Basler, K.  
STRENGTH OF PLATE GIRDERS IN SHEAR,  
Journal of the Structural Division, ASCE, Vol. 87,  
No. ST7, October 1961.

REFERENCES (continued)

9. Basler, K.  
STRENGTH OF PLATE GIRDERS UNDER BENDING AND SHEAR,  
Journal of the Structural Division, ASCE, Vol. 87,  
No. ST7, October 1961.
10. Bathe, K. J., Wilson, E. L. and Peterson, F. E.  
SAPIV - A STRUCTURAL ANALYSIS PROGRAM FOR STATIC AND  
DYNAMIC RESPONSE OF LINEAR SYSTEMS,  
Report EERC 73-11, University of California, Berkeley,  
June 1973, revised April 1974.
11. Beedle, L. S. and Tall, L.  
BASIC COLUMN STRENGTH, Proc. ASCE, Vol. 86, No. ST7,  
July 1960.
12. Butzler, P. W., Colville, J. and Heins, C. P.  
ULTIMATE LOAD TESTS OF CONTINUOUS COMPOSITE-BRIDGE MODELS,  
Civil Engineering Report No. 61, University of Maryland,  
College Park, Maryland, June 1976.
13. Butzler, P. W. and Colville, J.  
CONTINUOUS COMPOSITE-BRIDGE MODEL TESTS,  
Journal of Structural Division, ASCE, Vol. 105,  
No. ST9, September 1979.
14. Burdette, E. G. and Goodpasture, D. W.  
FINAL REPORT ON FULL SCALE BRIDGE TESTING - AN EVALUATION  
OF BRIDGE DESIGN CRITERIA, University of Tennessee, 1971.
15. Chern, C. and Ostapenko, A.  
ULTIMATE STRENGTH OF PLATE GIRDERS UNDER SHEAR,  
Fritz Engineering Laboratory Report No. 328.7,  
Lehigh University, Bethlehem, PA, August 1969.
16. Chern, C. and Ostapenko, A.  
BENDING STRENGTH OF UNSYMMETRICAL PLATE GIRDERS,  
Fritz Engineering Laboratory Report No. 328.8,  
Lehigh University, Bethlehem, PA, November 1970.
17. Chern, C. and Ostapenko, A.  
UNSYMMETRICAL PLATE GIRDERS UNDER SHEAR AND MOMENT,  
Fritz Engineering Laboratory Report No. 328.9,  
Lehigh University, Bethlehem, PA, October 1970.

REFERENCES (continued)

18. Clough, R. W.  
THE FINITE ELEMENT METHOD IN STRUCTURAL MECHANICS,  
Chapter 7, of Stress Analysis, edited by O. C. Zienkiewicz  
and G. S. Hollister, John Wiley and Sons, New York,  
New York, 1965.
19. Dai, P. K., Thiruvengadam, T. R. and Siess, C. P.  
INELASTIC ANALYSIS OF COMPOSITE BEAMS, Engineering  
Extension Series No. 15, Proc. ASCE Specialty Conference  
on Steel Structures, University of Missouri, Columbia,  
June 8-12, 1970.
20. Dimitri, J. R. and Ostapenko, A.  
PILOT TEST ON STATIC STRENGTH OF UNSYMMETRICAL PLATE  
GIRDERS, WRC Bulletin No. 156, November 1970.
21. Doyle, S. K. and Burdette, E. G.  
A COMPARISON OF MEASURED AND COMPUTED LOAD DEFLECTION  
RELATIONSHIPS FOR FOUR HIGHWAY BRIDGES, The  
University of Tennessee, March 1972.
22. duPlessis, D. P.  
INTERACTION OF FLOORS AND FRAMES IN MULTISTORY BUILDINGS,  
Ph.D. Dissertation, Lehigh University, Bethlehem, PA, 1974.
23. Engineering News Record  
BRIDGE CRISES, Engineering News Record, Vol. 198, No. 10,  
March 10, 1977.
24. Evans, R. H. and Marathe, M.S.  
MICROCRACKING AND STRESS-STRAIN CURVES FOR CONCRETE  
IN TENSION, Materiaux et Constructions, Vol. 1,  
Janvier - Fevrier, 1968.
25. Fu, C. C., Colville, J. and Heins, C. P.  
INELASTIC ANALYSIS OF CONTINUOUS COMPOSITE HIGHWAY  
BRIDGES, Civil Engineering Report No. 62, University  
of Maryland, College Park, Maryland, June 1976.
26. Gustafson, W. C. and Wright, R. N.  
ANALYSIS OF SKEWED COMPOSITE GIRDER BRIDGES, Journal  
of the Structural Division, ASCE, Vol. 94, ST4, April  
1968.

REFERENCES (continued)

27. Hall, J. C. and Kostem, C. N.  
INELASTIC ANALYSIS OF STEEL MULTIGIRDER HIGHWAY BRIDGES,  
Fritz Engineering Laboratory Report No. 435.1, Lehigh  
University, Bethlehem, PA, August 1980.
28. Hall, J. C. and Kostem, C. N.  
FURTHER STUDIES ON THE INELASTIC OVERLOAD RESPONSE OF  
STEEL MULTI-GIRDER BRIDGES,  
Fritz Engineering Laboratory Report No. 435.2, Lehigh  
University, Bethlehem, PA, March 1981.
29. Hamada, S. and Longworth, J.  
ULTIMATE STRENGTH OF CONTINUOUS COMPOSITE BEAMS,  
Journal of the Structural Division, ASCE, Vol. 102,  
No. ST7, July 1976.
30. Hand, F. R., Pecknold, D. A. and Schnobrich, W. C.  
A LAYERED FINITE ELEMENT NONLINEAR ANALYSIS OF REINFORCED  
CONCRETE PLATES AND SHELLS, Civil Engineering Studies,  
Structural Research Series No. 389, University of  
Illinois, Urbana, Illinois, August 1972.
31. Hand, F. R., Pecknold, D. A. and Schnobrich, W. C.  
NONLINEAR LAYERED ANALYSIS OF RC PLATES AND SHELLS,  
Journal of the Structural Division, ASCE, Vol. 99,  
No. ST7, July 1973.
32. Heins, C. P. and Colville, J.  
LOAD FACTOR DESIGN RECOMMENDATIONS FOR STEEL I BEAM  
COMPOSITE HIGHWAY BRIDGES, Civil Engineering Report No.  
63, University of Maryland, College Park, Maryland,  
September 1976.
33. Highway Research Board  
THE AASHO ROAD TEST, Report 2, MATERIALS AND CONSTRUCTION,  
Special Report 61B, 1962.
34. Highway Research Board  
THE AASHO ROAD TEST, Report 4, BRIDGE RESEARCH,  
Special Report 61D, 1962.
35. Highway Research Board  
OVERSIZE-OVERWEIGHT PERMIT OPERATION ON STATE HIGHWAYS,  
National Cooperative Highway Research Program Report  
80, 1969.

REFERENCES (continued)

36. Hsu, T. T. C., Slate, F. O., Stuman, G. M. and Winter, G.  
MICROCRACKING OF PLAIN CONCRETE AND THE SHAPE OF THE  
STRESS-STRAIN CURVE, Journal of the American Concrete  
Institute, Vol. 60, No. 2, February 1963.
37. Hughes, B. P. and Chapman, G. P.  
THE COMPLETE STRESS-STRAIN CURVE FOR CONCRETE IN DIRECT  
TENSION, BULLETIN RILEM, No. 30, March 1966.
38. Johnson, R. P.  
RESEARCH ON STEEL-CONCRETE COMPOSITE BEAMS,  
Journal of Structural Division, ASCE, Vol. 96, ST3,  
March 1970.
39. Johnston, B. G., Editor  
GUIDE TO STABILITY DESIGN CRITERIA FOR METAL STRUCTURES,  
3rd Edition, John Wiley & Sons, New York, New York, 1976.
40. Kulicki, J. M. and Kostem, C. N.  
THE INELASTIC ANALYSIS OF REINFORCED AND PRESTRESSED  
CONCRETE BEAMS, Fritz Engineering Laboratory Report  
No. 378B.1, Lehigh University, Bethlehem, PA, November  
1972.
41. Kulicki, J. M. and Kostem, C. N.  
USER'S MANUAL FOR PROGRAM BEAM, Fritz Engineering  
Laboratory Report No. 378B.2, Lehigh University,  
Bethlehem, PA., February 1973.
42. Kulicki, J. M. and Kostem, C. N.  
FURTHER STUDIES ON THE NONLINEAR FINITE ELEMENT ANALYSIS  
OF BEAMS, Fritz Engineering Laboratory Report No. 378A.5,  
Lehigh University, Bethlehem, PA., April 1973.
43. Kulicki, J. M. and Kostem, C. N.  
THE INELASTIC ANALYSIS OF PRESTRESSED AND REINFORCED  
CONCRETE BRIDGE BEAMS BY THE FINITE ELEMENT METHOD,  
Fritz Engineering Laboratory Report No. 378A.6, Lehigh  
University, Bethlehem, PA., September 1973.
44. Kulicki, J. M. and Kostem, C. N.  
TORSIONAL CONSIDERATIONS IN NONLINEAR BEAM-SLAB  
BRIDGE SUPERSTRUCTURES, Bulletin No. 58 of the  
International Association for Shell and Spatial  
Structures, Madrid, Spain, September 1975.

REFERENCES (continued)

45. Kupfer, H., Hilsdorf, H. K., and Rusch, H.  
BEHAVIOR OF CONCRETE UNDER BIAXIAL STRESSES,  
Journal of the American Concrete Institute, Vol. 66,  
No. 8, August 1969.
46. Lay, M. G.  
FLANGE LOCAL BUCKLING IN WIDE-FLANGE SHAPES,  
Journal of the Structural Division, ASCE, Vol. 91,  
No. ST6, December 1965.
47. Lin, C. S.  
NONLINEAR ANALYSIS OF REINFORCED CONCRETE SLABS AND  
SHELLS, Ph.D. Dissertation, University of California,  
Berkeley, California, September 1972.
48. Liu, T. C.  
STRESS-STRAIN RESPONSE AND FRACTURE OF CONCRETE IN  
BIAXIAL COMPRESSION, Ph.D. Dissertation, Structural  
Engineering Department, Cornell University, Ithaca,  
New York, 1971.
49. Liu, T. C., Nilson, A. H. and Slate, F. O.  
BIAXIAL STRESS-STRAIN RELATIONS FOR CONCRETE,  
Journal of Structural Division, ASCE, Vol. 98,  
No. ST5, May 1972.
50. Neilissen, L. J. M.  
BIAXIAL TESTING OF NORMAL CONCRETE, HERON,  
Vol. 18, No. 1, 1972, Stevin-Laboratory of the  
Department of Civil Engineering of the Technological  
University and Institute TNO for Building Materials  
and Building Structures, Delft, The Netherlands
51. Newmark, N. M.  
A DISTRIBUTION PROCEDURE FOR THE ANALYSIS OF SLABS  
CONTINUOUS OVER FLEXIBLE BEAMS, University of Illinois  
Engineering Experiment Station Bulletin No. 304,  
University of Illinois, Urbana, 1938.
52. Peterson, W. S., Kostem, C. N. and Kulicki, J. M.  
THE INELASTIC ANALYSIS OF REINFORCED CONCRETE SLABS,  
Fritz Engineering Laboratory Report No. 378B.3, Lehigh  
University, Bethlehem, PA., May 1974.

REFERENCES (continued)

53. Peterson, W. S., Kostem, C. N. and Kulicki, J. M.  
DISCUSSION OF "FULL RANGE ANALYSIS OF ECCENTRICALLY STIFFENED PLATES", by A. W. Wegmuller, Journal of the Structural Division, ASCE, Vol. 100, ST9, September 1974.
54. Peterson, W. S. and Kostem, C. N.  
THE INELASTIC ANALYSIS OF BEAM-SLAB HIGHWAY BRIDGE SUPER STRUCTURES, Fritz Engineering Laboratory Report No. 378B.5, Lehigh University, Bethlehem, PA., March 1975.
55. Peterson, W. S. and Kostem, C. N.  
THE INELASTIC ANALYSIS OF BEAM-SLAB BRIDGES, Fritz Engineering Laboratory Report No. 400.20, Lehigh University, Bethlehem, PA., July 1975.
56. Proctor, M. H.  
ANALYTICAL AND EXPERIMENTAL STUDY OF LIGHTWEIGHT CONCRETE-STEEL COMPOSITE BEAMS, M.S. Thesis, University of Missouri, Columbia, August 1963.
57. Ramberg, W. and Osgood, W. R.  
DESCRIPTION OF STRESS-STRAIN CURVES BY THREE PARAMETERS, NACA, TN 902, July 1943.
58. Rockey, K. C. and Skaloud, M.  
THE ULTIMATE LOAD BEHAVIOR OF PLATE GIRDELS LOADED IN SHEAR, The Structural Engineer, No. 1, Vol. 50, January 1972.
59. Siess, C. P., Viest, I. M. and Newmark, N. M.  
STUDIES OF SLAB AND BEAM HIGHWAY BRIDGES, PART III - SMALL SCALE TESTS OF SHEAR CONNECTORS AND COMPOSITE I-BEAMS, University of Illinois Engineering Experiment Station Bulletin No. 396, University of Illinois, Urbana, 1952.
60. Smith, G. M. and Young, L. E.  
ULTIMATE FLEXURAL ANALYSIS BASED ON STRESS-STRAIN CURVES OF CYLINDERS, Journal of the American Concrete Institute, Vol. 53, No. 6, December 1956.
61. Tall, L., editor  
STRUCTURAL STEEL DESIGN, Roland Press, Chapter 17, Local Buckling, New York, New York, 1964.

REFERENCES (continued)

62. Teraszkiewicz, J. S.  
STATIC AND FATIGUE BEHAVIOR OF SIMPLY SUPPORTED AND CONTINUOUS COMPOSITE BEAMS OF STEEL AND CONCRETE, Ph.D. Thesis, Imperial College of Science and Technology, University of London, September 1967.
63. Tottenham, H. and Brebbia, C.  
FINITE ELEMENT TECHNIQUES IN STRUCTURAL MECHANICS, Southampton University Press, Southampton, England, 1970.
64. Tumminelli, S. C. and Kostem, C. N.  
FINITE ELEMENT ANALYSIS FOR ELASTIC ANALYSIS OF COMPOSITE BEAMS AND BRIDGES, Fritz Engineering Laboratory Report No. 438.3, Lehigh University, Bethlehem, PA., March 1978.
65. Viest, I. M.  
REVIEW OF RESEARCH ON COMPOSITE STEEL-CONCRETE BEAMS, Journal of the Structural Division, ASCE, Vol. 86, ST6, June 1960.
66. Wegmuller, A. W. and Kostem, C. N.  
ELASTIC-PLASTIC ANALYSIS OF PLATES, Proceedings of the IASS Symposium on Shell Structures and Climatic Influences, pp. 379-386, Calgary, Canada, July 1972.
67. U. S. Department of Transportation, Federal Highway Administration,  
STANDARD PLANS FOR HIGHWAY BRIDGES, Vol. IVA, Typical Continuous Bridges, Load Factor Design, June 1973.
68. Wegmuller, A. W. and Kostem, C. N.  
FINITE ELEMENT ANALYSIS OF PLATES AND ECCENTRICALLY STIFFENED PLATES, Fritz Engineering Laboratory Report No. 378A.3, Lehigh University, Bethlehem, PA., February 1973.
69. Wegmuller, A. W. and Kostem, C. N.  
FINITE ELEMENT ANALYSIS OF ELASTIC-PLASTIC PLATES AND ECCENTRICALLY STIFFENED PLATES, Fritz Engineering Laboratory Report No. 378A.4, Lehigh University, Bethlehem, PA., February 1973.

REFERENCES (continued)

70. Whang, B.  
ELASTO-PLASTIC ORTHOTROPIC PLATES AND SHELLS,  
Proceedings of the Symposium on Application of  
Finite Element Methods in Civil Engineering,  
Vanderbilt University, Nashville, Tennessee,  
November 1969.
71. Wu, Y. C.  
ANALYSIS OF CONTINUOUS COMPOSITE BEAMS, Ph.D.  
Dissertation, Lehigh University, Bethlehem, PA.,  
December 1970.
72. Yam, L. C. P. and Chapman, J. C.  
THE INELASTIC BEHAVIOR OF SIMPLY SUPPORTED COMPOSITE  
BEAMS OF STEEL AND CONCRETE, Proceedings of the  
Institution of Civil Engineering, London,  
December 1968.
73. Ziekiewicz, O. C.  
THE FINITE ELEMENT METHOD IN ENGINEERING SCIENCE,  
McGraw Hill, New York, New York, 1971.
74. Kostem, C. N.  
SHEAR PUNCHING OF BRIDGE DECKS, Fritz Engineering  
Laboratory Report No. 378B.4, Lehigh University,  
Bethlehem, PA., July 1975.
75. Kostem, C. N.  
OVERLOADING BEHAVIOR OF BEAM-SLAB TYPE HIGHWAY  
BRIDGES, Fritz Engineering Laboratory Report No.  
378B.8, Lehigh University, Bethlehem, PA.,  
July 1977.
76. Hall, J. C. and Kostem, C. N.  
USER'S MANUAL, BOVAS-BRIDGE OVERLOAD ANALYSIS -  
STEEL, Fritz Engineering Laboratory Report No. 435.3,  
Lehigh University, Bethlehem, PA., April 1981.

### ACKNOWLEDGMENTS

Parts of the reported investigation were sponsored by the Pennsylvania Department of Transportation and the United States Department of Transportation, Federal Highway Administration. Their support is gratefully acknowledged.

The authors extend their gratitude to the Lehigh University Computing Center for making the facilities available for an extensive computer based investigation.

Thanks are also due to Mesdames D. Fielding, P. M. Vidanage and K. M. Kostem for typing this manuscript; to Mr. J. Gera and Mrs. S. Balogh for preparation of the drawings; and to Ms. Jamie I. Moyer for her editorial contributions.